The callosal contribution to cortical microcircuits

Alejandro Sempere Ferràndez, 2016

Supervisor: Emilio Geijo Barrientos

Instituto de Neurociencias UMH-CSIC

Consejo Superior de Investigaciones Científicas
Universidad Miguel Hernández
Instituto de Neurociencias

Prof. Salvador Martínez
Director

A QUIÉN PUEDA INTERESAR,

Prof. Salvador Martínez Pérez, Director del Instituto de Neurociencias, Centro Mixto de la Universidad Miguel Hernández-UMH y la Agencia Estatal Consejo Superior de Investigaciones Científicas-CSIC,

CERTIFICA:

Que la Tesis Doctoral titulada "The callosal contribution to cortical microcircuits" ha sido realizada por D. Alejandro Sempere Ferràndez (NIE 74370275M) bajo la dirección del Dr. Emilio Geijo Barrientos y da su conformidad para que sea presentada a la Comisión de Doctorado de la Universidad Miguel Hernández.

Para que así conste a los efectos oportunos, firma el presente certificado en San Juan de Alicante a 10 de noviembre de 2016

Salvador Martínez

Director

dirección.in@umh.es
dirección.in@csic.es
www.ina.umh.es

Tel: +34 965 919220 (s)
+34 965 919221 (d)
Fax: +34 965 919561

Av. Ramón y Cajal s/n
Campus de San Juan
03550 SAN JUAN DE ALICANTE - ESPAÑA

Consejo Superior de Investigaciones Científicas
Universidad Miguel Hernández
Instituto de Neurociencias

D. Emilio Geijo Barrientos, Catedrático de Universidad en la Universidad Miguel Hernández de Elche,

CERTIFICA,

Que D. Alejandro Sempere Ferràndez, licenciado en Biología, ha realizado bajo mi dirección el trabajo experimental que recoge su Tesis Doctoral "The callosal contribution to cortical microcircuits".

Que el que suscribe ha revisado los contenidos científicos y los aspectos formales del trabajo y da su conformidad para su presentación y defensa públicas.

Para que así conste, y a los efectos oportunos, firma el presente certificado en San Juan de Alicante, a 10 de noviembre de 2016.

Fdo. Emilio Geijo Barrientos

Av. Ramón y Cajal s/n
Campus de San Juan
03550 SAN JUAN DE ALICANTE - ESPAÑA

I

No importa la rima
no hay que contar sílabas.
Primero la sangre,
los demás luego,
más tarde.

II

A las calles encendidas,
que bajo un negro cielo
anuncian una despedida,
el fin de lo convencional.

A los fracasos sentados
en la barra de un bar
que en nada quedan
cuando la mano levanta el vaso
y la risa, entre amigos,
se abre paso.

Al sí rotundo
sin reproches
de todos los que conmigo
compartieron ese mundo,
el de la oscuridad y la noche.

CONTENTS

LIST OF ABBREVIATIONS

5HT3aR	serotonin ionotropic receptor 3a
τm	membrane time constant
A1	primary auditory cortex
A2	secondary auditory cortex
ACSF	artificial cerebro-spinal fluid
ADVR	anterior dorsal ventricular ridge
AMPA	α-amino-3-hydroxy-5-methyl-4-isoxazolepropionic acid
AP	action potential
ATP	adenosine triphosphate
CPN	callosal-projection neuron
DAPI	4',6-diamidino-2-phenylindole
DNA	deoxyribonucleic acid
EGTA	ethylene glycol-bis(β-aminoethyl ether)-N,N,N',N'-tetraacetic acid
E/I balance	excitatory to inhibitory balance
EPSC	excitatory postsynaptic current
	cEPSC compound EPSC
	uEPSC unitary EPSC
EPSP	excitatory postsynaptic potential
GAD67	glutamic acid decarboxylase isoform 67
GFP	green fluorescent protein
GTP	Guanosine-5'-triphosphate
HEPES	4-(2-hydroxyethyl)-1-piperazineethanesulfonic acid
Ihold	holding current
IPSC	inhibitory porstsynaptic potential
	cIPSC compound IPSC
	mIPSC miniature IPSC
	uIPSC unitary IPSC
IR-DIC	infrared differential interference contrast
L1, 2/3, 4, 5, 5B, 6	cortical layer 1, 2/3, 4, 5, 5B, 6
L5m	medium-size pyramidal neurons from layer 5
L5Bm	medium-size pyramidal neurons from layer 5B

L5BL	large pyramidal neurons from layer 5B
LFP	local field potential
NBQX	2,3-dihydroxy-6-nitro-7-sulfamoyl-benzo[f]quinoxaline-2,3-dione
NeuN	neuronal nuclei protein
PBS	phosphate buffer solution
PFA	paraformaldehyde
PSP	postsynaptic potential
PV	parvalbumin
PV-FS	parvalbumin-expressing fast-spiking interneuron
Rm	membrane input resistance
Rs	series resistance
RSC	retrosplenial cortex
	aRSC agranular RSC
	gRSC granular RSC
SST	somatostatin
SVZ	subventricular zone
V1	primary visual cortex
V2	secondary visual cortex
Ve	voltage error
Vm	membrane potential
Vrest	resting membrane potential
Vss	steady-state voltage
VIP	vasoactive intestinal peptide
VZ	ventricular zone

RESUM

El cos callós es la major comissura del cervell dels mamífers placentaris. Els axons callosos realitzen una contribució fonamental al funcionament del còrtex cerebral al permetre la comunicació interhemisfèrica, principalment entre regions homotòpiques contralaterals. En aquest treball, hem investigat la influència de les neurones de projecció callosa de les capes 2/3, el subtipus més abundant, als circuits del còrtex retrosplenial, una regió involucrada en la cognició espacial y contextual.

Les nostres dades indiquen que aquesta via corticocortical projecta, específicament, sobre les neurones piramidals de capa 2/3 i les grans piramidals amb projeccions extratelencefàliques de descàrrega en ràfega que es situen a la part superficial de capa 5B. Per contra, les neurones piramidals de tamany mitjà de les capes 5A, 5B i 6, i les grans piramidals de la part profunda de la capa 5B responen de manera residual, tant a l'entrada excitatòria callosa directa com a la inhibició associada.

A banda, demostrem que l'entrada callosa té un efecte contrari a les seues dianes principals: suprimeix l'activitat de les neurones contralaterals de capa 2/3, mentre que recluta les grans piramidals de capa 5B. Aquesta diferència depén, en primer lloc, d'una major convergència d'axons callosos excitadors sobre les segones. A més, posem de manifest l'existència d'una dependència laminar en la dinámica de reclutament de les interneurones de descàrrega ràpida (FS per les sigles en anglés) en resposta a l'entrada callosa, que també afavoreix el comportament oposat d'ambós tipus neuronals. A les capes superficials, les interneurones FS són reclutades de manera directa per l'excitació callosa, i actuen inhibint a les neurones piramidals superficials de forma potent i ràpida, reduïnt sensiblement la probabilitat d'aquestes últimes d'arribar a l'umbral de descàrrega. En canvi, a capes més profundes, la resposta de les interneurones FS es moderada, i el

seu reclutament també requereix l'entrada excitatòria de les grans piramidals de capa 5B, que disparen previament a aquestes per l'efecte excitador dominant dels axons callosos.

Concluïm, per tant, que les neurones piramidals superficials i de descàrrega en ràfega de capa 5B formen un subxarxa que integra ambdós àrees retrosplenials contralaterals, i que es troba aïllada, almenys parcialment, de xarxes locals en la que participen els altres tipus de neurones piramidals mencionats. A més, aportem resultats novedosos respecte a l'organització laminar dels circuits corticals inhibidors, dels quals es deriven implicacions directes sobre les estratègies de codificació implementades per les neurones superficials i profundes. Finalment, discutim aquestos resultats en el context del coneixement actual de la fisiología dels circuits corticals.

SUMMARY

The corpus callosum is the largest commissure in the brain of placental mammals. Callosal axons exert a major contribution to cortical function by mediating interhemispheric communication, mainly between homotopic contralateral regions. Here, we have studied the influence of superficial callosal projecting neurons (CPNs), the most abundant subtype of CPN, in the entire columnar extension of the retrosplenial cortex, a region involved in spatial cognition and context recognition.

Our data indicate that this form of cortical input specifically targets superficial pyramidal neurons and the large bursting extratelencephalic-projecting pyramidal neurons in upper layer 5B. In contrast, the medium-size pyramidal neurons in layers 5A, 5B and 6 and the large pyramidal neurons from lower layer 5B remained largely unresponsive, both to the direct callosal excitatory input and to PV-FS dependent inhibition.

The effect of callosal input on their two main contralateral targets was opposed, suppressing the activity of layer 2/3 pyramidal neurons and potently recruiting the large pyramids of layer 5B. A larger convergence of callosal axons on the latter and the large responsiveness of superficial parvalbumin-expressing fast-spiking interneurons (PV-FS), which potently inhibit pyramidal neurons in layers 2/3, explain the differential recruitment of both pyramidal subtypes. In addition, we demonstrate a laminar dependence in the dynamics of PV-FS recruitment by callosal input. While PV-FS cells in superficial layers are directly recruited by callosal excitation, acting on superficial pyramidal neurons in a feed-forward manner and markedly reducing their opportunity to reach the firing threshold, those PV-FS neurons from deeper layers only weakly respond

to callosal input, but require the previous activation of the surrounding large bursting pyramidal neurons to fire an action potential.

Overall, our data suggests that superficial and bursting pyramidal neurons with subcortical projections from upper layer 5B form an integrated subnetwork across contralateral retrosplenial areas, and that this is, at least partially, isolated from microcircuits including other pyramidal subtypes. In addition, we also provide new insights in the organization of cortical inhibitory networks across layers with relevant implications in the coding strategies of superficial and deep pyramidal neurons. A discussion of these results in the context of our current understanding of the general principles of cortical function is also provided.

INTRODUCTION

In this introduction I provide a brief summary of (what I know about) isocortical circuits, with emphasis in the functional implications of its architecture. First, I discuss their origin, as often, evolutionary aspects provide interesting cues to interpret biological phenomena. I then proceed with an historical overview on the general principles of isocortical architecture (lamination, regionalization and columnar organization), followed by a short discussion of the connectivity rules between the diverse neurons of the isocortex, both at the local and long-range levels. Finally, I review the issue of interhemispheric connectivity across the corpus callosum.

Hypothesis on the origin and evolution of the isocortex

The isocortex develops from the dorsalmost area of the pallium, in the roof of the telencephalic vesicle (Puelles et al. 2013). In mammals, this region undergoes a great surface expansion, becoming the largest nervous center of the brain. Despite the existence of remarkable structural commonalities with other pallial centers, including the hippocampal formation and the piriform cortex, the isocortex can be easily distinguished from them by a more complex arrangement in six layers (Lewis 1880, Brodmann 2006). The special character of this architecture is reflected in the current controversy regarding its evolutionary origin, a topic I briefly discuss below.

Our closest extant relatives, the modern (non-avian) reptiles, diverged from our lineage about 300 million years ago. Nevertheless, as in mammals, the reptilian pallium can be divided in three major segments (Puelles 2001, Naumann et al. 2015): (a) a lateral olfactory cortex, receiving direct projections from the main olfactory bulb (*piriform cortex*), (b) a medial *limbic* cortex (*hippocampus)* and (c) an intermediate region, which, in contrast with mammals, not only has a cortical domain, the reptilian dorsal cortex, but

also a nuclear region protruding from the pallial surface close to the ventricle, the anterior dorsal ventricular ridge (ADVR). Similarly to the isocortex, the dorsal cortex and the ADVR of reptiles are largely occupied by modality-specific sensory areas, including gustatory, visual, somatosensory and auditory domains (Donkeelar 1998). Of particular interest is the reptilian dorsal cortex, which position and structure noticeably resembles those of the mammalian isocortex. In fact, it is often assumed that the stem amniote had a three layered cortex with a similar organization to the reptilian dorsal cortex, being the mammalian isocortex, and also probably the ADVR, apomorphic characters.

The reptilian dorsal cortex has a monolayer of glutamatergic excitatory pyramidal neurons which send their apical and basal spiny dendritic trees to the upper and lower scarcely cellular layers, respectively; in addition, a diversity of stellate gabaergic inhibitory interneurons are disposed in the three layers of the cortex (Connors and Kriegstey 1986). Local reciprocal connections are established within these pyramidal neurons, which also have distal intra and extracortical projections. Additionally, several neuromodulatory inputs from the brainstem (cholinergic, adrenergic, serotonergic…) and modality-specific sensory input from glutamatergic thalamic afferents reach the outer part of the upper molecular layer, exciting both the pyramidal and the stellate cells, which in turn inhibit the formers (Reiner 1993, Ulinski 2007). In general, these scheme also applies for the mammalian cortical circuits.

A relevant question is how a monolayer of pyramidal neurons became the five pyramidal layers of the mammalian neocortex. An answer to this may come from comparative studies on the neurogenic compartments of the developing telencephalon. In all amniotes, cortical excitatory neurons are produced by progenitors that divide along the ventricular surface (Rakic 1971 and 1972) a region called the ventricular zone (VZ). However, in mammals, cortical excitatory neurons are also produced in the subventricular

zone (SVZ), a zone superficial to the VZ. Recent work suggests that this neurogenic niche, mostly absent in non-avian reptiles, importantly contributes to the production of superficial pyramidal cells in the mammalian isocortex (Cheung et al. 2007). Interestingly, the SVZ has been described in other telencephalic regions that, as the isocortex, undergo a prominent expansion phase during development, including the avian pallium (Nomura 2016). Following this view, it is often assumed that deep isocortical layers (layers 5-6) constitute the pleisomorphic character of the cerebral cortex, while the incorporation of superficial pyramidal neurons (layers 2-4) is a mammalian innovation. If this was correct, it becomes of major significance to determine which functional novelties were incorporated with superficial neurons.

Two other relevant differences exist between both structures. One is the presence of areas directly implicated in motor control in the mammalian cerebral cortex, a function mediated through the corticospinal and corticobulbar projections emerging from the large pyramidal neurons of layer 5; these areas are missing in the reptilian pallium, whose influence on motor control is indirect and depends on the cortical projection to the striatum (Donkelaar 1998). In fact, in reptiles, the striatopallidal complex and not the cortex itself is the main output of the telencephalon. Then, one must consider that even if isocortical deep layers are homologous to the pyramidal layer of the dorsal cortex of the reptilian brain, both entities must have diverge during the course of evolution.

Additionally, in the reptilian brain, topographically-organized sensory maps are restricted to mesencephalic levels (there is only a non-topographic or just crude topographic order in the cortical projections from the subcortical sensory centers), while already in extant *primitive* mammals those homologous projections are highly topographical (Allman 1990). Speculating on the reasons for this difference, one wonders if the surface expansion of the cerebral cortex, and the appearance of the numerous and

smaller pyramidal cells in superficial layers of the mammalian isocortex were necessary conditions for the establishment of more specific sensory projections.

An old structural scheme for the isocortex: layers, regions and columns

The term *iso*cortex was introduced by Vogt to reflect its homogeneity, clearly contrasting with the larger structural variability of the *allo*cortical structures (the hippocampal formation and the piriform cortex). In this sense, the isocortex is characterized by three structural *constancies* common to all mammals: (1) in the horizontal dimension, neurons are arranged in layers and the layer identity of a given cell determines many of its morphological and physiological features; (2) regional discontinuities exist, reflecting the differential laminar organization, size, density and distribution of neurons and (3) in the radial dimension, neurons are stereotypically interconnected forming what many have interpreted as unitary functional columns.

Lamination of the isocortex

As neurogenesis advances, new pools of pyramidal neurons are formed and travel radially from the periventricular surface to their final destination, close to the pia (Rakic 1971, 1972). In the mammalian isocortex, this migration follows an inside-out pattern, this is, those pyramidal neurons from deeper layers are formed and reach their destination before those in superficial layers, which will have to travel through the former to reach their final position (Rakic 1974). During this process, heterogeneous genetic programs and environmental conditions (including afferent systems) exist for those neurons generated asynchronously, explaining the variability in the pyramidal types across the cortical depth.

As a consequence of this developmental program, the laminar patterning of the isocortex is *easily* recognizable. Our current golden-standard six-layer model for the isocortex is quite old (Lewis 1880), and was based on classical histological staining techniques. What is more difficult to reach is a generalizable consensus regarding the identity of such layers. Cajal disagreed with the idea of a general six-layer scheme for all mammalian species, defending that a different degree in the complexity of the isocortical lamination could be distinguish across mammalian orders (referred in Brodmann 2006). In primates, superficial layers are relatively thicker than in rodents, in which deep layers are relatively larger (Hustler et al. 2005). It has been suggested that in larger brains, where a large diversity of areas appear, there is a concomitant need to increase corticocortical communication, and this may have exert a positive selective pressure on superficial layers, which are responsible of the majority of the communication between different cortical areas (Rockel et al. 1980). Sublaminar differentiation also exists, with different degrees of complexity across mammalian species, for instance in the case of layer 4 of primary visual cortex (Brodmann 2006).

Overall, cortical layers should not be considered as clearly defined compartments formed by homogeneous neuronal populations, as pyramidal neurons with diverse morphological, hodological, electrophysiological and functional properties coexist within the boundaries of each single layer (Mólnar and Cheung 2006, Thomson 2010, Yamashita et al. 2013, Kim et al. 2015).

Cortical enlargement and regionalization

A landmark of mammalian evolution is the massive surface expansion of the cerebral cortex, particularly of the isocortex (DeFelipe 2011). However, this was not a homogeneous process, but happened independently in several groups, namely in

primates, whales and dolphins and elephants. In fact, while in basal mammals, such as the hedgehog, the isocortex is similar in size to the allocortical regions, in primates it constitutes by far the largest center of the brain (Azevedo et al. 2009). The different degree of neocorticalization across mammalian species has been linked, again, to differences in neuronal progenitor cell biology. In mammals with larger brains, these cells are able to enter more self-sustaining cycles of division, therefore increasing the size of the neuronal pool derived from each initial progenitor (Borrel and Reillo 2012, Florio and Huttner 2014).

Concomitant to the surface expansion of the isocortical sheet was the emergence of areas with new or more specific functions. Variations in the cytoarchitecture of these areas, this is, in the shape and packing of their neurons and layers, prompted classical attempts of cortical parcellation, the most famous of which is Brodmann's *Localisation in the cerebral cortex* (Brodmann 2006, for a recent study on the parcellation of the human cerebral cortex see Glasser et al. 2016). It is believed that in the stem mammal, the isocortex was dominated by a basic set of areas containing the limbic structures and those allowing for rudimentary sensory and motor processing (Allman 1990). This seems to be the case of those extant species that are considered to resemble the primitive condition (*primitive* marsupials such as the Virginia opossum). Already in prosimians, the modality-specific primary sensory cortices of primitive mammals are separated by a strip of association cortex, and another area of association cortex is present in front of the motor cortex (Nieuwenhuys et al. 1998). In primates, both the posterior (parietotemporal) association area and the anterior (prefrontal) one are considerably expanded. It seems reasonable to think that the enlargement of the isocortex allowed for a more accurate representation of the environmental sensorium, which, in combination with the formation and progressive expansion of high-order integration centers (unimodal and multimodal

association areas), potentiated the behavioral flexibility shown by mammals with larger brains.

Sensorimotor integrative centers exist all over the vertebrate subphylum. In amphibians, sensory processing largely depends on the tectum, the roof of the anterior part of the mesencephalum, which it is usually believed to be a visuomotor area, but which also receives non-visual sensory input (Donkelaar 1998b). In these animals, the striatum also emerges as an important integrative region linking multimodal sensory information with motor commands. In reptiles, most of sensory processing is already shifted to pallial domains, and as in mammals, the medial cortex (hippocampus) is known to receive projections from the other specific sensory areas of the pallium. Birds constitute a branch within the reptilian tree, and despite they lack cortical domains, their pallium is very well developed into different nuclear centers. Interestingly, the avian pallium is similarly organized to the mammalian isocortex. It also comprises primary target areas of the three major sensory systems (visual, auditory and somatosensory), which are surrounded and strongly interconnected with secondary areas; contains a primary output (motor) area and a large region of substantial integration defined by massive intrahemispherical connections with primary and secondary sensory areas on one side, and output areas on the other side, similarly to the mammalian prefrontal cortex (Rehkamper et al. 1991, Shanahan et al. 2013). Therefore, the same strategy of regional differentiation has been followed in the avian and mammalian telencephalon. In addition, a recent study indicates that parrots and corvids, despite having smaller brains, contain comparable amounts of neurons in their forebrains than larger primates (Olkowicz et al. 2016). Both mammals and birds are thought to excel in their cognitive abilities over other vertebrates. The fact that in both cases the pallium is well-developed following a similar plan and that a

comparable amount of neurons can be found in their forebrain reinforces the idea that cognition is largely dependent on this set of telencephalic structures.

Modularity of cortical circuits

Classical studies on lamination and regionalization did not study the complete morphology and the pattern of dendritic and axonal branching of single neurons, precluding any kind of functional interpretation based on microconnectivity. For these reasons, it has been indicated that this approach was like making a *"road map without roads"* (Valverde 2002). It was Santiago Ramón y Cajal who started the description of the cortical microcircuits by means of a powerful technique, the *Golgi staining*. With it, the dendritic and axonal arborizations of the intrinsic cortical neurons and the afferent fibres could be revealed in fine detail, allowing neuromorphologists to start scratching, still very superficially, the intricate mazes of cortical circuits. Cajal's disciple Lorente de Nó, applying the same approach, proposed the existence of a unifying columnar principle in the structure of local cortical circuits (Lorente de Nó 1938). According to him, it consisted on the vertical arrangement of the neuronal elements needed to carry a nerve impulse to the cortex, process it, and sent it back to another cortical or subcortical region. He also indicated that this principle could not be generalized in their fine details, as the neuronal types and their connectivity rules were variable across columns of different cortical regions.

In the late 50s, during the course of *in vivo* electrophysiological recordings in the somatosensory cortex of the anesthetized cat and monkey, Mountcastle observed neurons similarly tuned for their specific stimulus modality and peripheral receptive fields when the recording microelectrode was radially advanced through the cortical depth, but not when moved tangentially (Mountcastle 1957). This is the consequence of the

topographical disposition of the sensory afferents to the mammalian neocortex already noticed by Lorente de Nó. Very soon, similar results were obtained in the cat and monkey striate cortex by Hubel and Wiesel (Hubel & Wiesel 1963, 1968).

Two additional approaches reinforced the idea of the vertical bias in cortical architecture. Absolute neuron counts in radial volumes of cortical tissue from the pial surface to the underlying white matter revealed the constancy of neuron number across several cortical regions (frontal, motor, somatosensory, parietal, temporal) and species (mouse, rat, cat, monkey and human), with the only exception of the primate striate cortex, where the constant amount of neurons was increased 2.5-fold (Rockel et al. 1974 and 1980). This observation deserved the scepticism of many (Rakic 2008), and still recently, conflicting studies appear regarding this issue (Herculano-Houzel et al. 2008, Collins et al. 2010, Carlo and Stevens 2012). In parallel to this, Rakic's studies on monkey corticogenesis showed that the adult columnar disposition of the isocortex was the reflection of the organization of the neuroepithelium during developmental stages, in which the precursor cells located in the ventricular zone were already divided by glial-septa into well-defined columns (Rakic 1971, 1972). According to this model, each group of separated precursor cells, the *proliferative unit*, gives rise to a cohort of neurons that migrate in succession along the same radial glial guides, therefore adopting a close position in the postnatal cortex. In this way, all the postmitotic neurons coming from the same proliferative unit constituted an *ontogenetic column*.

Deeply influenced by the diversity of sources pointing to a vertical bias in the microstructure of the isocortex, Mountcastle presented his hypothesis on the columnar organization of neocortex in an influential essay entitled *"An organizing principle for cerebral function: the unit module and the distributed system"* (Mountcastle 1978). In his proposal, the cortical column was described as a large processing and distribution unit

with diameters of 500-1000μm, with the potential to represent many variables submapped in irreducibly smaller units, the minicolumns. Many neuroscientists have adopted this hypothesis as a comfortable axiom from which interpreting cortical function (Markram et al. 2015). As already mentioned, several variables can be distributed in a columnar fashion within cortical circuits, particularly in sensory areas where the topographic organization of ascending inputs may become a major determinant, but also in motor and association domains (Goldmann and Nauta 1977, Georgopoulos et al. 1982 and 2007).

Others interpret cortical modularity not as a functional unifying principle, but as an epiphenomena imposed by morphological and developmental constraints, and not necessary following a columnar fashion (Purves et al. 1992, Horton and Adams 2005). The iso-oriented columns of primary visual cortex of cat (Hubel and Wiesel 1963) and macaque (Hubel and Wiesel 1968, Blasdel GG 1992) have been claimed not to exist in the rodent brain, where neurons with different orientation tuning to visual stimuli are intermingled, following the so-called *salt and pepper* distribution (Lee et al. 2016, but see Ringach 2016). The horizontal expansion of dendritic and axonal arbours of the many cellular constituents of the cortical circuit can surpass the proposed extension of the theoretical column, contributing to the formation of cortical representations that exceed the vertical bias (Narayanan et al. 2015). Indeed, it has been argued that the contribution of neuronal input arising from the surrounding (external to the putative column) quantitatively dominate the *columnar* connectivity (Boucsein et al. 2011)

Additionally, Mountcastle's initial proposal also included the universality of the columnar function, this is, that cortical columns across cortical areas and species had the same function. In a recent formulation of his ideas, this point was totally rejected: *"...the processing chains are not everywhere identical [...] the differences in afferent input are*

convolved with different intrinsic operations in different cortical areas to produce what we call different functions" (Mountcastle 2003).

The debate between those focusing in the variability (*splitters*) and those supporting the universality of the cortical processing (*lumpers*) is still on (Nelson 2002). In my opinion, it seems obvious that some general rules may apply to the organization of cortical circuits. In line with this, Douglas and Martin have proposed the existence of a *canonical circuit* for the isocortex (Douglas & Martin, 2010), a term which has been widely adopted, and intelligently skips the anatomical limitations of the columnar hypothesis. Of course, this is not to say that functional diversity has not imposed some degree of circuit specialization (as an example of the divergent organization of different cortical areas see Watkins et al. 2014). I will discuss the general plan of local cortical circuits in the following section.

The neighborhood: local circuits in the isocortex

When studying local cortical circuits, there are two immediate issues that seem *easily* resolvable, the first regarding the diversity of cell types and the second, which relays on the first, the hodological relationship between them. Diversity can be studied according to several rules (morphological traits, genetic/transcriptomic analysis, molecular marker expression, electrophysiological properties, input/output organization…). An exhaustive consideration of all these properties can lead to the useless conclusion that each neuron is one cell-type. Despite the existence of intralayer diversity, a reasonable starting point for the hodological analysis of the cortical local circuits is layer identity. I will first consider the excitatory population.

An excitable skeleton: pyramidal connectivity in local circuits

Fueled by the work of Hubel and Wiesel, the cat visual cortex initially became the model system to study the intrinsic organization of local cortical circuits (for a relatively recent study in this area see Bizegger et al. 2004). Other primary sensory regions have also received strong attention, particularly in rodents. The discovery of the fine somatotopy of the rodent whisker system (Woolsey & van der Loose 1970) explains why the barrel cortex of mice and rats became another preferred model for this type of studies. The introduction of the patch-clamp technique (Neher and Sackmann 1974), and its application to whole-cell recordings in acute cortical slices prompted the demonstration of synaptic connectivity between simultaneous recorded pairs or groups of neurons (Thomson et al. 1989). This technique has been extensively used in several cortical regions and species, greatly expanding our understanding of local cortical circuits (Deuchars et al. 1994, Markram et al. 1997, Thomson and Bannister 1998, Feldmeyer et al. 1999, Feldmeyer et al. 2002, Feldmeyer et al. 2006, Frick et al. 2008, Lefort et al. 2009, reviewed in Thomson and Lamy 2007).

Overall, these studies, agree in a general one-way processing thalamocortical pipeline for cortical local circuits, according to which, layer 4 spiny cells are directly thalamorecipient and their response properties are similar in many ways to those of their presynaptic thalamic relay cells. These neurons project to layers 2/3, where different response properties already emerge, and more complex stimuli are required to evoke a response. In turn, these superficial pyramidal neurons project back to layer 5 from where a highly processed signal is then sent out to other cortical and subcortical structures (Hirsch and Martinez 2006, Thomson and Lamy 2007). In addition, a dense recurrent circuit exist in each step, possibly for gain amplification.

Of course, this view is a simplification of the reality. As already mentioned, layers are not unified entities, and different pyramidal types exist within the boundaries of single layers. In layer 5, at least two main pyramidal types can be distinguished. Thin-tufted regular spiking pyramidal neurons with medium size somas, and intratelencephalic projections are intermingled with thick-tufted pyramidal neurons with large somas that project to extratelencephalic territories and typically fire bursts of action potentials (Molnár and Cheung 2006). Layer 6 contains corticothalamic, corticoclaustral and corticocortical pyramidal neurons (Thomson 2010), and their role within the cortical matrix is still poorly understood.

Furthermore, the complexity of local cortical circuits extends far beyond the relationships between different subtypes of pyramidal neurons. It is known that bidirectional connectivity between pyramidal cells is overrepresented, not only in terms of probability but also in terms of unitary EPSP amplitude (Song et al. 2005). Several studies show that connected pairs of pyramidal neurons tend to share their inputs from other sources, a feature that is not present, or at least in a lesser extent, in unconnected pairs, suggesting that within a cortical column, a set of partially segregated subnetworks coexist. There is evidence for the existence of such subnetworks in the L4 to L2/3 and L2/3 to L2/3 (Yoshimura et al. 2005, Ko et al. 2011, Morgenstern et al. 2016), the L2/3 to L5 (Otsuka and Kawaguchi 2008) and L5 to L5 pathways (Song et al. 2005). These subnetworks are not instated by physical proximity, as the axons and dendrites of neurons from different ensembles pass near each other with roughly equal probability to those forming functional connections (Lee et al. 2016). In the mouse visual cortex, connection probability is elevated for neurons sharing orientation preference, and also for those responding similarly to natural movies (Ko et al. 2011). It has been suggested that this particular disposition may help to enhance cortical responses to a given input, minimizing

susceptibility to noise and prolonging responses, which in turn may facilitate the integration of high-order feedback or subsequent inputs (Harris and Mrsic-Flogel 2013).

Nonetheless, in my opinion, the major caveat of the serial model of columnar processing is that it does not fit with the dynamics of cortical responses. In a mouse barrel column, responses in some layer 5 pyramidal neurons to whisker deflections precede those evoked on superficial pyramidal cells, and show similar latencies to those in layer 4 (Constantinople and Bruno 2013, de Kock et al. 2007, Reyes-Puerta et al. 2014). Interestingly, *in vivo* pair recordings of thalamic and cortical neurons demonstrate an alternative thalamocortical pathway, with thalamic axons strongly targeting infragranular neurons, particularly in layer 5B thick-tufted pyramids (Constantinople and Bruno 2013). Moreover, inactivation of layer 4 with lidocaine suppressed sensory evoked responses in L4 and L2/3 but not in infragranular layers, where mean PSP amplitude and onset latencies were unaltered. These observations suggest the existence of a parallel loop of thalamocortical processing bypassing superficial layers (L2-4).

Sculpting cortical activity with inhibition

Functional units in the mammalian central nervous system are never built exclusively with excitatory cells. Positive feedback systems, such as a recurrent network of pyramidal neurons, are intrinsically unstable. Cortical inhibition imposes gain control (Isaacson and Scanziani 2011, Atallah et al. 2012), increasing the dynamic range of the network by reducing the size of the active pool of neurons in response to any biologically relevant circumstance. In addition to this, the existence of a balance between synaptic excitation and inhibition enhances the temporal resolution of the spiking activity of the pyramidal cells (Pouille and Scanziani 2001). Therefore, the existence of inhibition increases the spatial and temporal resolution of the neocortical network. Moreover, inhibition has been

demonstrated to be necessary to generate many of the rhythms shown by the neuronal activity in the cortex (Sohal et al. 2009, Stark et al. 2013, reviewed in Bartos et al. 2007). Some argue that these oscillations control the transmission of information across distal areas. In this sense, regional synchronization has been proposed as a mechanism to explain the unity of sensory experience (Mioche and Singer 1989, Gray et al. 1989). Given the fundamental implications of inhibitory neurons in cortical function, it is necessary to understand the architecture of these circuits.

Inhibition in cortical circuits is mainly provided by local-projecting gabaergic neurons. Despite only 15-20% of cortical neurons are inhibitory cells (Lee et al. 2010, Xu et al. 2010), the contribution of these neurons to the synaptic activity of the cortex is quantitatively more relevant than it may seem. Several factors compensate for their relative scarcity: (1) the connection probability between pyramidal and inhibitory neurons is higher, in both directions, than among pyramidal neurons (Avermann et al. 2012), (2) the strength of the unitary pyramidal to inhibitory neuron connection, at least for some types of interneurons, is larger than among pyramidal neurons (Hull et al. 2009). Then, even with weak excitatory input, inhibitory neurons can be recruited, and excitatory synaptic conductances on cortical neurons are almost synchronically counterbalanced by inhibitory input (Gabernet et al. 2005).

Classical Golgi studies revealed the existence of many morphological types of interneurons. Molecular, morphological and physiological properties have been combined to categorize this large diversity (Kawaguchi and Kubota, 1997; for review see Markram et al. 2004; Petilla group 2008, Fishell and Rudy 2011). In a recent study, parvalbumin (PV), somatostatin (SST) and the ionotropic serotonin receptor 5HT3a were shown to label three non-overlapping population of cells corresponding to the entire population of gabaergic interneurons in the mouse barrel cortex (Lee et al., 2010). PV+

cells (~40% of the whole gabaergic population) and SST+ (~30%) neurons are relatively more abundant on deep layers (L4 to 6), while 5HT3aR cells (~ 30%) dominate in superficial ones (L1 to 3). This seems to be a general landmark of cortical circuits as it also applies to frontal and visual areas (Xu et al. 2010).

Nonetheless, within each one of these three non-overlapping classes, further diversity exists. PV-FS interneurons include perisomatic targeting large and small basket cells and axoaxonic chandelier cells (Markram et al. 2004, Petilla group 2008), all of them sharing a fast-spiking firing pattern, with narrow spikes, large afterhiperpolarizations, high maximal firing frequencies and minimal firing frequency adaptation during sustained depolarization. Within the SST+ neurons, the Martinotti cell is the prominent cell type, but a diversity of SST+ interneurons with different morphological, electrophysiological, genetic and laminar distribution properties have been described (Ma et al. 2006). 5HT3aR+ cells are less characterized. Among them, VIP cells are often bitufted or bipolar with an irregular or fast-adapting firing pattern. Among non-VIP 5HT3aR neurons, reelin expressing cells are the majority and include neurogliaform or multipolar cells with late-spiking firing patterns (Fishell and Rudy 2011).

A fundamental question is whether inhibitory cells establish fine-scale subnetworks with their targets. An *a priori* requirement for specific connectivity is the existence of a low connection probability between local random pairs of neurons, which is the case for local pyramidal pairs, but pyramidal PV-FS/SST pairs show high connection probabilities in both ways (Avermann et al. 2011, Fino and Yuste 2011, for examples of PV-FS and SST to pyramidal connectivity, respectively). Accordingly, the responses of gabaergic neurons tend to reflect the pooled activity of the surrounding population (Kerlin et al. 2010, Bock et al. 2011). This implies that if there exists any kind of spatial segregation in the neuronal representation of a given variable, as is the case of

the orientation columns in cat primary visual cortex (V1), then a putative interneuron will maintain the sensory tuning of its environment. If differentially tuned neurons are intermingled, following a salt and pepper distribution, like in mouse V1, then the interneuron will be broadly tuned, or not tuned at all (Atallah et al. 2012). Despite some studies exist supporting the opposite scenario, according to which there is some kind of specific connectivity between pyramidal neurons and some types of interneurons (Yoshimura and Callaway 2005), the proposal of a dense and unspecific inhibitory connectivity matrix, with proximity as the major determinant of connectivity, is currently widely accepted (Fino and Yuste 2011, Packer and Yuste 2011) .

In agreement with this hypothesis, the main source of inhibitory input to the average pyramidal cell are gabaergic cells from the same layer (Kätzel et al. 2011). Nevertheless, the existence of interneurons whose axons travel across layers is well documented. A recent report indicates that in mouse primary visual cortex, layer 6 corticothalamic neurons recruit deep PV-FS interneurons whose axons ramify through the entire depth of the cortex, suppressing cortical responses in a columnar manner (Bortone et al. 2014). In primary visual and somatosensory areas, but not in primary motor cortex, some pyramidal neurons received the majority of their inhibition form other layers (Kätzel et al. 2011). In addition, columnar interlaminar excitatory pathways such as the dense L2/3 to L5 or the L4 to L2/3 projections, not only provide excitation to principal neurons but also to interneurons (Helmstaedter et al. 2008, Apicella et al. 2012).

On top of inhibitory-to-excitatory neuron interactions, interneurons also establish recurrent connections. PV-FS cells powerfully inhibit other PV-FS neurons while providing weak inhibitory input to non-PV-FS interneurons, and SST interneurons avoid each other but strongly inhibit all other interneurons populations (Pfeffer et al. 2013). In contrast, the VIP-expressing population is known to avoid pyramidal cells. Apparently,

their main postsynaptic partners are SST neurons (Pi et al. 2013; Lee et al. 2013; Pfeffer et al. 2013). Interestingly, these population seems to fire in response to feedback information such as reinforcement signals (Pi et al. 2013) or to motor feedback during active whisking (Lee et al. 2013), therefore creating a desinhibitory loop that facilitates the generation of plastic associations on pyramidal cells.

Beyond the neighborhood: long-range connectivity in isocortical circuits

If the description of the high-dimensional local circuit of a 500µm-width cortical column is already a scientific challenge, the task becomes much more difficult when the neocortical interareal connectivity is considered. In contrast to other brain areas such as the cerebellum or the superior colliculus, the isocortex is a highly distributed circuit, with distal regions strongly interacting between them (Felleman and Van Essen 1991). As stated previously, this long-range connectivity depends on the projections arising from medium-size pyramidal neurons in superficial and deep layers, including layers 2, 3, 5 and 6.

A prominent principle of cortical architecture is the existence of a regional hierarchy (Felleman and Van Essen 1991). In some degree, this feature resembles the organization of the information flow in a (sensory) cortical column discussed before. Layer 4 spiny cell responses where in many ways similar to the responses of sensory thalamic relay neurons and as the information flow *advances* within the column, specific neuronal representations appear diverging from those typical from the initial stages. The classical model to study the regional cortical hierarchy has been the macaque visual cortex. The hierarchy is reflected by the receptive field properties of neurons in each area: neurons in the primary visual cortex show preferences for very simple and spatially restricted features like oriented lines, whereas neurons in higher areas respond to more

complex stimulus aspects such as objects, irrespective of their size or orientation. This scheme goes beyond specific sensory modalities, as areas exist that integrate different sensory modalities (multimodal association areas). On the top of the hierarchy, the prefrontal cortex, a group of executive regions, is in charge of selecting behavioral plans according to the incoming highly processed sensory information and, importantly, according to the individual experience (Fuster and Bressler 2014).

The existence of a hierarchical processing architecture does not imply that a strictly serial stream applies. Cortical computations advance in parallel and are highly reciprocal, with *higher* areas projecting back to *lower* ones. In the primate cortex, forward (or bottom-up) projections tend to originate in superficial layers and terminate in layer 4 (resembling the sensory thalamocortical input to primary sensory areas), while feedback (or top-down) connections arise both from deep and superficial layers but avoid layer 4 as their target (Felleman and Van Essen 1991). In rodents, evidence for hierarchical organization also exists, but its relation to lamination is less clear. In mouse visual cortex, feedback avoids L4 and cells giving rise to feedforward and feedback projections are not laminarly distributed but form segregated populations (Berezovskii et al. 2011). In the close future, a better understanding of the genetic mechanisms that explain the specification of distinct subclasses of pyramidal neurons with characteristic long-range cortical projections might provide a cellular explanation for inter-areal connectivity patterns.

It has been proposed that projections from higher to lower areas are of modulatory nature, shaping bottom-up determined receptive fields, according to behavioral states (Lamme et al. 1998). An alternative suggestive hypothesis states that within a loop between two cortical areas, the feedback projection transmits an elaborated prediction or a set of predictions, based on previous experience, of what is happening (of the causes of

the sensorium), while the lower region sends an error signal to update the prediction, or to select among the possibilities (Mumford 1992).

Regarding the synaptic organization of long-range interactions across cortical regions, two recent studies compare the synaptic properties of bottom-up and top-down pathways in the auditory and visual cortices in the rat (Covic and Sherman 2011, De Pasquale and Sherman 2011). The main conclusion is that similar response properties apply for the excitatory input in the forward (A1 to A2, V1 to V2) and feedback (A2 to A1 and V2 to V1) pathways. However, a different study indicates that in rat cortex, responses of V2 pyramids to V1 stimulation, the bottom-up pathway, show a excitation/inhibition balance much more favorable to inhibition than in the top-down direction, from V2 to V1 (Shao and Burkhalter 1996). Therefore, at least some projections arising in higher areas seem to be in position to exert a powerful influence on lower regions.

The callosal pathway

In placental mammals, both cortical hemispheres are strongly interconnected by a massive axonal bundle, the corpus callosum. Interhemispheric communication through this commissure is a general principle of the isocortex of these animals, as areas through the entire rostrocaudal axis, from lower sensory and motor regions to associational ones send and receive axons to and from the opposite hemisphere. Importantly, most callosal axons terminate on the homotopic region of the contralateral side, and therefore mediate reciprocal communication between homologous regions (Yorke and Caviness 1975), but heterotopic projections have also been reported (Mitchell and Macklis 2005, Decosta-Fortune et al. 2015). In contrast, monotremes and marsupials do not develop the corpus callosum, but a large anterior commissure instead, through which isocortical (also

paleocortical) neurons project to contralateral territories, at the cost of a longer distance and latency of this pathway. It has been proposed that corticocortical commissures developed in the mammalian brain to integrate the two topographic hemirepresentations of the sensory world which are segregated across hemispheres, the left sensory hemifield being displayed in the right brain hemisphere and *vice versa* (Aboitiz and Montiel 2003).

This hypothesis was initially based on studies in the cat visual system, where callosal fibers were shown to arise and terminate in the boundary between areas 17 and 18, where the vertical midline of the visual field is represented (Choudhury et al. 1965 referred in Hubel and Wiesel 1967). These studies demonstrated the role of visual callosal fibers in the formation of binocular receptive fields of visual cortical neurons, and therefore in depth perception (Blakemore et al. 1983). Similar ideas have been proposed to explain the role of callosal connectivity in other sensory systems, among them, sound localization in the auditory cortex and bimanual coordination for the somatosensory cortex. In both behavioral paradigms, coordination between sensory information initially restricted to contralateral equivalent areas is required for proper function. In this sense, it is not surprising that cortical somatosensory neurons with bilateral receptive fields are more abundant in the cortical territory representing the fingers than the toes (Iwamura 2000).

In addition to the integration of sensory information across hemispheres, callosal connectivity is also involved in the transfer of higher cognitive information, including attentional resources. During visual search tasks performed by human patients with complete callosotomy, each cortical hemisphere is able to independently scan their respective visual hemifield, indicating the existence of intrahemispheric attentional mechanisms that apparently fuse in one combined attentional spot in control subjects, whose callosum is intact (Luck et al. 1989). Moreover, some argue that the implication

of this pathway increases with the computational demand of the task, this is, that callosal transfer is enhanced during complex task resolution (Holtzman and Gazzaniga 1982). In relation to this, an independent and influential idea suggests the possibility that hemispheric lateralization emerged as a consequence of the reduction in the efficacy of interhemispheric transfer in larger brains due to increased conduction delays (Ringo et al. 1994). This idea relies in the observation that median callosal fiber diameter is conservative across species, and despite the maximal diameter tends to be higher in larger brains, this may not be sufficient to maintain a constant interhemispheric transmission time (Olivares et al. 2001).

Altogether, these evidence seems to support the role of the callosum as an integrative pathway across hemispheres. According to this *excitatory model*, callosal input allows the recruitment of contralateral ensembles therefore increasing the computational potential disposable to perform a given task. In fact, it has been demonstrated that callosal input is required to generate synchronous oscillations across contralateral areas (Engel et al. 1991). Nonetheless, in opposition to the excitatory model, it has also been shown that the activation of one hemisphere can induce the inhibition of the contralateral region (Hlushchuk and Hari 2006, Reis et al. 2007, Beaulé et al. 2012, Palmer et al. 2012). Accordingly, it has been proposed that callosal axons sustain competition between contralateral ensembles, leading to lateral dominance (for a review on these two opposed hypothesis of callosal function see Bloom and Hynd 2005, van der Knaap and Ham 2011).

Classical morphological and electrophysiological studies show that callosal projecting neurons are pyramidal neurons mainly located in layers 2/3, with a minor contribution from layers 5 and 6 (Yorke and Caviness 1975, Ramos et al. 2008) and that callosal axons densely innervate superficial and deep layers, avoiding the thalamo-

recipient layer 4 (Yorke and Caviness 1975, Mizuno et al. 2007, Wang et al. 2007). Contralateral targets of callosal fibers include not only different subtypes of pyramidal cells (Vogt and Godmann 1982, Kawaguchi 1992, Kumar and Huguenard 2001, 2003) but also inhibitory interneurons (Carr and Sesack 1998, Cissé et al. 2003, 2007, Karayannis et al. 2006, Petreanu et al. 2007), which in turn innervate local pyramidal neurons. Therefore, the effect of this cortical input on their postsynaptic targets will depend on the balance between the direct callosal excitation and the disynaptic inhibitory component (Kawaguchi 1992, Chowdhury and Matsunami 2002, Irlbacher and et al. 2007).

The lack of a detailed description of the connectivity diagram between CPNs and their contralateral targets is still a major limitation in our understanding of the functional role of the callosal transfer. Given the diversity of regions with reciprocal callosal connections, and the diversity of callosal projecting neurons, I expect the function of interhemispheric communication to be divers. Nevertheless, for each particular case, must be a microcircuit explanation for the final output of callosal transfer. The aim of our work is to study the influence of the CPNs on contralateral cortical microcircuits. Despite several attempts have been done to characterize the impact of CPNs on contralateral circuits (Karayannis et al. 2007; Palmer et al. 2012; Lee et al. 2014; Rock and Apicella 2015), so far, this is the first study considering the contribution of this pathway within the entire columnar extension of the contralateral cortex. For this, we have performed a detailed electrophysiological screening across different categories of pyramidal and gabaergic neurons in the retrosplenial cortex, a high-order association area involved in spatial cognition and context recognition (Wolbers and Buchel 2005, Smith et al. 2012, Czajkowski et al. 2014, reviewed in Vann et al. 2009). The selection of the retrosplenial

cortex as the model region responds to, again, a methodological consideration: in coronal cortical slices, callosal projections are best conserved in this area.

OBJECTIVES

In this project we aimed to characterize the contribution of superficial callosal projection neurons in the agranular retrosplenial cortex (RSC), focusing in the following objectives:

1. To unravel the connectivity diagram between callosal axons from superficial CPNs and pyramidal neurons in the contralateral homotopic cortex:
    - 1.1 To characterize the diversity of pyramidal neurons in the agranular RSC,
    - 1.2 To determine the laminar organization of the terminal arbors of callosal axons from superficial CPNs of the agranular RSC in the homotopic contralateral cortex,
    - 1.3 To determine the identity of the postsynaptic pyramidal targets of callosal axons from superficial CPNs in the agranular RSC,
    - 1.4 To determine the distribution of the inhibitory input recruited by callosal axons from superficial CPNs among the different pyramidal neuron subtypes of the agranular RSC;

2. To compare the synaptic mechanisms governing the integration of callosal input from superficial CPNs among the different contralateral postsynaptic targets.

MATERIAL AND METHODS

Ethical approval

Mice were maintained, handled, and sacrificed in accordance with national and international laws and policies (Spanish Directive "Real Decreto 1201/2005"; European Community Council Directive 86/609/EEC). The Ethical Committee for the Experimental Research of the Universidad Miguel Hernández approved the experimental protocols.

Morphological study of the mouse retrosplenial cortex

The cytoarchitecture of the mouse anterior retrosplenial cortex (-2.30 to -1.70 from Bregma) was studied with anti-NeuN immunohistochemistry in wild-type animals. The laminar distribution of parvalbumin cortical interneurons in this region was studied with anti-GFP immunohistochemistry in the Pvalb-Cre;RCE or with anti-PV immunohistochemistry in wild-type animals.

In each case, mice of either sex (3-4 postnatal weeks) were anesthetized with isufluorane and perfused with PFA 4% in PBS. Brains were removed and postfixed overnight in PFA 4% at 4ºC. 40 µm coronal sections were cut in the vibratome from agarose embedded brains. Floating slices were immunostained using the following antibodies: NeuN mouse monoclonal antibody 1:500 (MAB377/Chemicon); GFP rabbit polyclonal antibody 1:1000 (A 11122, Molecular Probes); GFP chicken polyclonal antibody 1:500 (GFP1020, AVES); PV rabbit polyclonal antibody 1:1000 (MAB388, Chemicon); goat antibody to mouse AlexaFluor594 1:500 (A 11032, Molecular Probes); donkey antibody to rabbit AlexaFluor488 1:500 (A 21206, Molecular Probes); goat antibody to chicken AlexaFluor488 1:500 (A 11039 Molecular Probes); donkey antibody to rabbit AlexaFluor594 1:500 (A 21206, Molecular Probes). Slices were prepared for

fluorescent microscopy in Mowiol4-88 (Sigma). Images were acquired in an upright confocal microscope (DM-5500, Leica Microsystems) with a 40x oil immersion objective using Leica Application Suite X (LASX) software.

In confocal z-stacks from NeuN-immunostained slices, representative cortical territories expanding through the whole cortical depth were processed with an automatized cell counting algorithim (Imaris® software) supervised visually. This allowed us to determine the neuronal density across a cortical column by the quantification of $NeuN^+$ somas in 50µm-depth segments. For the study of the laminar distribution of cortical interneurons, confocal z-stacks of the region of interest were analyzed using the image processing package ImageJ. Laminar boundaries were established with fluorescent nuclear DAPI dye (Sigma-Aldrich) counterstaining, and the number of labelled neurons in each laminar compartment was counted manually. Interneuron density per layer was computed as number of labelled neurons/area.

Callosal axon labeling by in utero electroporation

We used a green fluorescent protein (GFP) expressing plasmid (pCX-GFP) to label superficial CPNs by *in utero* electroporation. Plasmid DNA was purified using an extraction midi kit (NucleoBond® xtra midi, Macherey-Nagel). DNA was dissolved at a final concentration of 1µg/µl in milliqH_2O with 1% fast green. E16.5 pregnant dams (C57-BL6 strand) were anesthetized with isofluorane. The uterus was accessed via a 1.5cm incision of the abdominal wall, and individual embryos were injected through the intact uterine wall using glass microcapillaries under a fiber optic light source. After electrodes were placed strategically, 5 pulses of 40V current of 50ms duration were applied at intervals of 950ms using an electroporator (Square Wave model CVY21SC, Nepa Gene). The surgical incision was sutured and mice were administered a single

subcutaneous injection of 0.1mg/kg buprenorphine analgesic (Buprex®, Schering Plough), and then orally with 0.03mg of buprenorphine per food pellet. Electroporated mice at 3-4 postnatal weeks were anesthesized with isufluorane and perfused with PFA 4% in PBS. Brains were removed and postfixed overnight in PFA 4% at 4ºC. 40µm coronal sections were cut in the vibratome from brains embedded in agarose. Immunohistochemistry to GFP was performed in floating slices with GFP chicken polyclonal antibody 1:500 (GFP1020, AVES) and goat antibody to chicken AlexaFluor488 1:500 (A 11039 Molecular Probes).

Slice preparation

Brain slices of neocortex were prepared from mice of either sex (C57-BL6 strand; 18-21 postnatal days). Animals were killed by cervical dislocation and their brains were quickly excised and submerged in ice-cold low Ca^{2+} / high Mg^{2+} cutting solution (composition in mM: NaCl 124, KCl 2.5, $NaHCO_3$ 26, $CaCl_2$ 0.5, $MgCl_2$ 2, NaH_2PO_4 1.25, glucose 10; pH 7.4 when saturated with 95% O_2 + 5% CO_2). Coronal slices (350 µm thick) were cut using a vibratome (Leica VT-1000; Germany) and transferred to a glass beaker, in which the tissue was submerged in artificial cerebrospinal fluid (ACSF; composition in mM: NaCl 124, KCl 2.5, $NaHCO_3$ 26, $CaCl_2$ 2, $MgCl_2$ 1, NaH_2PO_4 1.25, glucose 10; pH 7.4 when saturated with 95% O_2 + 5% CO_2) at 34°C for 30 min. The slices were stored submerged in ACSF for at least one hour at room temperature before recordings were made. One slice at a time was transferred to a submersion-type recording chamber, and kept at 32–34°C during the recording period. The ACSF used to bath the slices was fed into the recording chamber at a rate of 2-3 $ml \cdot min^{-1}$ and was continuously bubbled with a gas mixture of 95% O_2 + 5% CO_2.

Stimulation of superficial CPNs

Slices were stimulated with a concentric bipolar electrode (CBAFC75, Frederick Haer & Co, USA) connected to a stimulus isolator unit (A365, WPI) and placed on layer 2/3 of the homotopic contralateral cortex with respect to the recording region. Integrity of the projection was assessed by extracellular recordings prior to intracellular experiments (see example in figure 1, results section). Unless otherwise mentioned, single pulses (stimulus intensity 50-800μA, 0.1ms) were applied at a frequency of 0.2Hz to elicit AP firing in superficial CPNs contralateral to the recording site.

To evoke putative unitary synaptic responses, this is, single-axon responses, we used a minimal stimulation protocol. This method consists in setting the lower stimulus intensity in which responses to contralateral stimulation appear with a success rate of ~ 50%. A typical experiment starts with a stimulus intensity below threshold and is increased successively is steps of ~10μA until a clear response is reliably evoked, stage at which the intensity is re-set to evoked positive responses with a success rate of ~50% by reducing the stimulus intensity in steps of 1-5μA. Exclusion of possible compound responses is performed off-line under visually inspection when discontinuities in the slope of the rising phase or changes in the peak amplitude of the response are observed. For putative unitary EPSCs, strong jitter (>few tenths of milliseconds) is also considered as an exclusion criteria, but not for putative unitary IPSC, which disynaptic nature increases their temporal degrees of freedom.

Intracellular recordings

Somatic whole-cell recordings from neurons located all across the cortical depth of the anterior part of agranular RSC cortex were made under visual control using an upright microscope (Olympus BX50WI) equipped with Nomarski optics and a water immersion

lens (40x). Recordings were obtained in current-clamp or voltage-clamp mode with a patch-clamp amplifier (Multiclamp 700B, Molecular Devices, USA). No correction was made for the pipette junction potential (which was estimated to be about −10 mV using the junction potential calculator included in the pClamp software). Voltage and current signals were low-pass filtered at 2-4 kHz and digitized at 20 kHz with a 16-bit resolution analog to digital converter (Digidata 1322A, Axon Instruments). The generation and acquisition of pulses were controlled by pClamp 9.2 software (Axon Instruments). Patch pipettes were made from borosilicate glass (1.5 mm o.d., 0.86 mm i.d., with inner filament) and had a resistance of 4–7 MΩ when positive pressure was applied.

Current-clamp experiments were performed with an intracellular solution containing (in mM): 130 K-gluconate, 5 KCl, 5 NaCl, 5 EGTA, 10 HEPES, 2 Mg-ATP, 0.2 Na-GTP, 0.01 AlexaFluor594; pH 7.2 adjusted with KOH; 285–295 mOsm). Voltage-clamp recordings were performed with an intracellular solution containing (in mM): 135 Cs-methanesulfonate, 10 NaCl, 5 EGTA, 10 HEPES, 2 Mg-ATP, 0.2 Na-GTP, 0.01 Alexa Fluor 594; pH 7.2 adjusted with CsOH; 285–295 mOsm. The theoretic Nernst equilibrium potentials for the K-based internal solution were (in mV): E_K=-105.7, E_{Na}=89.3, E_{Cl}=-68.5). The theoretic Nernst equilibrium potentials for the Cs-based internal solution were (in mV): E_{Na}=71.4, E_{Cl}=-68.5.

Current clamp recordings were performed at the resting membrane potential of the neuron. Series resistance (Rs) was measured and balanced on-line under visual inspection assisted by the Bridge Balance tool of Clampex software. Rs was monitored at the beginning and at the end of each protocol, and re-balanced if needed. Cells in which Rs>40MΩ were discarded (typical Rs<25MΩ).

For voltage clamp experiments, EPSCs and IPSCs were recorded with holding potentials of -70 and 0mV, the measured reversal potential for the inhibitory and

excitatory synaptic currents, respectively. Neurons in which Rs>30MΩ were discarded (typical Rs was between 10-25MΩ). The error in the measure of the membrane potential (Ve) was computed as Ve = Ihold·Rs; Ihold stands for the holding current needed to set the holding potential (Vh). To hold the cell at the desired membrane potential (Vm), we set Vh = Vm + Ve. Quantification of intrinsic membrane properties and synaptic responses was performed on Clampfit10.3.

Analysis of intrinsic membrane properties and synaptic responses

Intrinsic membrane properties were analyzed in Clampfit10.3 from recordings of the voltage responses to 1.5s rectangular current pulse injections of different amplitudes (starting at -300pA, 30pA steps) (figure M1). Resting membrane potential (V_{rest}) was measured as the average potential of a 5 seconds time window just after giga-seal rupture. Neurons were discarded if V_{rest}>-55mV. Membrane resistance (R_m) was computed from the slope of the linear fit from steady state voltage responses to low intensity current square steps (figure M1A-B). Membrane time constant (τ_m) was estimated form the exponential fit of the voltage response to a hyperpolarizing current step of less than -100pA or as the time at which the change in the membrane potential (ΔV_m) reached 67% of the steady state potential (V_{ss}) from the response onset (t_o) (figure M1C). The voltage sag (V_{sag}) was calculated from the voltage response to a -300pA square current injection as $V_{sag} = (V_{peak}-V_{ss})/V_{peak}$ (figure M1D).

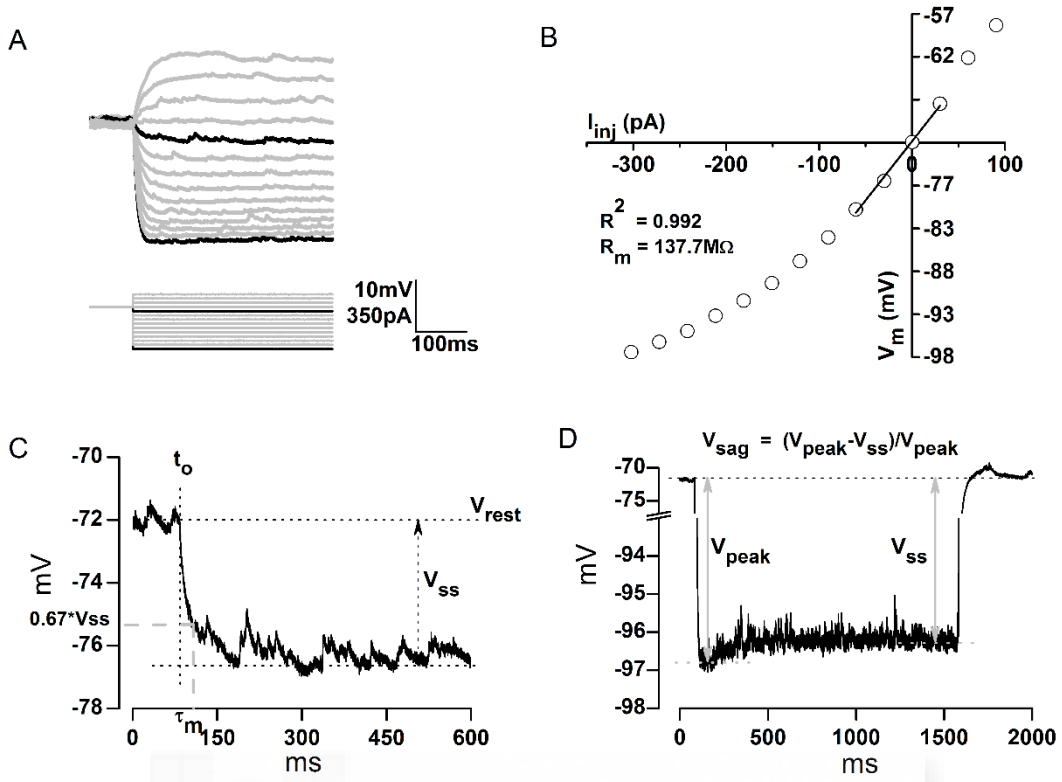

Figure M1. Analysis of passive electrophysiological properties of a recorded neuron. A. Example of the voltage responses of a superficial pyramidal neuron (upper panel) to the injection of square current pulses of increasing amplitude at 30pA steps (lower panel). Notice that the signals are truncated after 500ms (pulse duration 1500ms). B. IV curve from responses in A. Membrane resistance was compute as the slope of a linear fit of the region in which linearity was conserved (black line). Notice that the resting potential for this neuron is -72mV. C. Measure of the membrane time constant (τ_m). The response to the smallest hyperpolarizing pulse (-30pA) was employed. D. Measure of the voltage sag (V_{sag}). The response to a -300pA pulse was employed. Notice that V-axis is truncated.

AP properties were measured in the first action potential fired by the first suprathreshold depolarizing current injection (figure M2). Action potential peak amplitude (AP_{amp}) was measured from the AP threshold (AP_{thres}) to the AP peak (AP_{peak}). The AP_{thres} was measured at the abrupt slope change in the depolarizing phase under visual inspection and the AP width (AP_{width}) was measured at half amplitude. The firing frequency was measured as the average AP frequency in response to a 600pA depolarizing square pulse. An accommodation index (flast/f2) of the firing frequency was computed

as the ratio between the last and the second interspike interval in response to a 600pA depolarizing square pulse.

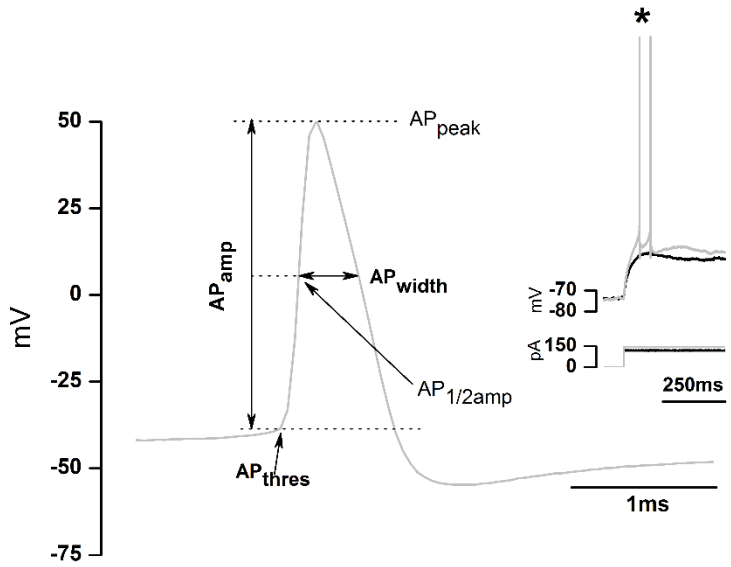

Figure M2. Analysis of action potential properties. Example of the first AP evoked in a superficial pyramidal neuron by intracellular injection of depolarizing rectangular current pulses and the measurement of its properties. The inset shows the first response at which the neuron fires (red trace) and the previous one at which AP threshold was not reached (black trace). The asterisk indicates the spike shown expanded in the main panel.

For synaptic responses (PSPs, EPSCs and IPSCs), peak amplitude, area, rise time (from 20 to 80% of peak amplitude) and decay time (from peak to half amplitude) were computed from the average trace of at least 10 sweeps with the Statistics tool of Clampfit 10.3 (figure M3). Latency was determined as the time difference between the onset of the stimulus artifact and the time point at which the amplitude of the response reached the 20, 50 or 80%, as indicated in the text.

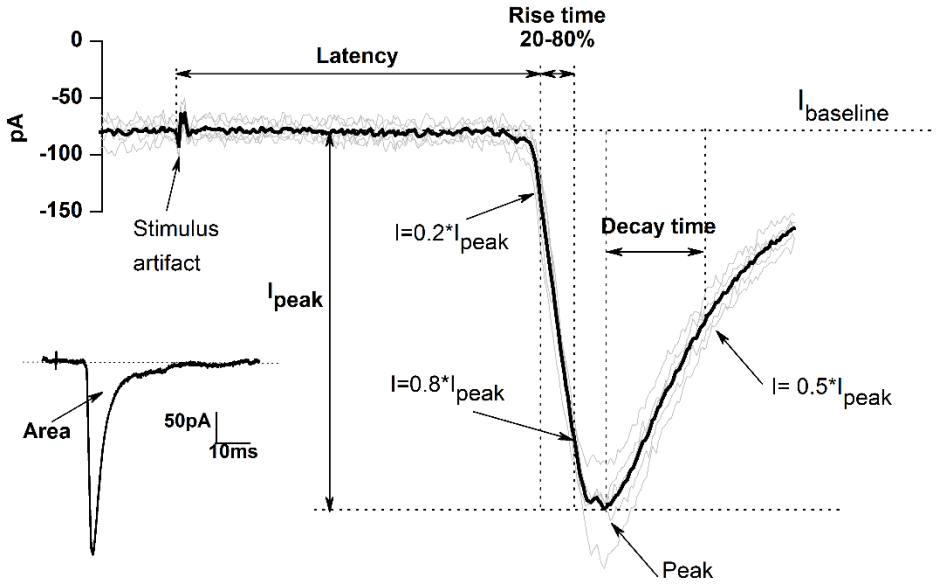

Figure M3. Analysis of synaptic properties. Example of an excitatory postsynaptic current recorded in a layer 2/3 pyramidal neuron in response to the contralateral stimulation of superficial layers. Latency, rise time, decay time and peak amplitude (I_{peak}) measurements are exemplified in the main panel. All measurements were done on the average of 10 responses (red trace in the main panel). The inset in the left represents the same response shown in the main panel to demonstrate complete $I_{baseline}$ recovery and EPSC area measurement (area delimited in between the average trace in red and $I_{baseline}$). Gray traces in the main panel are individual responses.

Neuron-type identification

Recorded cells were identified as pyramidal neurons by intracellular labelling with the fluorescent dye AlexaFluor 594, which was added to the recording solution. These neurons showed a characteristic pyramidal soma and a dominant apical spiny dendrite oriented to layer I while basal dendritic arbors were tangentially oriented (see examples in figure M4). In addition, pyramidal neurons were assignated to one of the following groups, according to laminar identity and size: layer 2/3, when their soma was above 300µm from pia; layer 5A, if the soma was below 300µm from pia and before the presence of large pyramidal neurons in layer 5B large; layer 5B large pyramids (see figure 1C results section, lower panel in the left); layer 5B medium-size pyramids, sorrounded by the previous ones; and layer 6 pyramids, below layer 5B large ones.

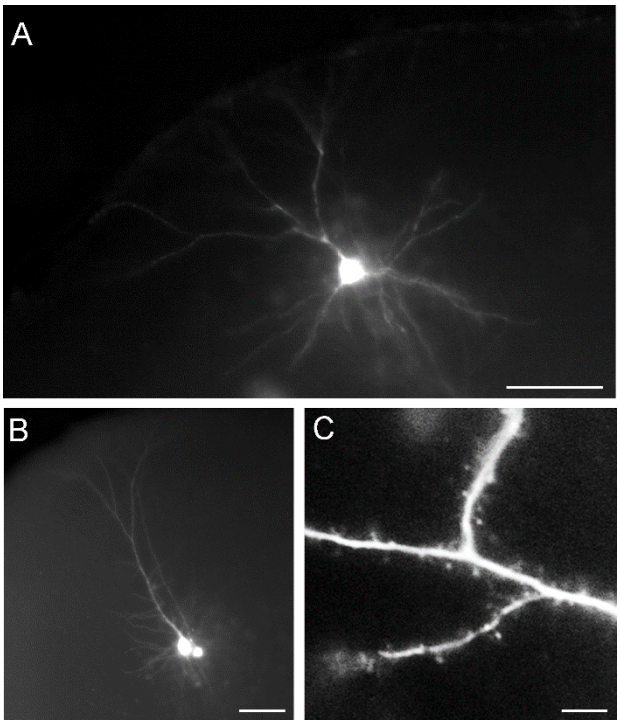

Figure M4. Morphological identification of pyramidal neurons. A. Example of a pyramidal neuron from layer 2/3 of the aRSC labeled intracellularly with AlexaFluor594 observed after patch clamp recording. B. A pair of L5BL and L5Bm pyramidal neurons simultaneously recorded. C. Detail of the apical dendrite of a layer 5 pyramidal neuron in which dendritic spines are clearly seen. Scale bars 40, 80 and 6µm, respectively.

Parvalbuming-expressing fast spiking interneurons (PV-FS) were identified by their characteristic spiking pattern, briefly, tonic discharges of narrow action potentials with little accommodation and large afterhiperpolarization in response to suprathreshold square current pulses. To increase the probability of patching PV-FS interneurons, we used the Pvalb-Cre;RCE mouse in which PV-expressing neurons are labeled with GFP. These animals were made by crossing Palvb-Cre mice (Hippenmeyer et al. 2005) with the Cre-dependent EGFP reporter line RCE;FRT (Sousa et al. 2009); or the GAD67-GFP line (Tamamaki et al. 2003), in which all types of gabaergic interneurons are labeled with GFP. Non PV-FS neurons were identified as GFP+ neurons from the GAD67-GFP line lacking the typical properties of FS cells.

Statistics

Data are given as the mean ± standard error of the mean (s.e.m.), and the number of cases, unless otherwise indicated. For comparison of the distribution of one variable among two non-paired samples, the two-tailed Mann–Whitney rank sum test was employed. In the case of neuron pairs recorded either simultaneously or sequentially (for the latter case, the position of the stimulus electrode and the intensity was kept constant), the two-tailed Wilcoxon signed rank test was employed. For comparison of proportions among two samples, the two-tailed Z-score test for two population proportions was employed. For linear correlation among two variables, the Pearson correlation coefficient was computed. For analysis of variance across more than two samples, the one-way ANOVA test was employed. If significant (p-value < 0.05), Bonferroni post-hoc corrections were applied. Statistical analysis were performed on OriginPro8 (Origin Lab Corporation) and Sigma Stat 3.11 (Systat Software Inc.). The degree of statistical significance is indicated by * ($p < 0.05$), ** ($p < 0.01$) or *** ($p < 0.001$).

RESULTS

PART 1. A transhemispheric subnetwork formed by superficial and large bursting pyramidal neurons from upper layer 5B in the retrosplenial cortex of the mouse

Coronal slices including the anterior region of the RSC maintained the integrity of the callosal pathway across hemispheres. Synaptic responses sensitive to the AMPA antangonist CNQX 40μM were evoked in the agranular RSC by the electrical stimulation of the superficial layers of the contralateral homotopic cortex (figure 1). This allowed us to study the physiology and connectivity of callosal synapses in retrosplenial cortical circuits.

However, given the symmetry of the callosal projection, electrical stimuli applied to layer 2/3 could also stimulate antidromically contralateral neurons projecting to the stimulus site, therefore making possible that the evoked postsynaptic responses were a mixture of contralateral (callosal) and ipsilateral inputs. To assess the contribution of this non-desired source of synaptic input, we quantified the ratio of contralateral pyramidal neurons in which antidromic spikes were evoked. Antidromic spikes were easily identified as low latency jitter, all-or-not action potentials arising directly from the resting membrane potential (see an example in figure 1E and compare with ortodromic spikes in figure 4D). In our sample of layer 2/3 neurons, where most CPNs are located (Fame et al. 2011), antidromic responses were quite uncommon: with stimulus intensities of 100 μA we observed antidromic spikes in 1 out of 92 neurons; with 200μA in 2/90 neurons, and with 500μA in 6/76 neurons. In the pyramidal neurons recorded in deeper layers we never recorded an antidromic spike. This very low proportion of neurons showing antidromic spikes indicated that in our experimental conditions, and at least when using stimuli of low and medium strength (100-200μA), we stimulated mainly the soma of ipsilateral CPN

neurons and not the axons of contralateral neurons and therefore the observed synaptic responses were mostly induced by callosal input, being minimal the contribution of local synapses activated antidromically.

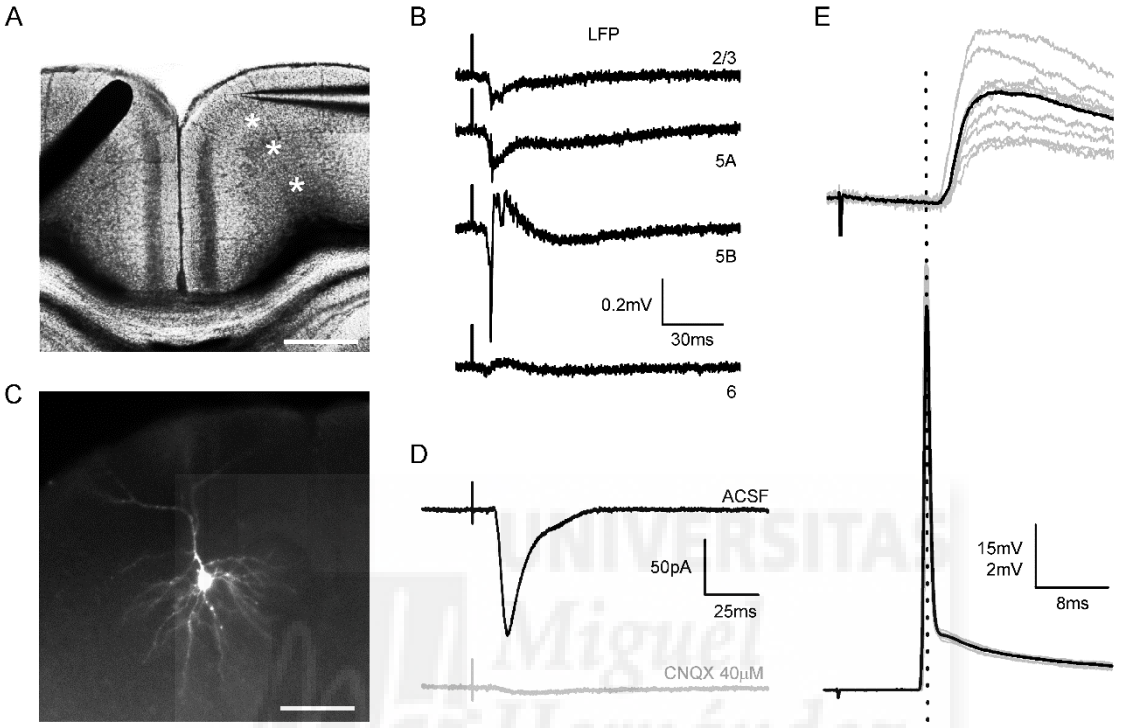

Figure 1. Coronal slices conserving callosal connections. A. DIC micropotograpth of a cortical slice containing the anterior part of the RSC and showing the position of the stimulus electrode (left) on the superficial layers of one hemisphere and a recording pipette (right) in the contralateral homotopic region. Scale bar 450µm. B. Local field potential (LFP) recordings in layers 2/3, 5A, 5B and 6 (sites marked with asterisks in panel A) in response to contralateral stimulation (each trace is the average of 10 consecutive responses). C. A layer 2/3 pyramidal neuron observed by fluorescence microscopy after intracellular staining with AlexaFluor 594. Scale bar 50µm. D. Postsynaptic current evoked in the pyramidal neuron from C (stimulus intensity 200µA) with the stimulus configuration shown in A. Notice that the application of the AMPA receptor antagonist CNQX (40µM) blocked the response (gray trace). Each trace is the average of 10 responses. E. PSPs evoked in a superficial pyramidal neuron by a 400µA stimulus (upper panel). Increasing the stimulus intensity to 500µA evoked an antidromic spike (lower panel). Gray traces are successive responses and the black trace is the average.

Pyramidal neurons diversity in the agranular retrosplenial cortex

We divided the agranular retrosplenial cortex (RSC) in 5 layers (1, 2/3, 5A, 5B and 6) according to changes in neuronal density measured by neuron soma counts in NeuN stained slices (Fig. 2A-B). This laminar distribution is in agreement with previous cytoarchitectonic studies on the mouse RSC, including the fact that in the mouse anterior agranular RSC, layer 4 is almost undetectable (Vogt and Paxinos 2012). Recorded neurons were assigned to one of these layers according to the criteria described in methods. Medium-size regular spiking neurons with spiny vertically oriented apical dendrites (see example in figure 1C and M4) were recorded all through layers 2-6. These neurons responded with adapting trains of action potentials in response to suprathreshold current pulses (figure 2D) and were considered as pyramidal neurons. Layer 5B also contained large pyramidal neurons (figure 2C); therefore, we grouped pyramidal neurons in five categories: L2/3, L5A, L5B medium-size (L5Bm), L5B large-size (L5BL) and L6 pyramidal neurons. A summary of the intrinsic properties of these neurons is given in tables 1 and 2.

L5BL pyramidal neurons were clearly different from the rest, and showed the typical properties of extratelencephalic projecting neurons (Mólnar and Cheung, 2006): large somas, a low membrane input resistance, a large voltage sag in response to somatic injection of hyperpolarizing current pulses and a tendency to fire bursts of action potentials (figure 2D-E). Despite the similarities among the medium-sized regular spiking pyramids, those from layer 2/3 were more hyperpolarized at rest and had a smaller voltage sag than those in layer 5 (see table 1); these differences were statistically significant ($p<0.05$ in both cases) and this fact allowed as to set the limit between layer 2/3 and 5A at 300µm from the pia. L5A and L5Bm pyramidal neurons had similar intrinsic electrophysiological properties (therefore they are grouped together in tables 1 and 2 as

L5m pyramidal neurons), while L6 pyramidal neurons show an intermediate profile, with an hyperpolarized resting potential, like superficial ones, but larger voltage sag in response to -300pA current steps, like those in layer 5. Overall, this is the general scheme of pyramidal organization across layers described in other neocortical regions (Connors and Gutnick, 1990).

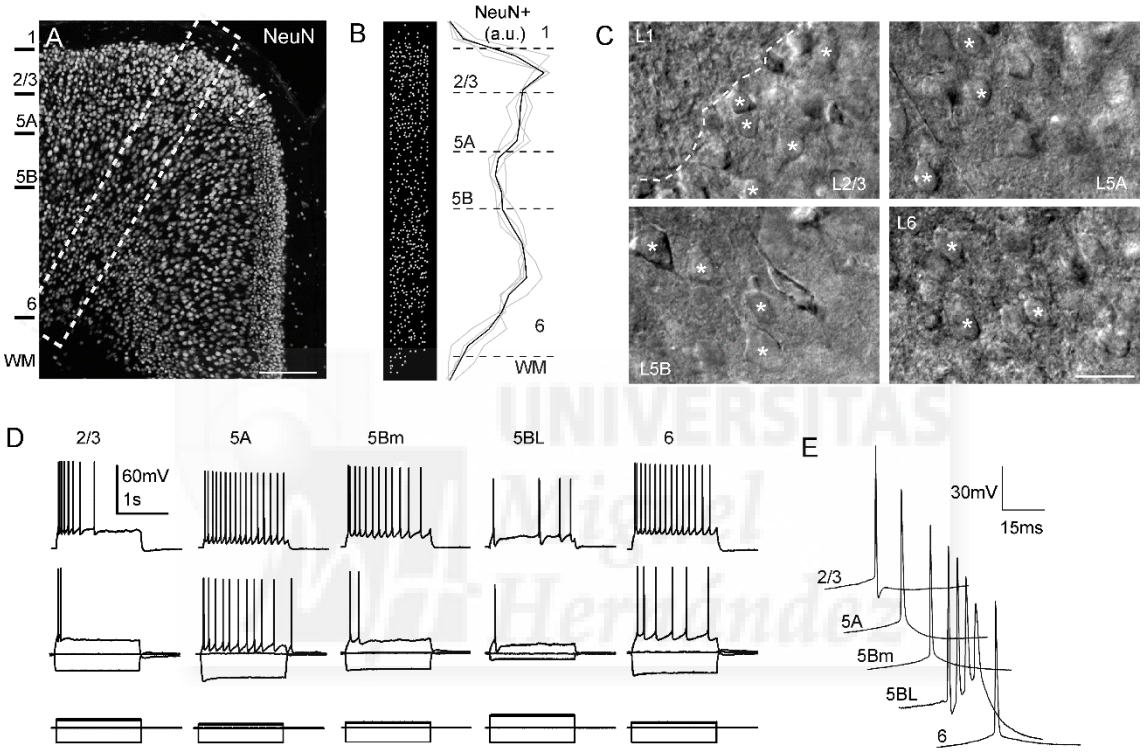

Figure 2. Pyramidal neurons in the agranular RSC. A. Confocal z-stack image of the anterior RSC immunostained for the neuronal marker NeuN. The short discontinuos line indicates the limit between the agranular RSC (aRSC, dorsal) and the granular RSC (gRSC, ventral). B. Left, Imaris reconstruction of the position of NeuN+ somas from neurons in the columnar inset shown in A (546 NeuN+ cells); right, NeuN+ cell density across an aRSC column measured with a 50μm bin width (n=7 slices from 4 mice; selected columns were 300-400μm wide, mean number of NeuN+ cells per column: 466). Grey traces represent individual cases and the black trace the mean. C. DIC micropotographs of the agranular RSC in a slice placed in a recording chamber. Notice the presence of large pyramidal somas in L5B but not in layers 2/3, 5A and 6. D. Membrane voltage responses from a L2/3, L5A, L5Bm, L5BL and a L6 pyramidal neuron to 1500ms current pulses. Responses were recorded at resting membrane potential ($I_{holding}$ = 0 pA). E. First action potential from the first suprathreshold response shown at larger scales. Scale bars 250 and 20μm in A and C, respectively.

Table 1. Subthreshold electrophysiological properties of pyramidal neurons in the agranular RSC

	n	Age (days)	Distance to pia (µm)	Vrest (mV)	Rm (peak) (MΩ)	Vsag	τm (ms)
Pyr 2/3	25	19,2 ± 1,1	190,6 ± 33,0	-75,5 ± 4,1	166,4 ± 55,0	0,04 ± 0,03	22,6 ± 7,7
Pyr 5m	26	19,9 ± 1,4	396,0 ± 71,5	-65,2 ± 5,4	211,7 ± 67,6	0,11 ± 0,06	21 ± 4,9
Pyr 5BL	21	19,4 ± 0,9	547,2 ± 71,1	-65,7 ± 2,2	46,9 ± 13,2	0,25 ± 0,04	11,8 ± 2,0
Pyr 6	17	19,5 ± 0,8	941,6 ± 114,5	-72,7 ± 5,2	215,0 ± 62,7	0,16 ± 0,05	15,9 ± 4,1

Pyr 5m stands for 5A (n=18) and 5Bm (n=8) pyramidal neurons. Data as mean±s.d.

Table 2. Action potential and firing properties of pyramidal neurons in the agranular RSC

	APthr (mV)	Vm-AP thr (mV)	APamp (mV)	AP width (ms)	Firing freq (Hz)	Adaptation index
Pyr 2/3	-40,2 ± 3,0	-35,2 ± 4,0	93,6 ± 4,7	0,62 ± 0,11	50,6 ± 14,7	2,8 ± 0,9
Pyr 5m	-40,6 ± 2,9	-24,6 ± 5,8	92,7 ± 4,7	0,59 ± 0,07	55,1 ± 15,4	2,8 ± 1,0
Pyr 5BL	-43,1 ± 3,4	-22,6 ± 3,3	97,1 ± 7,6	0,5 ± 0,07	34.9 ± 9.1	1,1 ± 0,3
Pyr 6	-37,7 ± 4,1	-35,0 ± 4,2	85,1 ± 4,5	0,63 ± 0,11	48.0 ± 8.9	1,9 ± 0,7

Same neurons as in table 1. Data as mean±s.d.

Laminar branching specificity of callosal axons from superficial CPNs

To characterize the arborization of the terminal branches of callosal axons across the layers of the contralateral cortex, we performed unilateral *in utero* electroporation of E16.5 embryos with an eGFP-expressing plasmid (pCX-GFP). At this age, superficial pyramidal neurons are being produced in the ventricular zone of the developing necortex. Consistently, in postnatal coronal slices (P30), GFP+ neurons were found in the superficial layers of the RSC in the electroporated hemisphere (figure 3, lower panel in the left). The axons of these neurons could be followed crossing the midline through the dorsal, but not the ventral part of the corpus callosum, as expected for a medial cortical region (Nishikimi et al. 2011). These axons invaded the contralateral homotopic cortex (figure 3, right panel), where they developed a bimodal pattern of arborization. Similarly

to what happens in other cortical areas (York and Caviness 1975, Mizuno et al. 2007, Wang et al. 2007), extensive branching was observed in a territory including superficial layers and layer 5. Nonetheless, in the agranular RSC, callosal terminal arbours specifically branched in the upper part of L5B, but not in L5A and the lower part of L5B.

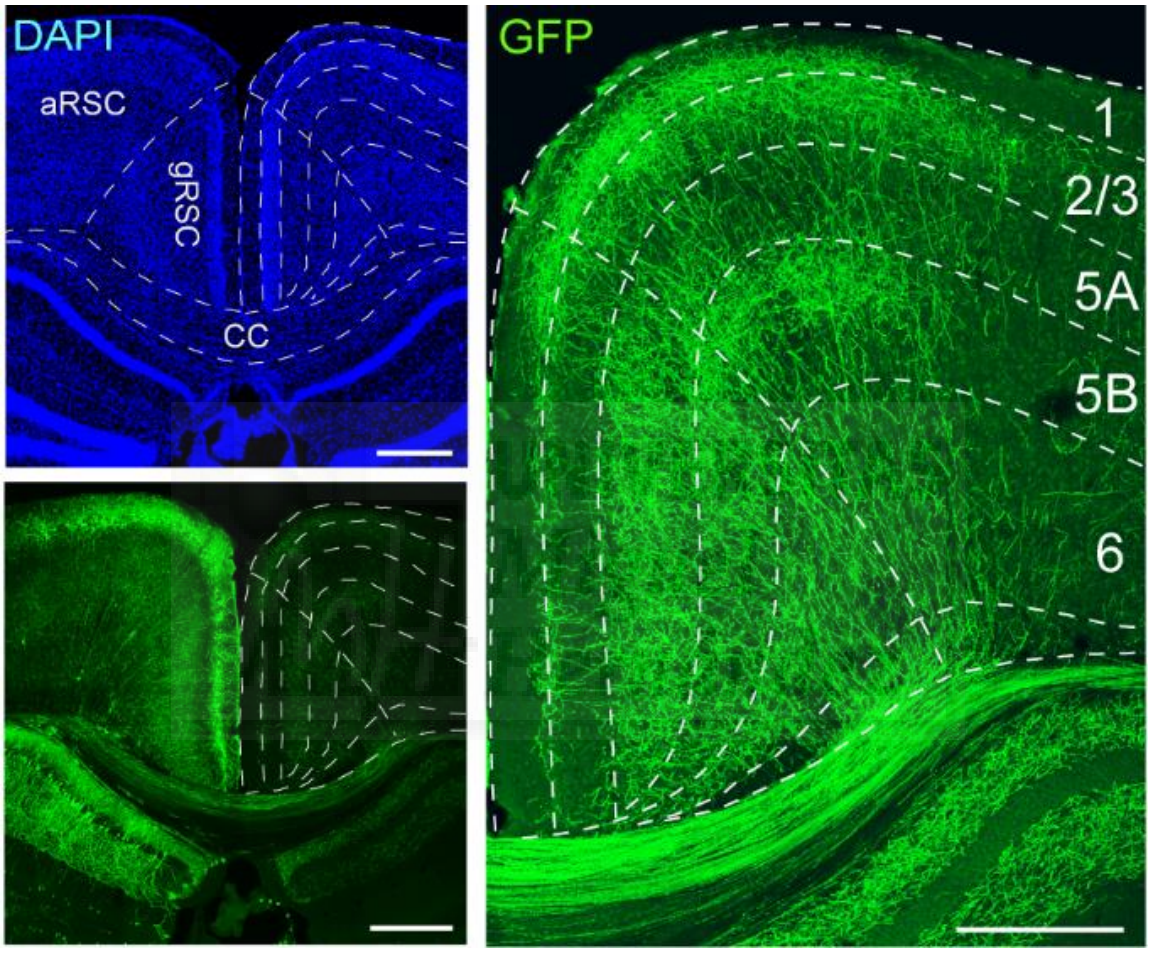

Figure 3. Branching of callosal axons in the retrosplenial cortex. Maximal projection of a confocal z-stack from a 40µm slice of a P30 mouse brain electroporated with an eGFP-expressing plasmid at E16.5 (lower panel in the left). Laminar boundaries were established according to DAPI counterstaining (upper panel in the left). Notice that in the neocortex, only neurons from superficial layers were electroporated (lower panel in the left), and that their axons crossed the midline and invaded the contralateral cortex (right panel). Scale bars 400µm (left panels) and 300µm (right panel).

Callosal axons preferentially target L2/3 and L5BL pyramidal neurons

The post-synaptic potentials (PSPs) recorded in L2/3 (n=21), L5A (n=17), L5BL (n=19) and L6 (n=23) pyramidal neurons in response to callosal input are shown in figure 4. In

most neuron, three different stimulus intensities were tested (100, 200 and 500 μA). Altogether, the amplitude of the callosal PSPs exhibited a bimodal distribution, being larger in L2/3 and L5BL than in L5A and L6 pyramidal neurons (figures 4B-C; see an example in figure 4A). A one-way ANOVA analysis of the data obtained at 200μA stimulus revealed significant differences among the groups ($F=10.44$, $p<0.00001$). A Bonferroni post hoc analysis only found significant differences in the amplitude of the response between L2/3, L5A and L5BL with L6 pyramidal cells (Bonferroni corrected p-value 0.007, computed p-value for Mann-Whitney two-sample comparisons: L2/3 vs L5A 0.080, L2/3 vs L5BL 0.749, L2/3 vs L6 $2.6 \cdot 10^{-6}$, L5A vs L5BL 0.022, L5A vs L6 $5.4 \cdot 10^{-6}$, L5BL vs L6 $5.6 \cdot 10^{-7}$). Within this sample, only in 2/21 L2/3 and 2/19 L5BL pyramidal neurons the callosal PSP were able to fire action potentials (see examples in figure 4D). The two L2/3 pyramidal neurons fired in response to 500μA stimulus, while the L5BL pyramidal neurons did it with lower stimulus intensity (200μA). The fact that the bimodal distribution of PSP amplitudes was clearly present with 100μA and 200μA stimulus intensities, where ortodromic and antidromic spikes were rare, strongly suggests that this pattern is mostly established by direct callosal input. The onset latency of the evoked responses is shown in figure 4E; for latency measurements we only analyzed neurons from experiments in which at least one pyramidal cell were recorded from layers 2/3, 5A and 5B in the same slice. A one-way ANOVA analysis of these data revealed significant differences in the onset latency across neuron types ($F=6.002$, p-value 0.00543). A Bonferroni post-hoc analysis found significant differences in the onset latency of the responses of L2/3 and L5A with respect L5BL pyramidal neurons (Bonferroni corrected p-value 0.0167, computed p-value for two-sample Mann-Whitney comparisons: L2/3 vs L5A 0.169, L2/3 vs L5BL 0.0167, L5A vs L5BL 0.004).

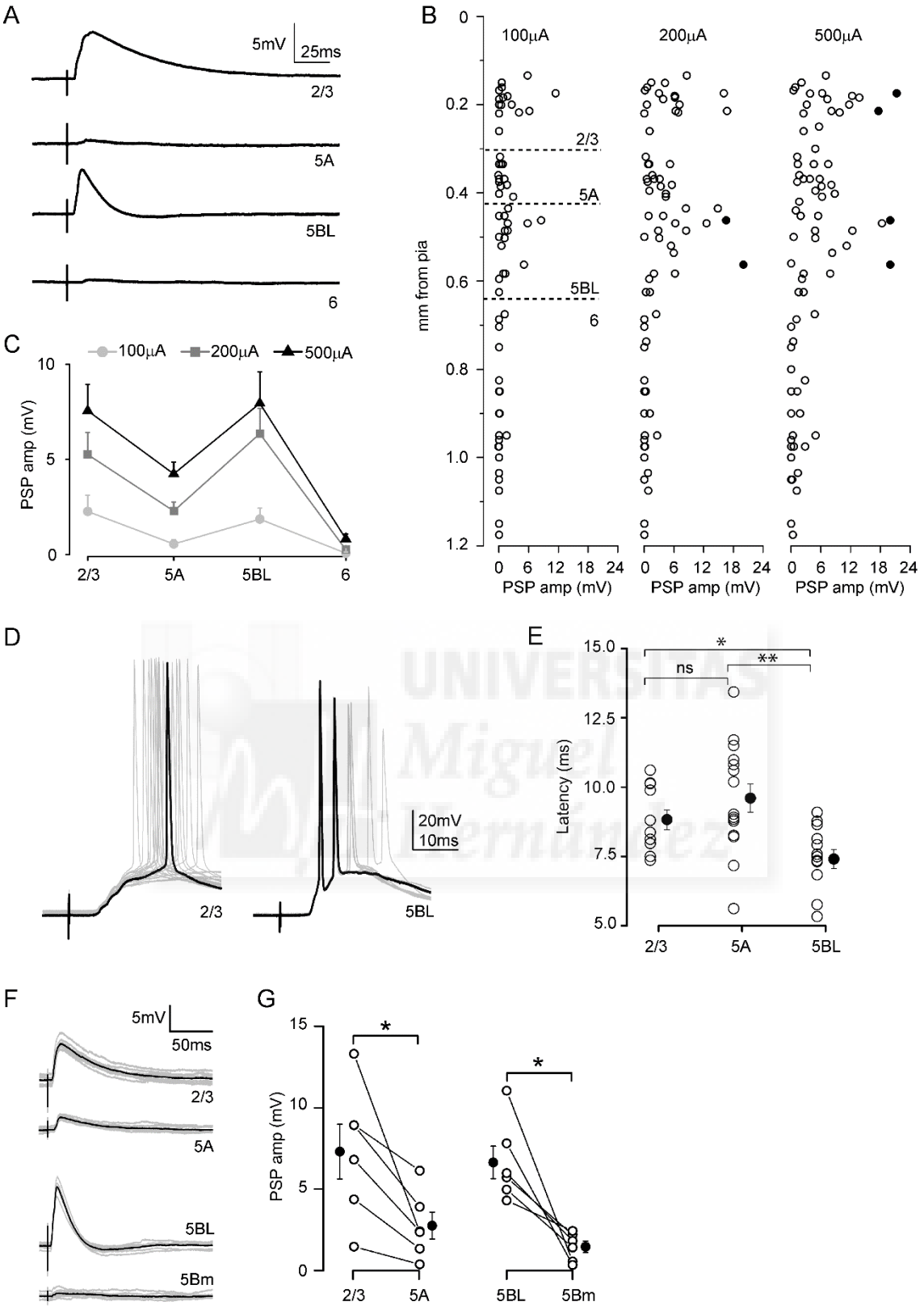

Figure 4. Laminar organization of callosal connections in the agranular RSC. A. An example of callosal PSPs recorded sequentially from 4 pyramidal neurons from the same cortical column in response to single pulse stimulation of the contralateral cortex (stimulus intensity 200µA). Each trace is the mean of at least 10 responses. B. Callosal PSP peak amplitude in a sample of pyramidal neurons (n = 21 L2/3, 17 L5A, 19 L5BL

and 23 L6 pyramidal neurons, n=16 slices from 16 mice) at three stimulus intensities (100, 200 and 500μA). Each circle is an individual neuron and filled circles represent neurons in which the an action potential was elicited. Soma to pia distance in μm was (mean ± s.d.): L2/3=190±31, L5A=371±39, L5BL=526±71, L6=927±136. C. Population PSP peak amplitude across pyramidal categories from the sample shown in B. D. Example of two neurons in which firing was evoked by suprathreshold postsynaptic potentials (stimulus intensity 500μA). Each trace is an individual response and one of the responses is highlighted in black. E. Onset latency of the callosal PSPs evoked in L2/3, L5A and L5BL pyramidal neurons, measured from stimulus artifact onset to 10% of PSP peak amplitude. Only slices in which at least 1 neuron of each category were sequentially recorded were analyzed (n=14 L2/3, 15 L5A and 11 L5BL pyramidal neurons; 8 slices of 8 mice; stimulus intensity 200μA, L6 neurons were excluded). F. Example of the responses evoked in a L2/3 vs 5A pair and in a L5BL vs L5Bm pair of pyramidal neurons simultaneously recorded (stimulus intensity 200μA). G. Callosal PSP peak amplitude in a sample of L2/3 vs L5A pairs (left panel, n=6) and L5BL vs L5Bm pairs (right panel, n=6). Stimulus intensity 200μA. Grey traces show individual responses and the black trace is the average. PSPs were recorded at resting membrane potential. Data in C, E and G as mean±s.e.m.

The above data revealed a tendency in the amplitude of the PSPs evoked in L5A pyramidal neurons to be smaller than in L2/3 and L5BL ones. To increase the potency of the statistical analysis, as well as to extend our analysis to L5Bm pyramidal neurons, we performed a set of experiments in which we simultaneously recorded from pairs of L2/3 vs L5A and L5BL vs L5Bm pyramidal cells (figure 4F-G, n=6 simultaneous pairs of each type). In the case of L2/3-L5A pairs, special care was taken to select neurons whose apical dendrites were radially aligned; in the case of L5BL-L5Bm pairs, intersomatic distance was <50μm (see example in figure M4B). These experiments revealed that callosal PSPs were significantly larger in L2/3 than in L5A neurons and in L5BL than in L5Bm pyramidal neurons, extending our previous results. Overall, these data indicated that L2/3 and L5BL pyramidal neurons were the preferred targets of the callosal axons within contralateral pyramidal neurons.

Strong recruitment of upper, but not lower, L5BL neurons by callosal input

The observation that callosal axons from superficial CPNs branched extensively in the upper part of layer 5B but not in its lower part (figure 3) suggested further specificty of callosal input on layer 5 circuits. In agreement with this, a detailed analysis of the data from our sample of L5BL neurons described above (figure 4A-C), revealed that the amplitude of their callosal PSPs was negatively correlated with their somatic distance from pia and with their membrane input resistance (figure 5A). In contrast, in layer 2/3 there was no correlation between the size of the PSPs and the position whitin the layer ($r = -0.007$, $p=0.98$).

Moreover, in a wider sample of L5BL pyramidal neurons, we observed that the membrane input resistance of L5BL pyramidal neurons was negatively correlated with their columnar depth (figure 5B), suggesting the existence of a further specialization between L5BL neurons placed in the upper and the lower part of layer 5B. To test if there was a bias in the callosal connectivity towards upper L5BL neurons, we compared the callosal PSP amplitude in pairs formed by an upper and lower L5BL pyramidal neurons that were sequentially recorded. In all cases the callosal PSP was larger in the upper L5BL neuron (figure 4D-E). To estimate the firing probability of the upper L5BL pyramidal neurons, we recorded from a total of 14 neurons whose soma was in the upper half of layer 5 (including the 8 neurons from the pairs); in this sample 4/14 (28%) and 6/14 (43%) neurons fired by the PSPs evoked by 200μA or 500μA contralateral stimuli, respectively (see an example in figure 5C). This proportion of firing neurons in upper layer 5B was clearly larger than the 10% (2/19, $p=0.032$) found in our initial sampling covering the whole layer 5B.

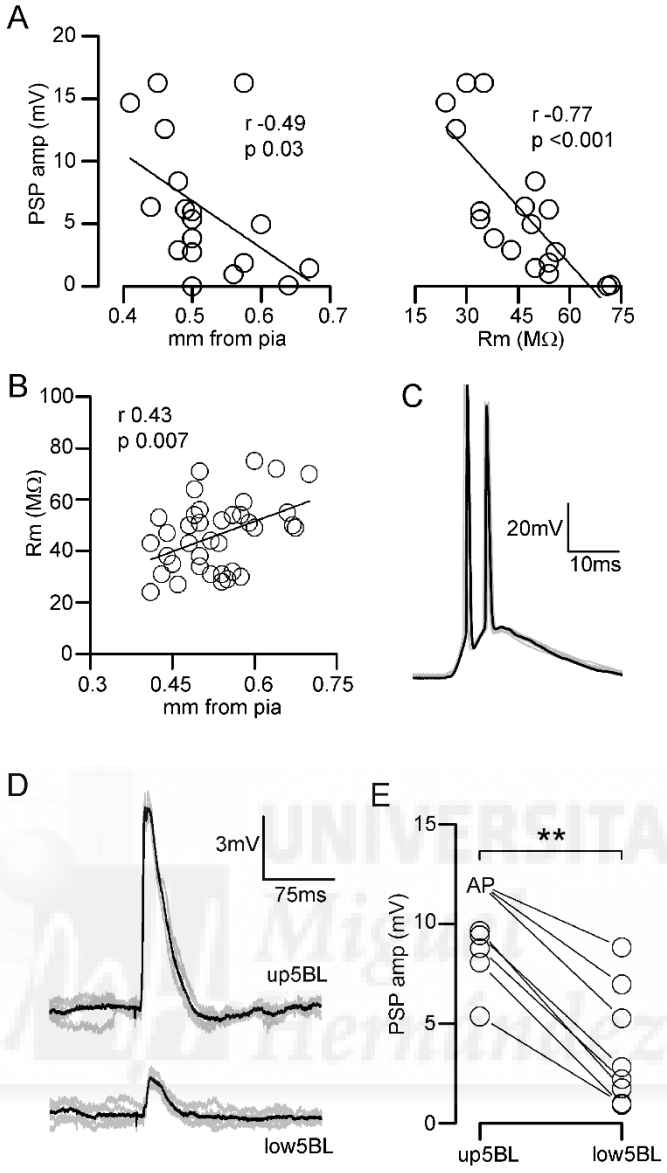

Figure 5. Strong recruitment of upper L5BL pyramidal neurons by callosal input. A. Callosal PSP peak amplitude in L5BL pyramidal neurons was negatively correlated with somatic distance from pia (left panel) and with membrane input resistance (right panel); same sample as in figure 4A-C; stimulus intensity 200μA. B. In L5BL pyramidal neurons, membrane input resistance was positively correlated with somatic distance from pia (n=37). C. Response of a L5BL pyramidal neuron from the upper half of layer 5B to a 200μA stimulus. Individual responses are shown in grey and one is highlighted in black. D. PSPs evoked in an upper vs lower L5BL pyramidal neuron pair evoked by contralateral stimulation. Grey traces are individual responses and the black trace is the average. E. PSP peak amplitude in a sample of upper vs lower L5BL pairs (n=8 pairs of neurons sequentially recorded in current-clamp; 5 slices from 5 mice; upper L5BL 490 ± 47μm from pia, lower L5BL 593 ± 61μm). Stimulus intensity 200μA. For statistical comparison of PSP amplitude, in those cells in which firing was evoked we used the PSP amplitude of the largest subthreshold response in the sample.

These data indicated that, in the agranular RSC, one hemisphere could recruit the extratelencephalic output pathway of the opposed homotopic region by means of the callosal projection.

PV-FS dependent inhibition recruited by callosal input is biased towards L2/3 and L5BL pyramidal neurons

In addition to targeting pyramidal cells, CPNs also synapse on contralateral inhibitory neurons (Carr and Sesack 1998; Cissé et al. 2003, 2007; Karayannis et al. 2006, Petreanu et al. 2007) which in turn innervate surrounding pyramidal cells. To characterize the organization of the inhibition recruited by callosal input across the different pyramidal subtypes studied, we compared the IPSCs in sequentially recorded pairs of L2/3 vs L5A and L5BL vs L5Bm pyramidal neurons (figure 6, n=8 and 6 respectively). Within a pair, the stimulus electrode position was not changed and the stimulus intensities employed were the same for both neurons. By this, we assumed that the pool of neurons recruited by the stimulus was maintained. IPSCs were recorded at 0mV, the measured reversal potential of the excitatory synaptic currents.

IPSC peak amplitude was significantly smaller in L5A and L5Bm than in L2/3 and L5BL pyramidal neurons, respectively (figure 6B and D, right panel), mimicking the specific pattern of the callosal excitation on pyramidal neuron subtypes. This was particularly remarkable in L5BL-L5Bm pairs, which had their somas closely placed, and indicated a strong selectivity of interneuron to pyramidal connectivity in this layer. In addition to the differences in the IPSCs, and consistently with our results, we observed that callosal EPSCs, recorded in the same neuron pairs at -70mV, were larger on L2/3 and L5BL pyramidal cells with respect to L5A and L5Bm pyramidal neurons, respectively (figure 6B and D, left panel).

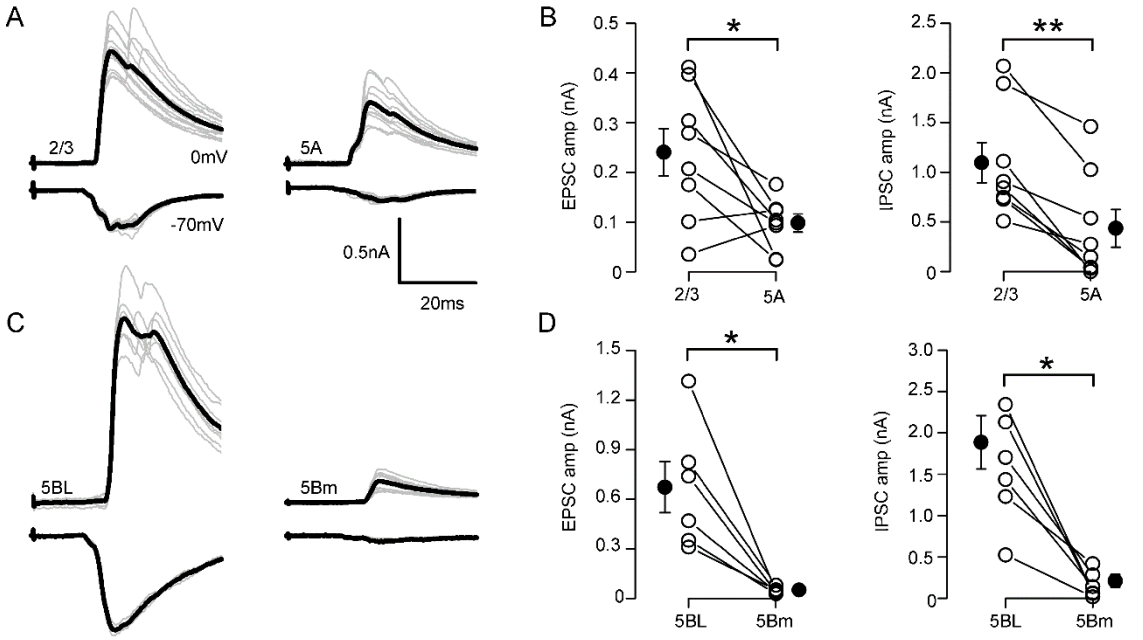

Figure 6. Inhibitory currents evoked on pyramidal neurons retained the specificity of callosal excitatory input. A. IPSCs (upper traces in each panel) and EPSCs (lower traces in each panel) evoked in a L2/3 vs L5A pair of pyramidal neurons sequentially recorded (stimulus intensity 200μA). Gray traces are individual responses and the black trace is the average. B. EPSCs (left panel) and IPSCs peak amplitudes (right panel) in a sample of sequential L2/3 vs 5Am pairs (n=8, 5 slices from 5 mice). C-D. Same as in panels A-B but for L5BL vs L5Bm pairs (n=6, 3 slices from 3 mice). Open circles in B and D are individual values and filled circles and error bars are the mean±s.e.m.

To determine which interneurons were responsible of this pyramidal subtype specific inhibition, we recorded from a sample of PV-FS and non PV-FS gabaergic neurons from all cortical layers. PV-FS cells were identified by their characteristic high frequency tonic discharges of narrow action potentials with little accommodation and large afterhiperpolarization in response to suprathreshold square current pulses. To increase the probability of patching PV-FS neurons, we used the Pvalb-Cre;RCE or the GAD67-GFP line, in which all types of gabaergic interneurons are labeled with GFP. Non PV-FS neurons were identified as GFP+ neurons from the GAD67-GFP line lacking the typical properties of FS cells (figure 7A-C and table 3).

Excluding layer 6, in which none, or only small responses were recorded, callosal PSPs evoked on PV-FS cells were larger than in non PV-FS interneurons (see example in

figure 7D). An important consequence of the smaller PSPs in non PV-FS interneurons was that none of these neurons fired in response to contralaterral input (0/31); in contrast, 8/36 PV-FS neurons, distributed in layers 2-5B, reached the action potential threshold in response to contralateral simulation (figure 7D-E). The latency of the action potentials evoked in PV-FS cells (range 7.5-13.5ms) overlapped but preceed the onset latency of IPSCs evoked on pyramidal neurons (range 8.2-15.0ms) (figure 7F). Altogether, these data strongly suggested that IPSCs evoked on pyramidal neurons were mainly PV-FS dependent, and that PV-FS interneurons responding to contralateral input had a strong preference to innervate L2/3 and L5BL pyramidal neurons.

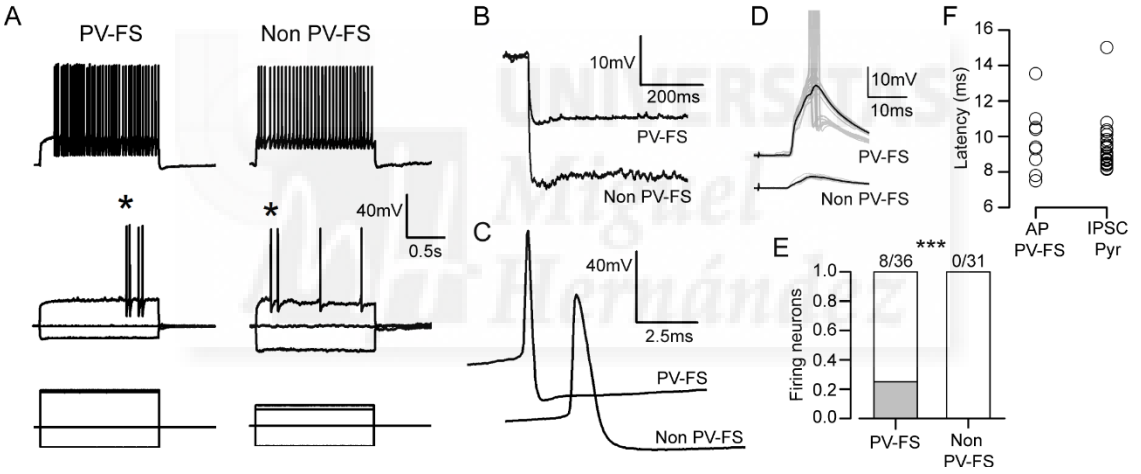

Figure 7. Inhibition triggered by callosal input is mediated by PV-FS interneurons. A. Membrane voltage responses from a PV-FS (left) and a non PV-FS interneuron (right) to -300pA, 0pA, first suprathreshold and second suprathreshol 1.5s current square pulses. Responses were recorded at resting membrane potential ($I_{holding}$=0pA). B. The response to a -300pA current pulse is hown amplified to illustrate the difference in the membrane input resitance of both neurons. C. The first AP from the first suprathreshold current injection is shown amplified. Notice that the narrower AP in the PV-FS neuron. D. PSPs evoked in a L2/3 PV-FS vs non PV-FS pair of closely placed interneurons sequentially recorded (stimulus intensity 200µA). Grey traces are individual responses and the black trace is the average of the subthreshold responses. Notice that in some cases the PV-FS neurons reaches the AP threshold (AP truncated). E. Proportion of firing neurons in a sample of PV-FS and non PV-FS interneurons from the agranular RSC (n=36 and 31 neurons respectively). Stimulus intensity range 200-800µA. F. AP latency (from stimulus onset to AP peak) in the sample of firing PV-FS neurons and IPSC latency (from stimulus onset to 10% of IPSC peak amplitude) in the sample of pyramidal neurons from figure 6.

Table 3. Electrophysiological properties of GABAergic neurons in the agranular RSC

	n	Age (days)	Distance to pia (µm)	Vrest (mV)	Rm (peak) (MΩ)	τm (ms)
PV-FS	45	19,7 ± 1,2	452,7 ± 217,7	-72,1 ± 5,1	70,8 ± 24,0	5,9 ± 1,9
Non PV-FS	16	19.2 ± 1.3	359,7 ± 206,5	-73,0 ± 2.8	196,7 ± 81,5	9,2 ± 5,4

	APthr (mV)	Vm-AP thr (mV)	APamp (mV)	AP 1/2 width (ms)	Firing freq (Hz)	Adaptation index
PV-FS	-37 ± 4,4	-35,1 ± 6,2	70,7 ± 7,8	0,21 ± 0,03	171,8 ± 8,9	1,0 ± 0,2
Non PV-FS	-35,6 ± 5,2	-37,0 ± 5,7	77,3 ± 8,31	0,47 ± 0,13	109,9 ± 45,7	2,4 ± 0,9

Data as mean±s.e.m.

Net inhibition in superficial pyramidal neurons by callosal input

In our experiments, the proportion of L2/3 pyramidal neurons in which the callosal input triggered an action potential was very low: 0/70 neurons with 200µA stimuli and 3/70 (4%) with 500µA (neurons in 39 slices from 34 mice), and significantly lower than in upper L5BL neurons (4/14 and 6/14 respectively, $p<0.001$ at both intensities tested). The fact that, in our conditions, L2/3 pyramidal neurons were more hyperpolarized at rest than other pyramidal neurons could difficult their recruitment. Nonetheless, the reversal potential of the callosal response in L2/3 pyramidal neurons was much more hyperpolarized than in L5BL pyramidal neurons, and even more negative than the threshold for AP firing (figure 8A-C, n=6 L2/3 vs L5BL pairs of pyramidal neurons sequentially recorded; see AP threshold values in table 2) causing a net inhibition in these neurons (see example in figure 8D), suggesting that the difference in the resting potential was not the main cause of the low firing probability among superficial pyramidal neurons in response to callosal input.

Alternatively, callosal PSPs evoked on L2/3 pyramidal neurons had a longer decay time than those on L5BL neurons (figure 8E-F), predisposing them for stronger temporal summation. We argued that in a context of sustained callosal activity, the recruitment of L2/3 pyramidal neurons could be supported by the temporal summation of successive

inputs. To test this hypothesis, we applied trains of stimuli instead of single-pulse stimulation. In the range of 10-15Hz stimulation, temporal summation of successive PSPs in a train was minimal in L2/3 pyramids ($4^{th}/1^{st}$ PSP amplitude 1.10±0.08, n=15). Therefore, we used higher stimulation frequencies (trains of 20-40 pulses at 40Hz) with the idea of shortening the interstimulus interval to facilitate the summation of successive responses. In 8 L2/3 vs L5BL pairs sequentially recorded, all L5BL neurons were recruited at some point during the train, while none of the L2/3 pyramidal neurons fired (see example in figure 8G).

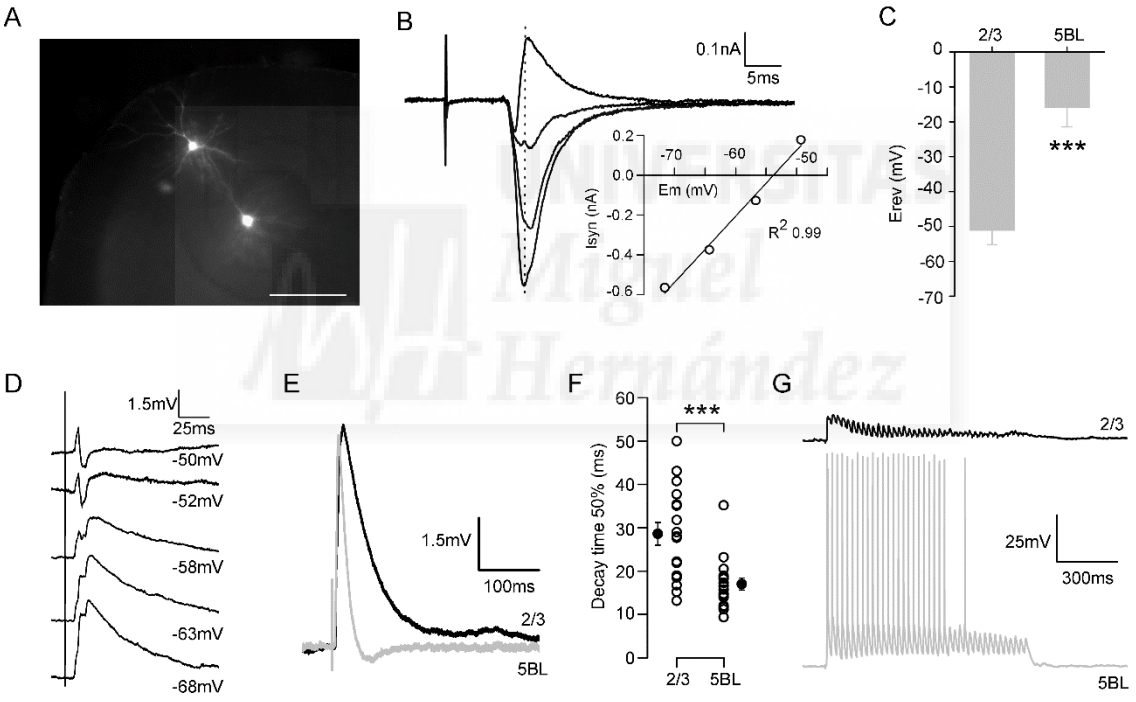

Figure 8. L2/3 pyramidal neurons are inhibited by callosal input. A-C. A. Example of a pair of L2/3 vs L5BL pyramidal neurons sequentially recorded; scale bar 200μm. B. PSCs in the L2/3 pyramidal neuron shown in A in response to contralateral stimulation measured at different holding potentials (from -72 to -50mV). Each trace is the average of at least 5 consecutive responses. The inset shows the IV curve measured at the PSC peak. C. Reversal potential of the callosal responses measured at the EPSC peak in a sample of L2/3 vs L5BL pairs (n=6 pairs, 5 slices from 5 mice, stimulus intensity 200μA). Notice that the reversal potential of the callosal responses is more hyperpolarized on L2/3 pyramidal neurons. D. Callosal PSP in a L2/3 neuron recorded at different membrane potentials. Notice that the response largely reverts at -50mV, below the action potential threshold. Each trace is the average of at least 5 consecutive responses. E. Callosal PSPs in a L2/3 vs L5BL pair (same as shown in figure 4A). F. Decay time to 50% of peak

amplitude of the callosal PSP in a sample of L2/3 and L5BL neurons (same as shown in figure 4A-E; stimulus intensity 200μA). G. Callosal PSPs evoked in a sequential L2/3 vs L5BL pair in response to a 40Hz train applied to the contralateral cortex (stimulus intensity 200μA). Population data as mean±s.e.m.

Even more, in a different sample of non-paired recordings, we tested the effect of 40Hz train of contralateral stimuli on the firing activity evoked in the recorded neuron by the injection of a suprathreshold current pulse (figure 9). In all L2/3 pyramids tested (n=8), the firing rate was decreased by contralateral stimulation. The opposite pattern was observed in L5BL neurons (n=8), and, as expected from their low responsiveness to callosal input, no change in the number of APs was detected in L5Bm pyramidal neurons (n=5). Altogether, these data indicates that, in our conditions, the firing activity of CPNs can suppress the activity of contralateral superficial pyramidal neurons, reinforcing the hypothesis of the inhibitory role of callosal projections on superficial layers of the retrosplenial cortex.

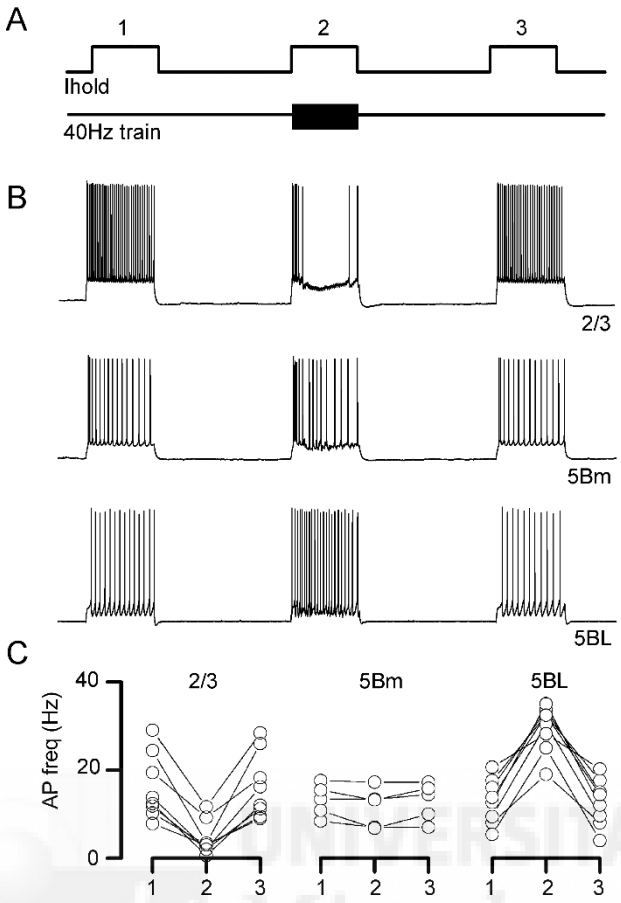

Figure 9. Firing in L2/3 pyramidal neurons is suppressed by callosal input. A. Experimental design: three suprathreshold current pulses (1s duration) were injected in the recorded neuron with a 2s interval; simultaneously to the second current pulse, a stimulus train was applied to the contralateral cortex (40Hz, 1s duration). B. Representative examples of the effect of contralateral stimulation on the firing frequency in a L2/3 (upper panel), L5Bm (middle panel) and L5BL (lower panel) pyramidal neuron. C. Change in the firing frequency induced by 40Hz stimulation of the contralateral cortex in a sample of L2/3 (n = 8), L5Bm (n = 5) and L5BL (n = 8) pyramidal neurons. Stimulus intensity 200μA.

PART 2. Synaptic mechanisms explaining the differential effect of callosal input in superficial and large bursting pyramidal neurons from upper layer 5B

Our mophological and electrophysiological analysis revealed that L2/3 and upper L5BL pyramidal neurons are the main targets of callosal axons from superficial CPNs. Nonetheless, in the conditions tested, the impact of this input in both neuronal types was opposed, with L2/3 pyramidal neurons being inhibited and upper L5BL pyramidal cells being strongly recruited. To further understand the synaptic mechanisms underlaying this divergent behaviour, we studied the properties of the excitatory and inhibitory postsynaptic currents evoked in both neuron types by contralateral input.

Synaptic properties of cortical responses in L2/3 and L5BL pyramidal neurons

Excitatory and inhibitory postsynaptic callosal currents were studied in a paired sample of L2/3 and L5BL pyramidal cells that were recorded sequentially (n=9). In each pair, several stimulus intensities were employed, covering the effective range of stimulation (intensity range 100-800µA, at least four different intensities were employed in each case), from perithreshold to submaximal responses (see example in figure 10A-C and 11A-C). Again, special attention was paid to select, in each pair, radially aligned neurons. For comparison of sample data, two stimulus intensities were used, one in the 150-400µA range (intermediate intensity), in which low-jitter EPSCs and IPSCs were reliably evoked without failures, and the other in the 400-800µA range (submaximal intensity), closer to the maximal response. Under these conditions, most of these postsynaptic currents were compound (multi-axon) responses.

The amplitude and area of the EPSCs evoked at both stimulus intensities were significantly larger in L5BL than in L2/3 pyramidal neurons (figure 10D-E). In contrast,

IPSCs amplitude and area were larger on the L2/3 pyramidal neurons at intermediate intensities, while these differences disappeared when submaximal stimulus intensities were employed (figure 11D-E). Overall, the excitatory to inhibitory balance of the response, measured as the EPSC/IPSC peak amplitude ratio, was more favorable to excitation in L5BL pyramidal neurons (0.10±0.01 vs 0.98±0.27 and 0.12±0.02 vs 0.55±0.13 with intermediate and submaximal intensities, respectively, p-value = 0.004 in both cases).

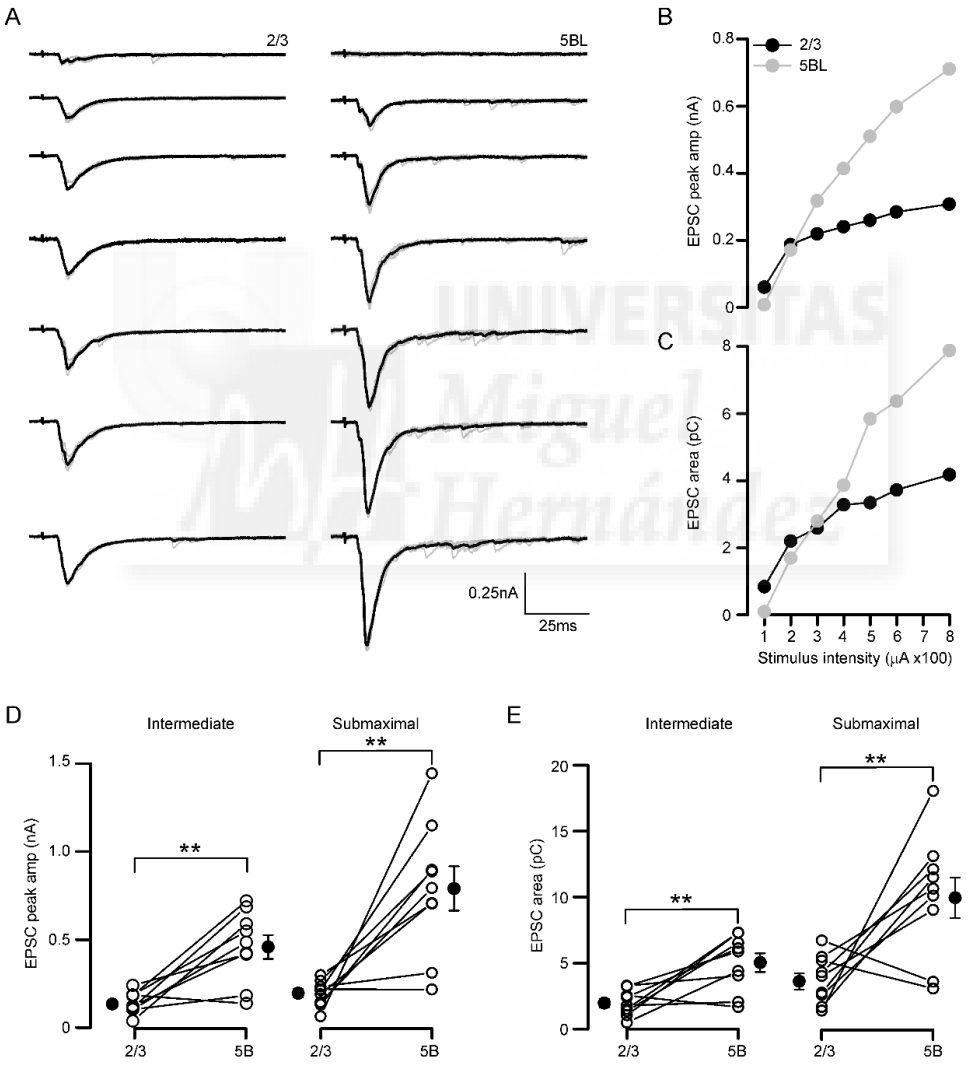

Figure 10. EPSCs in L2/3 and L5BL pyramidal neurons in response to contralateral cortical input. A. EPSCs evoked in a L2/3 vs L5BL pyramidal neuron pair in response to contralateral stimulation at increasing intensities (stimulus intensity range 100-800µA). Grey traces are individual values and the black trace is the average of at least 5 responses. B-C Peak amplitude and area of the evoked cEPSCs from the neurons in A at each stimulus intensity. D. Peak amplitude of the EPSC in a sample of 9 L2/3 vs L5BL

pyramidal neuron pairs sequentially recorded (5 slices from 5 mice) with intermediate (239±78µA, left panel) and high intensity stimulus (611±61µA, right panel). E. Same as D for EPSC area. EPSCs were recorded at -70mV. Open circles are individual values, filled circles and error bars are the mean±s.e.m.

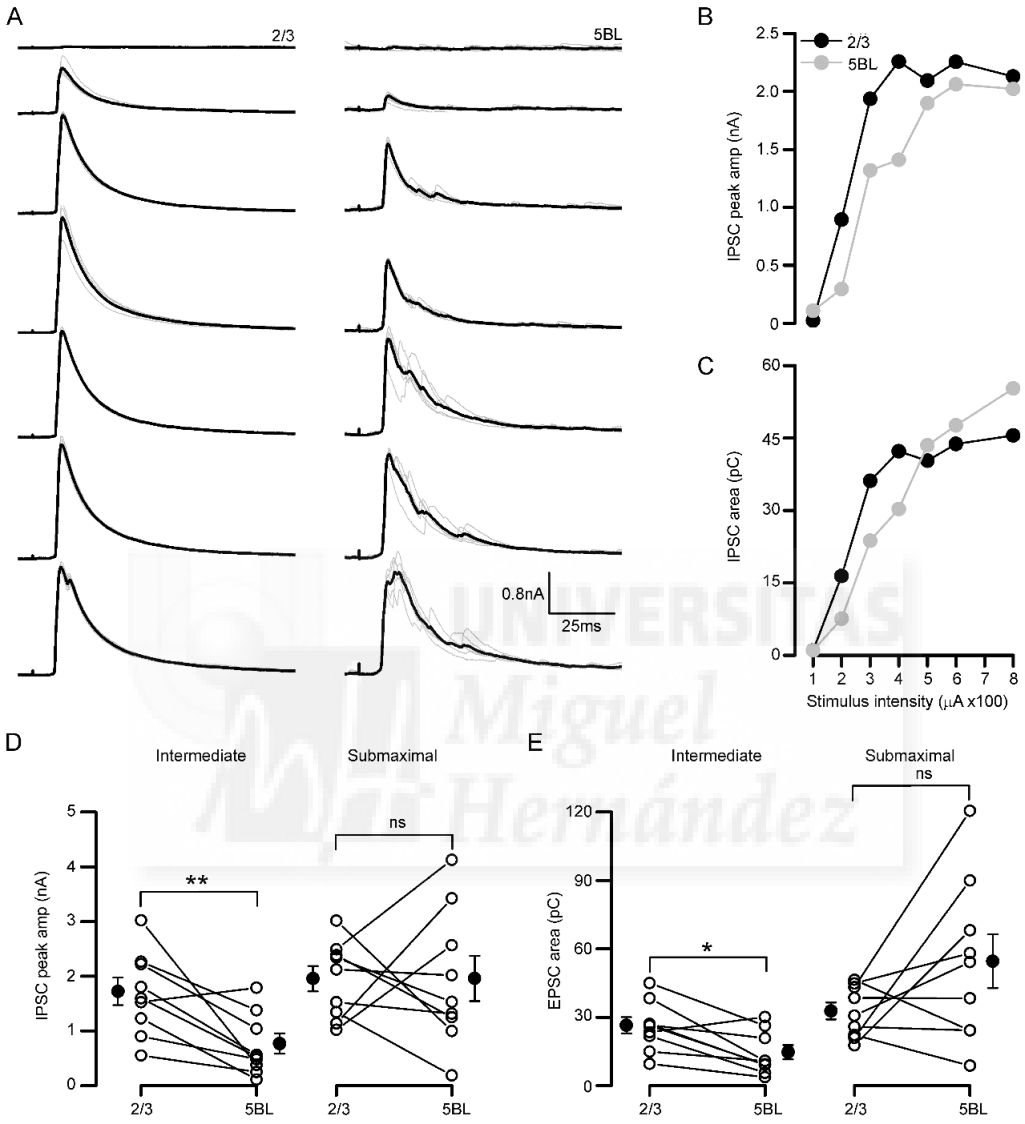

Figure 11. IPSCs in L2/3 and L5BL pyramidal neurons in response to contralateral cortical input. A. IPSCs evoked in a L2/3 vs L5BL pyramidal neuron pair (same as in figure 10A) in response to contralateral stimulation at increasing intensities (stimulus intensity range 100-800µA). Grey traces are individual values and the black trace is the average of at least 5 responses. B-C Peak amplitude and area of the evoked IPSCs from the neurons in A at each stimulus intensity. D. Peak amplitude of the IPSC in a sample of L2/3 vs L5BL pyramidal neuron pairs (same as in figure 10) with intermediate (239±78µA, left panel) and high intensity stimulus (611±61µA, right panel). E. Same as D for IPSC area. IPSCs were recorded at 0mV. Open circles are individual values, filled circles and error bars are the mean±s.e.m.

In addition, we measured the temporal course of the synaptic currents evoked by callosal input (figure 12, n=12 L2/3 vs 5BL sequential pairs). Importantly, IPSCs in L5BL pyramidal neurons were delayed with respect to those in L2/3 pyramidal neurons (figure 12A-B). As a consequence, the time window to integrate the excitatory component of the callosal synapse was longer in L5BL pyramidal neurons (figure 12C).

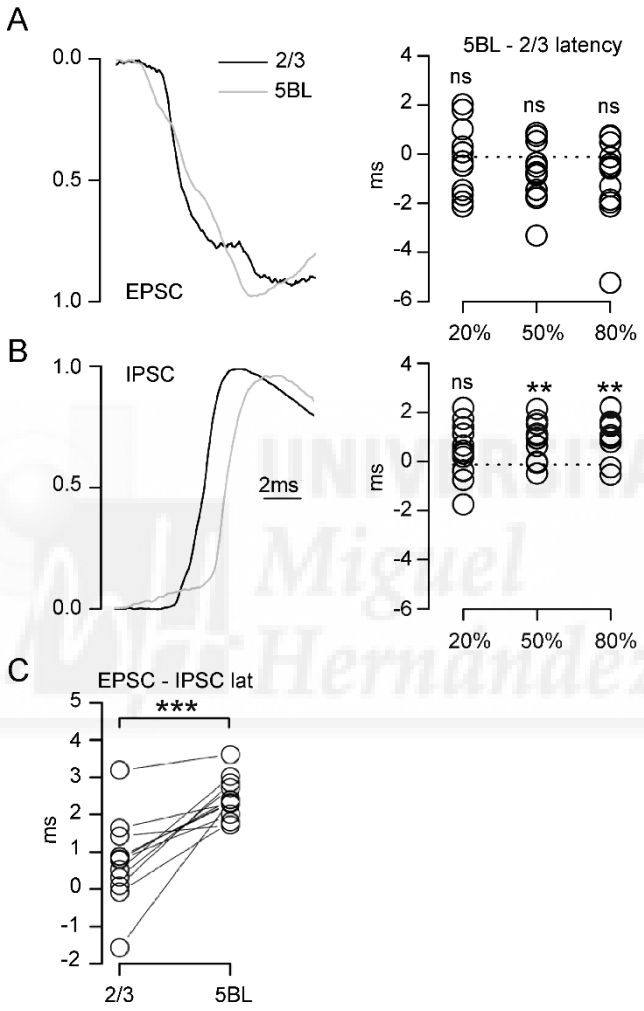

Figure 12. Longer IPSC latency on L5BL pyramidal neurons. A. Example of the rising phase of the EPSC evoked in a L2/3 vs L5BL pair of pyramidal neurons (left panel), and EPSC latency difference in a sample of L2/3 vs L5BL pyramidal neuron pairs (right panel, n=12 sequential pairs, 7 slices from 7 mice; stimulus intensity 229±56µA). Traces are the average of at least 5 responses and are normalized to peak amplitude. For comparisons, PSC latency was measured as the time point at which the response reached 20, 50 and 80% of peak amplitude with respect to stimulus onset and latencies for the same condition from each neuron in a pair were subtracted. B. In the same pairs, the IPSCs were also recorded. Panel B follows the same organization as in A. C. EPSC-IPSC latency measured at 50% of peak amplitude in the same 12 L2/3 vs L5BL pairs.

Overall, the differences detected in the E/I balance and in the time course of the inhibitory currents evoked on L2/3 and L5BL pyramidal neurons were in agreement with the different responsiveness of both pyramidal neuron subtypes, particularly, with our previous observation of a more hyperpolarized reversal potential of the callosal response in L2/3 pyramidal neurons (figure 8C).

Larger convergence of callosal axons in L5BL pyramidal neurons

The larger EPSCs evoked in L5BL neurons with respect to those in layer 2/3 could depend on 2 factors: (1) a larger amplitude of the unitary callosal EPSC (uEPSC) and/or (2) a larger convergence of callosal axons. To discriminate between both possibilities, we recorded uEPSCs in L2/3 and L5BL pyramidal neurons evoked with a minimal stimulation protocol (see methods) and computed the compund EPSC/unitary EPSC area, as an indicator of the number of firing presynaptic neurons contacting each pyramidal cell in figure 11.

Examples of putative uEPSCs recorded in a L2/3 and a L5BL pyramidal neurons are shown in figure 13. Notice the abundant presence of failures and the estability of the amplitude across successful trials, suggesting their single-axon nature. No significant differences were found in the amplitude and area of uEPSCs among both pyramidal subtypes (figure 13C, n=12 and 9 uEPSCs for L2/3 and L5BL pyramidal neurons, respectively). Accordingly, we observed a significant 2-fold larger cEPSC/uEPSC area ratio on L5BL neurons (figure 13C, right panel; for compound responses, those evoked with intermediate stimulation were employed), indicating that callosal convergence was larger in upper L5BL than in L2/3 pyramidal neurons.

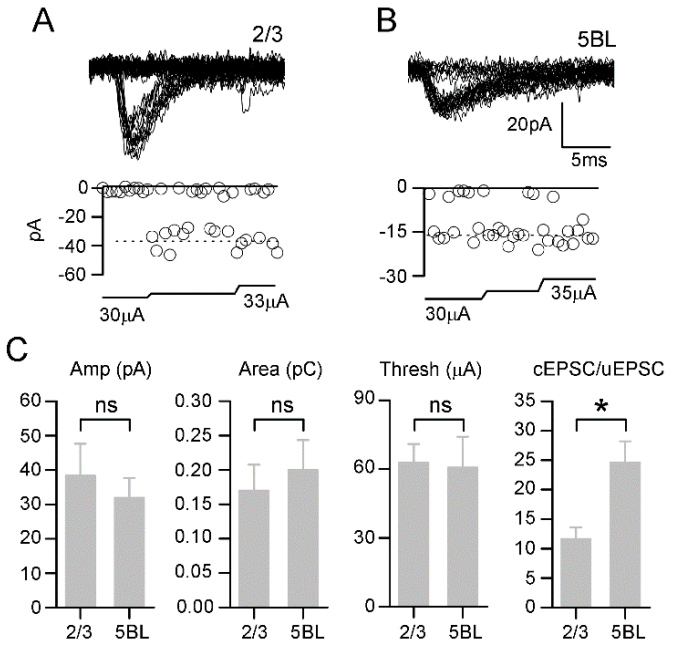

Figure 13. Similar properties of callosal unitary EPSCs in L2/3 and L5BL neurons. A-B. Example of putative unitary EPSCs evoked with a minimal stimulation protocol in a L2/3 (A) and a L5BL pyramidal neuron (B). The upper panel shows consecutive responses. Notice the abundant presence of failures. The lower panel shows the peak amplitude of the evoked response and the stimulus intensity employed for each response. C. Average peak amplitude, area and stimulus threshold for the putative uEPSCs and the cEPSC/uEPSC area ratio in a sample of L2/3 and L5BL pyramidal neurons (n=12 L2/3 and 9 L5BL). Data as mean±s.e.m.

Lower responsiveness of L5 PV-FS neurons explain the lower IPSC amplitude in L5BL neurons

Then, we focused in the difference in the IPSC amplitude among L2/3 and L5BL pyramidal neurons detected with intermediate stimulus intensities. Similarly to the case of compound EPSCs, three non-excluding hypothesis could explain this observation: (1) reduced amplitude of unitary IPSCs (uIPSCs) on L5BL pyramidal neurons, (2) lower PV-FS to L5BL connectivity, and/or (3) lower responsiveness of PV-FS neurons targeting L5BL neurons.

The amplitude and area of the uIPSCs were not significantly different among both pyramidal neuron subtypes (figure 14, n=19 and 12 uIPSCs for L2/3 and L5BL neurons, respectively), arguing against the first hypothesis. Accordingly, the cIPSC/uIPSC area

ratio was 2-fold larger on superficial pyramids (figure 14C, right panel), indicating that a larger number of PV-FS cells recruited in response to contralateral stimulation synapsed on L2/3 pyramidal neurons with respect to L5BL ones. In addition, the density of PV-FS neurons was similar across layers 2/3 and 5 (figure 15). Given that the total neuronal density is lower in layer 5B (figure 2B), the pyramidal to PV-FS ratio must be lower in superficial layers, arguing against the hypothesis of a larger PV-FS to pyramidal convergence on superficial layers.

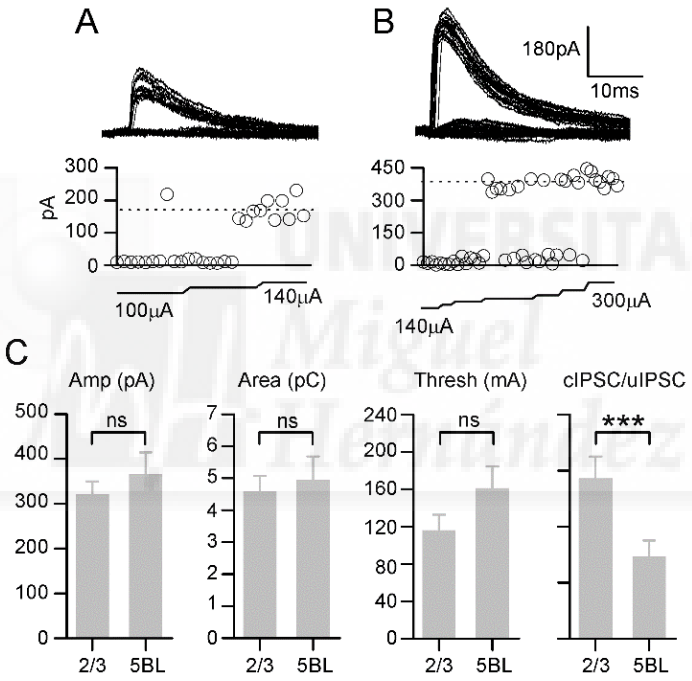

Figure 14. Similar properties of unitary IPSCs in L2/3 and L5BL neurons. A-B. Example of putative uIPSCs evoked with a minimal stimulation protocol in a L2/3 (A) and a L5BL pyramidal neuron (B). The upper panel shows consecutive responses. Notice the abundant presence of failures. The lower panel shows the peak amplitude of the evoked response and the stimulus intensity employed for each response. C. Average peak amplitude, area and stimulus threshold for the putative uIPSCs and the cIPSC/uIPSC area ratio in a sample of L2/3 and L5BL pyramidal neurons (n=19 L2/3 and 12 L5BL). Data as mean±s.e.m.

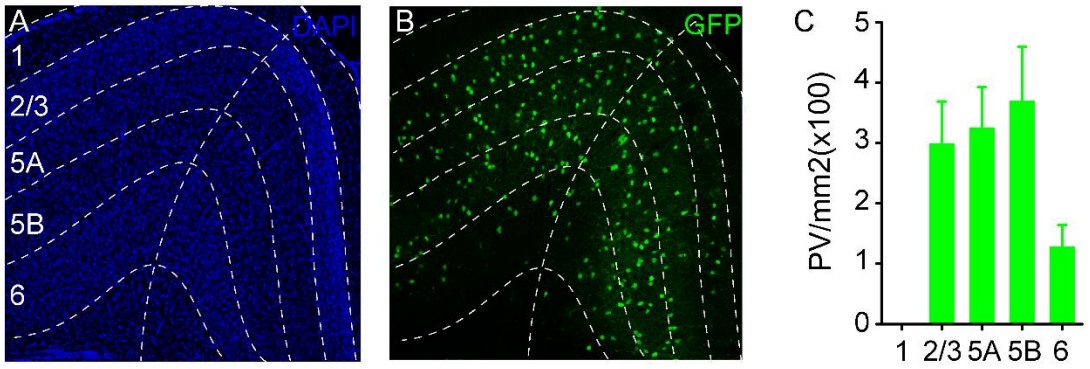

Figure 15. Distribution of PV+ cells in the agranular RSC. A. Laminar boundaries were stablished accordind to DAPI staining. B. Confocal z-stack of an 40µm slice from a Pvalb-Cre;RCE immunostained against GFP. C. GFP+ neurons in the agranular RSC (region in the left limited by the vertical dotted line) were counted for each layer (n=7 slices from 3 mice). Data as mean±s.d.

Therefore, we compared the responses of PV-FS interneurons from layers 2/3 and 5 to contralateral input with two different stimulus intensities (figure 16, n=17 L2/3 vs L5 PV-FS pairs sequentially recorded in current-clamp; stimulus intensity 165±50µA and 483±71µA). PSPs were significantly larger on L2/3 PV-FS neurons with respect to L5 ones at both stimulus intensities (figure 16A-C). With the weaker stimulus, already 2/17 superficial PV-FS cells reached the AP threshold, while none of the layer 5 PV-FS neurons fired. With the stronger stimulus 8/17 superficial and 2/17 deep PV-FS neurons fired in response to contralateral stimulation. Notice that the stimulus intensities used here were smaller than those employed for figures 10 and 11, and therefore, the ratio of recruited PV-FS cells may be larger in that case.

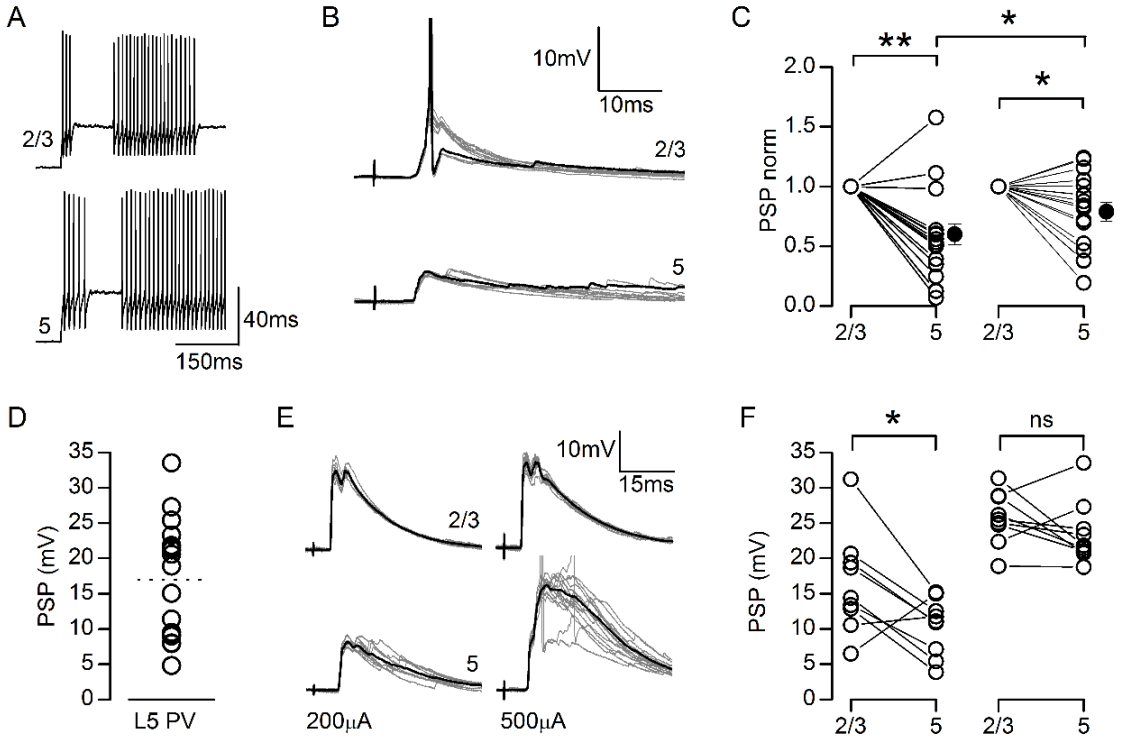

Figure 16. Smaller responsiveness of PV-FS interneurons in layer 5 to callosal input with respect to PV-FS in layers 2/3. A-C. PSPs in response to contralateral stimulation are larger on L2/3 PV-FS cells. A. Firing pattern of a pair of L2/3 and L5 PV-FS cells in response to somatic current injection (upper and lower panel, respectively). B. Postsynaptic response of a pair of PV-FS neurons (same pair shown in A). 10 consecutive traces are shown, one of them in black to facilitate visualization. In this case, the superficial, but not the deep PV-FS interneuron, reaches the AP threshold (AP truncated). C. Normalized PSP amplitude for L2/3 vs. L5 PV-FS pairs evoked at two different intensities (165±50µA and 483±71µA, left and right panel respectively). The population PSP amplitude is larger in the superficial PV-FS cells at both stimulus intensities tested, but this difference is reduced with the stronger one. Open circles represent individual values. Black circles represent the mean and error bars the standard error of the mean. Distance from pia was 236±62µA and 528±84µm for L2/3 and L5 PV-FS cells respectively; n=17 pairs, 11 slices from 10 mice. D. PSP peak amplitude for the sample of L5 PV-FS interneurons (same as in C) in response to the strong stimulus. E. Example of a L2/3 vs L5 PV-FS pair in which the AP threshold was reached in the deep neuron (AP truncated). Notice that for the superficial PV-FS cell, the responses at both intensities tested are similar, while for the deep PV-FS cell, the response at 200µA is smaller, but increases with 500µA stimulus. F. For those pairs in which the L5 PV-FS cell strongly responded (>15mV, above the dotted line in D, n=9 pairs from 6 slices and 5 mice), the PSP amplitude was larger in L2/3 PV-FS neurons with the weaker (164±55µA, left panel) but similar with the stronger stimulus (522±205µA, right panel).

Importantly, no differences were detected in the intrinsic properties of superficial and deep PV-FS cells that could predispose the formers to be more excitable (figure 17), indicating that the decreased responsiveness of L5 PV-FS neurons depended on weaker synaptic input from contralateral CPNs.

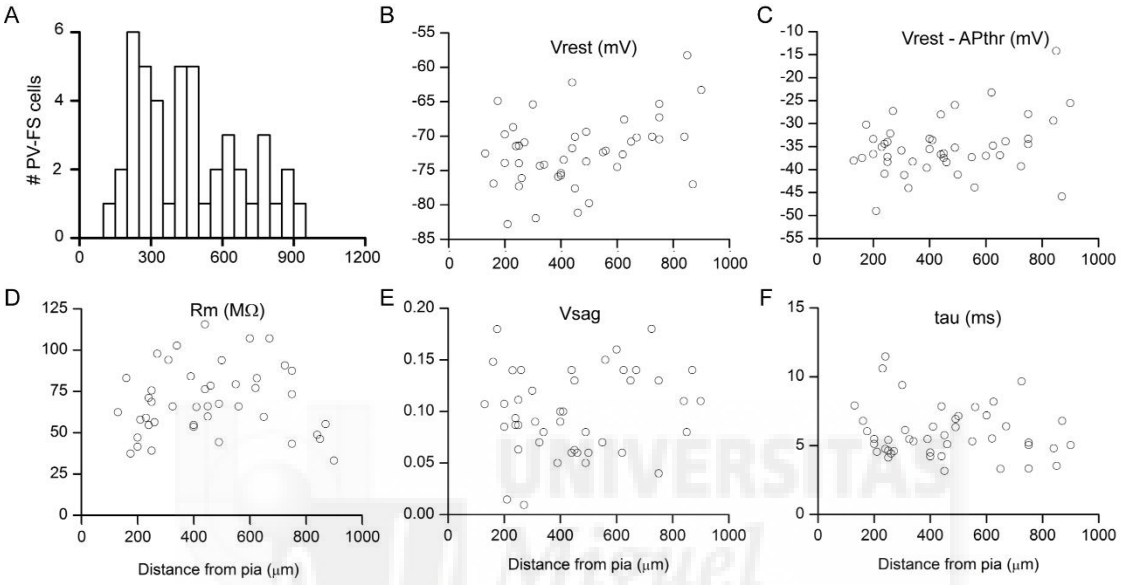

Figure 17. Intrinsic electrophysilogical properties of PV-FS neurons are not laminar dependent. A. Soma to pia distance distribution in a sample of PV-FS neurons for which the intrinsic electrophysiological properties were determined (n=45). B-F. Distribution of intrinsic electrophysiolog,ical properties (resting potential, resting potential to AP threshold difference membrane resistance, voltage sag and membrane time constant) in the sample of PV-FS cells from A. Notice that no differences exist in the intrinsic properties of PV-FS interneurons predisposing superficial ones to be more excitable.

The requirement of a higher stimulus intensity to evoke large PSPs and firing in L5 PV-FS cells, nicely fitted with the shifted input/output curve of IPSCs in L5BL pyramidal neurons towards intense stimuli (figure 11), suggesting that L5 PV-FS cells were the main source of the inhibitory responses evoked in these set of pyramidal cells. This is in agreement with a report indicating that most of the inhibitory synapses in a given pyramidal neuron arise from interneurons whose somas are located in the same layer (Kätzel et al. 2011).

Feedback inhibition in L5BL pyramidal neurons in response to callosal input

The PSP amplitude difference among superficial and layer 5 PV-FS interneurons significantly decreased when the stimulus intensity was increased (figure 16C). Indeed, after excluding those pairs in which the L5 PV-FS interneuron showed relatively low responses (figure 16D; <15mV with the strong stimulus, those below the dotted line), this difference disappeared for the higher intensities, but remained in the responses evoked with the weaker stimulus (figure 16E-F).

This effect pointed to the existence of a second source of excitation, compensating for the weaker callosal input on L5 PV-FS neurons. An obvious possibility was that this subpopulation of PV-FS interneurons were also integrating the ipsilateral input from L5BL pyramidal neurons. Several sources of evidence favoured this hypothesis: (1) L5BL pyramidal neurons in upper layer 5B were recruited by callosal input (figure 5 and 18), (2) the recuitment of L5BL pyramidal neurons occurred at lower stimulus intensities than in layer 5 PV-FS interneurons (figure 18 A-B), (3) L5BL pyramidal neurons are known to synapse on L5 PV-FS cells (Angulo et al. 1999) and (4) the first APs elicited by callosal input on L5BL pyramidal neurons preceded the onset of IPSCs in these neurons (figure 18 C-D).

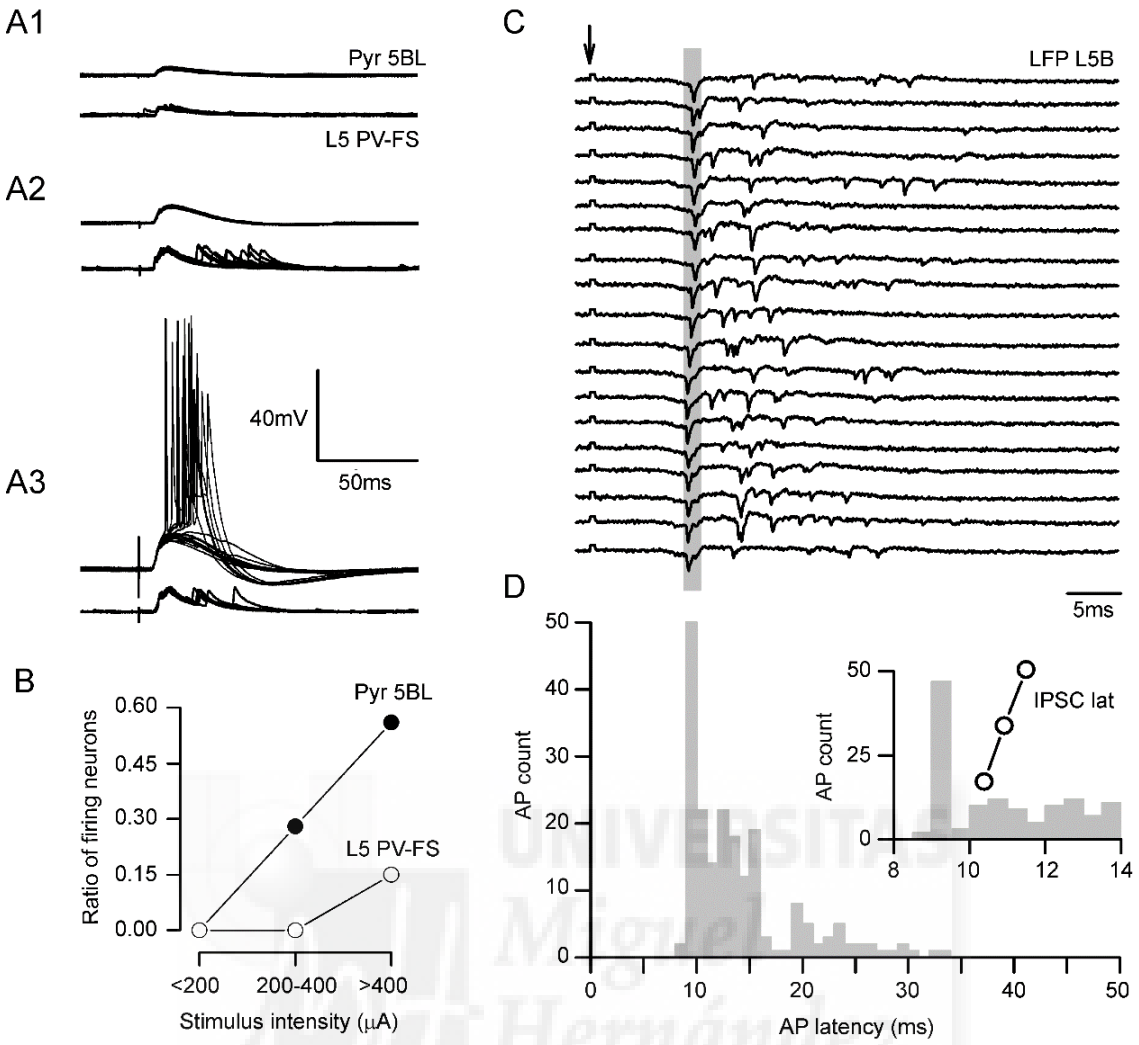

Figure 18. Recruitment of L5BL pyramidal neurons and L5 PV-FS cells by cortical input. A1-3. Example of the responses in a L5BL pyramidal neuron and a L5 PV-FS interneuron sequentially recorded evoked by contralateral stimulation at three different stimulus intensities (100, 200 and 500µA). At least 10 consecutive traces are shown superimposed. B. Ratio of firing neurons in a non-paired sample of L5BL pyramidal neurons and L5 PV-FS interneurons (n=20 and 18, respectively). C. Extracellular recording of the LFP in layer 5B in response to contralateral stimulation. Each trace is an individual response. D. AP latency histogram (1ms time bin) from a sample of L5BL pyramids (n=202 spikes, 10 L5BL pyramids from 8 slices and 7 mice; stimulus intensity 419±223µA). For each neuron, 10 consecutive traces and all the evoked AP were considered. Notice the high synchronicity of the first spike among the sample of pyramidal neurons, whose latency corresponds with the first peak shown in the LFP recording in C. Inset in D shows the same AP latency histogram with a 0.5ms time bin superimposed with the IPSC latency (open circles) measured at 20, 50 and 80% of peak amplitude in the sample of L5BL neurons from figure 11 (n=9; stimulus intensity 611±61µA). AP latency was measured from stimulus onset (indicated by arrows in C) to AP peak.

Moreover, we argued that if the hypothesis of feedback inhibition in layer 5 was correct, the temporal properties of the evoked PSPs in L5 PV-FS neurons should recapitulate the time course of the firing activity of L5BL pyramids. In fact, for the same 9 L2/3 vs L5 PV-FS pairs from figure 16D-F, the slope of the rising phase was slower, the peak amplitude was delayed, and the decay time was longer on L5 PV-FS PSPs (figure 19). Despite the PSP peak amplitude was similar among these PV-FS pairs, the total PSP area was significantly larger on L5 PV-FS ones (figure 19A-B). These differences are expected for neurons integrating two non-synchronic inputs (L5 PV-FS cells) with respect to those integrating the input from one source (L2/3 PV-FS).

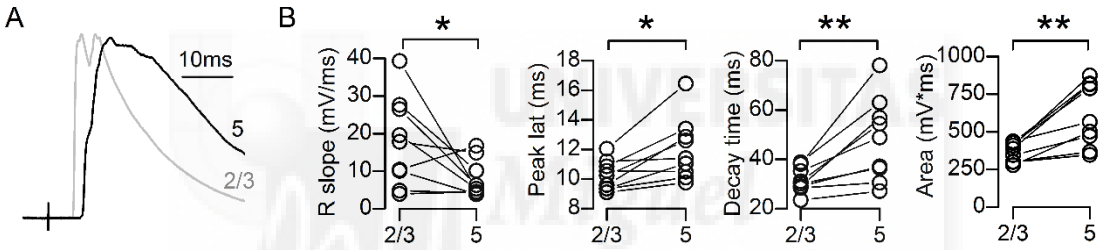

Figure 19. Delayed and prolonged callosal responses in L5 PV-FS interneurons. A. Normalized subthreshold PSP evoked on the L2/3 vs L5 PV-FS pair shown in figure 16E (stimulus intensity 500µA). B. PSP rise slope (20-80%), peak latency, decay time (from peak to 10% of PSP amplitude) and area for the 9 L2/3 vs L5 PV-FS pairs from figure 16F.

Altogether, these data indicate that L5 PV-FS neurons integrate callosal input from contralateral superficial CPNs with the ipsilateral activity of upper L5BL neurons before reaching the AP threshold, suggesting that, at least in part, inhibition on L5BL pyramidal neurons in response to contralateral input is dependent on a feedback mechanism.

Synaptic mechanisms for potent feedforward PV-FS dependent inhibition on superficial pyramidal neurons

As already shown, callosal input recruited a large number of superficial PV-FS interneurons. We recorded the responses evoked by contralateral stimulation in L2/3 pyramidal vs PV-FS neuron pairs at several stimulus intensities (figure 20A-B, n=13). The postsynaptic potentials were clearly larger on PV-FS cells at all intensities tested. With the strongest stimuli, 6/13 PV-FS neurons fired, while none of the pyramidal cells was recruited.

The larger responsiveness of PV-FS cells was explained by the larger amplitude and area of the compound EPSCs in response to callosal input with respect to pyramidal neurons (figure 20C, n=8 pairs). This was at least partially explained by the larger amplitude of unitary callosal EPSC on PV-FS cells (figure 20D). Aditionally, the temporal window to integrate the incoming excitation, this is, the latency between the EPSCs and the IPSCs, was larger on PV-FS cells than in pyramidal cells (figure 20E). Even more, both EPSCs and IPSCs appeared before in PV-FS cells than in pyramidal neurons (figure 20E), favoring their rapid recruitment. Therefore not only he size of the callosal input but also the dynamics of the postsynaptic currents on PV-FS cells also favored their larger responsiveness and their role as a feed-forward inhibitors of superficial pyramidal neurons.

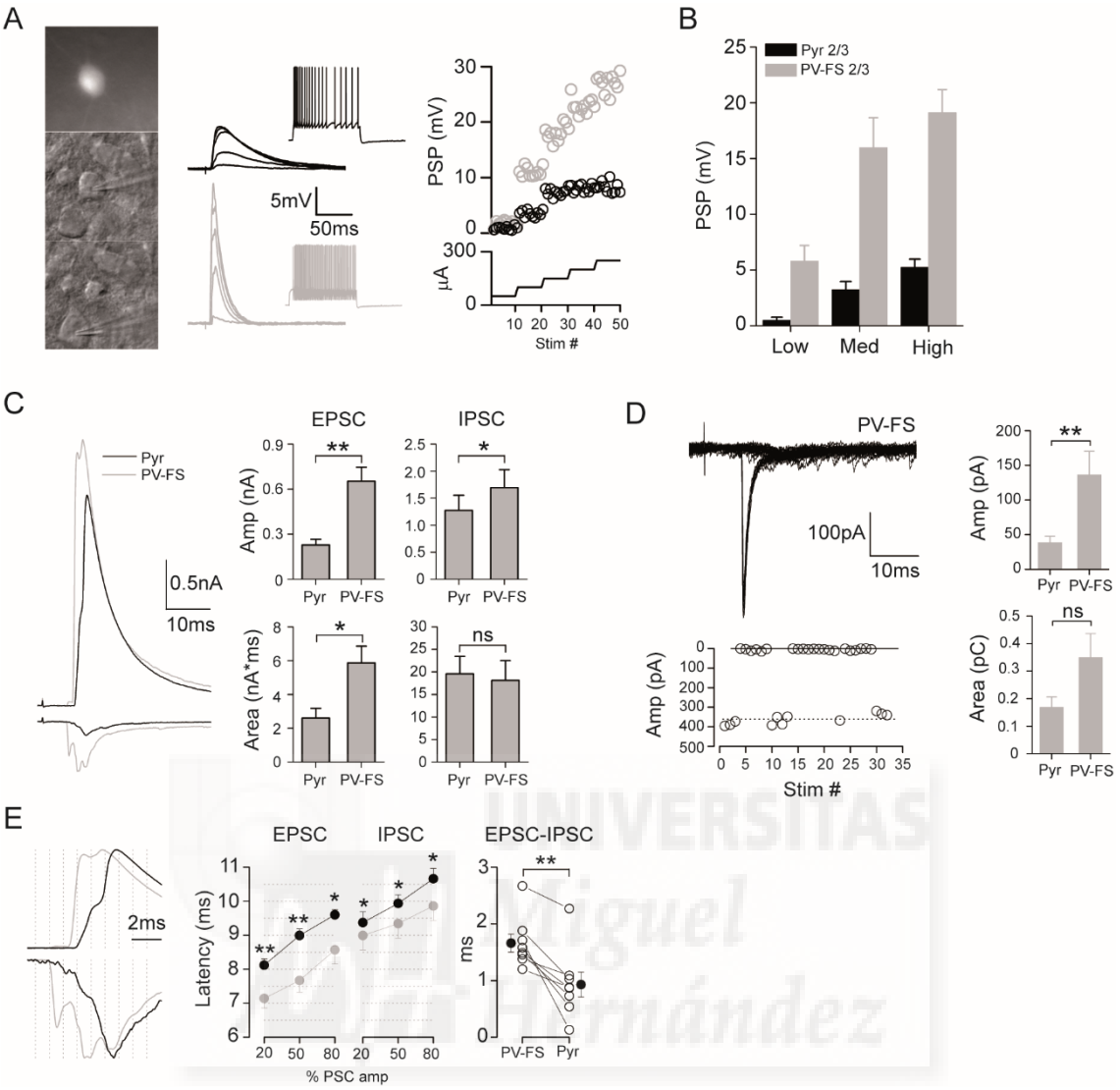

Figure 20. Synaptic mechanisms for potent feed-forward inhibition of L2/3 pyramidal neurons in response to callosal input. A. Left, example of a sequential recording in a superficial pair of neurons formed by a PV-GFP+ FS interneuron and an adjacent pyramidal cell; center; average PSPs evoked in this pair of neurons at increasing stimulus intensities; right, PSP amplitude for individual responses. B. PSP amplitude evoked in a sample of L2/3 pyramidal vs PV-FS interneurons from layer 2/3 (n=8 sequential and 5 simultaneous pairs) at three different intensities (79±25, 192±28 and 492±175μA). Notice that response amplitude is larger on PV-FS cells at the three intensities tested. C. Left, EPSC and IPSC recording in a sequential L2/3 pyramid vs PV-FS pair recorded (stimulus intensity 200μA). Traces are averages of at least 10 consecutive responses. Right, EPSCs evoked on PV-FS cells had a larger peak amplitude and area when compared to EPSCs evoked in pyramidal neurons, while IPSCs were similar (n=8 sequential L2/3 pyramidal vs PV-FS neurons, 6 slices from 5 mice; stimulus intensity 200-400μA). D. Left, example of a putative unitary EPSC evoked in a L2/3 PV-FS neuron (stimulus intensity 18μA); right, callosal uEPSC amplitude was larger on superficial PV-FS neurons with respect to pyramidal cells (n=12 pyramidal neurons from 6 slices and 6 mice and 11 PV-FS from 6 slices from 5mice). E. Left, the responses show in C are amplified to observe their temporal organization. Center, EPSC and IPSC latency measured at 20, 50 and 80% of peak amplitude in the sample of responses shown in C.

Notice that evoked PSCs on PV-FS neurons appear with a shorter latency. Right, temporal window for integration of the excitatory input is larger in PV-FS cells than in pyramidal neurons. Data as mean±s.e.m.

Different IPSC temporal dynamics in L2/3 and L5BL pyramidal neurons

In addition to the different responsiveness of L2/3 and L5BL pyramidal neurons to single pulse stimulation of the contralateral cortex, our previous results (figure 9) also showed a strong inhibitory effect of long-lasting, high frequency (40Hz) trains of callosal input on L2/3 pyramidal neurons. Nonetheless, in these conditions L5BL pyramidal neurons were still potently recruited by the callosal input. To explain this, we studied the temporal dynamics of the inhibitory currents evoked by contralateral stimulation on these neurons.

IPSCs depressed less in L2/3 than in L5BL pyramidal neurons (figure 21). IPSCs evoked in L2/3 pyramidal neurons in response to 4-pulse 40Hz trains were heterogeneous. In some L2/3 pyramidal neurons, IPSCs showed an initial depression that was reversed during the train, being the fourth IPSC larger that the second (figure 21A, upper panel; 21/38 L2/3 neurons), while in others, a steady depression was observed (figure 21A, middle panel; 17/38 L2/3 neurons). In constrast, inhibitory responses evoked on most L5BL showed a progressive depression during the train (figure 21A, lower panel, and 21B), with only 1/16 neurons showing a fourth IPSC larger than the second.

In a different sample of L2/3 vs L5BL pairs sequentially recorded (n=8), we studied the short-term dynamics of the EPSCs and IPSCs in response to 40Hz trains of 20 pulses (figure 21D-E). Both EPSC and IPSCs had similar short-term dynamics in L2/3 pyramidal neurons (figure 21D, upper panel). As a consequence, the E/I balance remained constant along the train in these cells (figure 21E). In contrast, the strong depression of the IPSCs in L5BL pyramidal neurons exceed the reduction in the excitatory conductance (figure 21D, lower panel), increasing the E/I balance of the callosal response through the train, that was mantained larger than in L2/3 pyramidal neurons (figure 21E). This could

explain why L2/3 pyramidal neurons were inhibited with long trains of high-frequency contralateral input while the recruitment of L5BL pyramidal neurons was sustained under these conditions (figure 8 and 9).

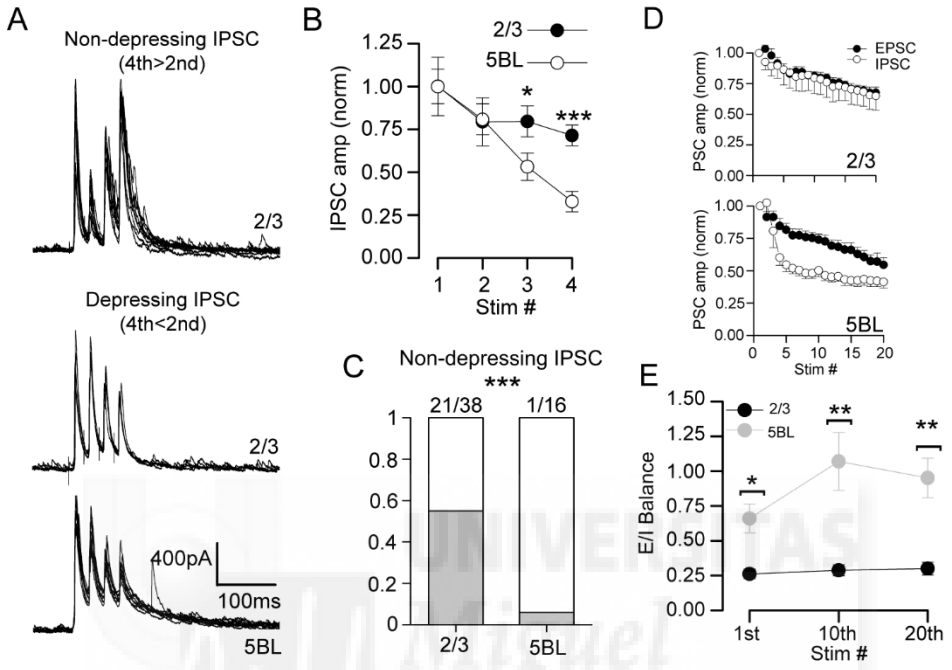

Figure 21. Weak IPSC depression on L2/3 pyramidal neurons. A. IPSCs evoked on two L2/3 and a L5BL pyramidal neurons in response to 40Hz train stimulation. Notice that in one L2/3 neuron, the last IPSC is larger than the second. B. IPSC amplitude for a non-paired sample of L2/3 and L5BL pyramidal neurons (n=38 and 16, stimulus intensity 468±29 and 332±40µA, respectively). IPSC amplitude was measured from valley to peak to remove the effect of temporal summation of successive responses. C. Ratio of non-depressing IPSCs evoked in the same sample as in C. D. Short-term dynamics of the EPSCs and IPSCs evoked in a sample of L2/3 vs L5BL pairs recorded senquentially in response to 20-pulse 40Hz trains of contralateral input (n=8). In this case, summation was included in the measured of amplitude. E. E/I balance measured at the 1st, 10th and last stimulus in the train from the responses in E. In D an E, PSC amplitude includes summation. Population data as mean±s.e.m.

Frequency-dependent recruitment of different superficial inhibitory neurons by callosal input

It has been shown that PV-FS interneurons reduce their responsiveness during high-frequency stimulus (Beierlein et al. 2003, Liu et al. 2014), an effect that depends on the depressing nature of the pyramidal to PV-FS neuron synapse. In addition, PV-FS dependent IPSCs on pyramidal neurons also show a marked short-term depression (Gabernet et al. 2005, Ma et al. 2012, Zaisev and Lewis 2013), reinforcing the reduction in the strenght of PV-FS dependent inhibition during continuous activity. To test if this also happened in response to callosal input, we recorded the responses of L2/3 PV-FS cells to trains of stimuli at different frequencies (range 15-100Hz, figure 22A-D). For subthreshold responses, successive PSPs were clearly depressing (figure 22B-C). As a consequence, the firing probability was markedly reduced through the train (figure 22A and D).

The strong reduction in the responsivenes of PV-FS along 4-pulse 40Hz trains did not match our observations of weak IPSC depression on superficial pyramidal neurons under the same consitions, with more than one half of them showing potentiating IPSCs (figure 21A and C). To explain this discrepancy, we recorded from non PV-FS interneurons of layer 2/3. In 4/12, we observed callosal EPSCs that strongly potentiated during 40Hz trains, but not with lower frequency stimulation (see an example in figure 22E-F). This behaviour should predispose these interneurons to be recruited by high frequency callosal input, becoming a major source of feed-forward inhibition on superficial layers in a context of sustained presynaptic activity, in which PV-FS interneurons are largely silenced. Therefore, it is likely that these non PV-FS interneurons mediated the inhibitory effect triggered by long trains of contralateral input on L2/3 pyramidal neurons.

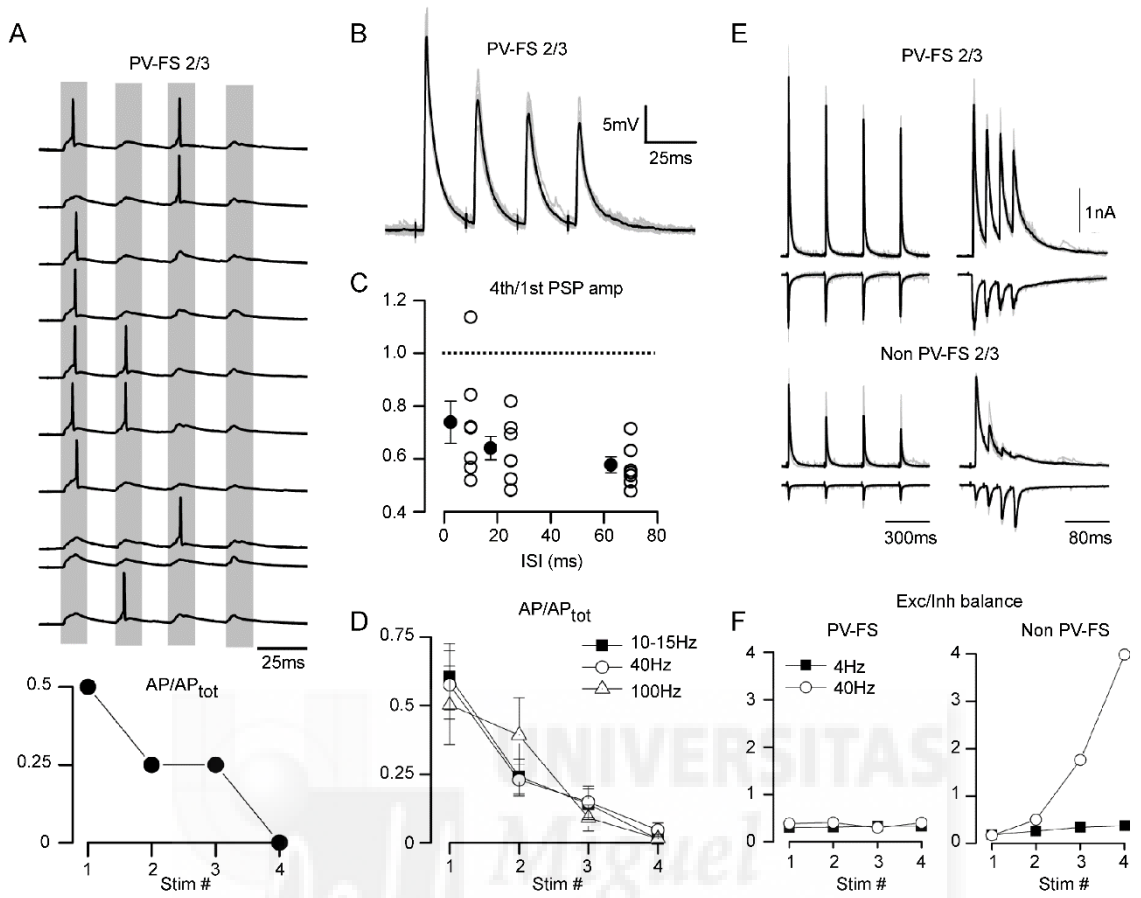

Figure 22. Frequency-dependent recruitment of two different inhibitory networks in superficial layers by callosal input. A. Upper panel, successive suprathreshold responses of a L2/3 PV-FS neuron in response to a 4-pulse 40Hz train applied to the contralateral cortex (stimulus intensity 200µA). Lower panel, number of APs evoked after each stimuli with respect to the total number of evoked APs within 10 consecutive responses. B. Subthreshold responses evoked in the same PV-FS neurons with a 40Hz train (stimulus intensity 100µA). C $4^{th}/1^{st}$ PSP amplitude ratio for subthreshold responses evoked in a sample of PV-FS neurons (n=7) at different stimulus frequencies (15, 40 and 100Hz, interstimulus interval 10, 25 and 70ms, respectively). D. AP ratio, computed as in A, from a sample of L2/3 PV-FS neurons (n=7, 64-96 spikes depending on the frequency tested). For each neuron, ten successive responses for 3 different frequencies (15, 40 and 100Hz) were considered. E. EPSC and IPSC recording from a pair of PV-FS and a non PV-FS interneurons from layer 2/3 in response to 4 (left panel) and 40Hz (right panel) contralateral sitmulus. Notice that the amplitude of the response falls along the train for the PV-FS cell, while the EPSC amplitude is strongly potentiated along the 40Hz train in the case of the non PV-FS neurons. F. E/I balance for the responses shown in E.

DISCUSSION

Specificity of the callosal response across pyramidal neuron subtypes

Our results clearly show that in the agranular RSC, superficial CPNs preferentially target contralateral L2/3 and L5BL pyramidal neurons. Callosal axons branched on two strips in the contralateral cortex, one in the border between layers 1 and 2 and the other in the upper layer 5B, overlapping with the dendritic arbors of these neurons. Indeed, postsynaptic responses elicited by contralateral input were larger on these than in other pyramidal neuron subtypes, including L5A, L5Bm and L6 ones. The observation that in layer 5, callosal connections are strongly biased towards L5BL pyramidal cells is in agreement with a study showing that in its home cortical column, superficial pyramidal neurons have a 10-fold larger connection probability with the large bursting neurons from layer 5B than with layer 5 regular-spiking pyramidal neurons (Thomson and Bannister 1998). Recently, the molecular mechanisms underlying this strong synaptic preference have been described (Harwell et al. 2012). Consistently with our results, the specific molecular interaction between L2/3 pyramidal neuron axons and L5BL pyramidal neuron dendrites also applies to callosal axons from contralateral superficial CPNs.

However, these results contradict two previous reports studying the contribution of callosal input in layer 5 circuits in the mouse cortex. In one, a similar response amplitude was found between thick-tufted and thin-tufted L5 pyramidal neurons of the medial prefrontal cortex (Lee et al. 2014) (notice that thick-tufted neurons correspond to our L5BL pyramidal neuron subtype, while thin-tufted neurons correspond to L5A and L5Bm subtypes). In the auditory cortex, callosal EPSCs were found to be larger in L5 thin-tufted pyramidal neurons than in thick-tufted ones (Rock and Apicella 2015). The divergence between those studies and our results suggests that the local structure of callosal circuits is highly specialized across different cortical areas. One may also

consider that in our case, we focus in the contribution of callosal input from superficial CPNs, while in both other studies no distinction was done regarding the laminar origin of the callosal axons.

In addition, we found that responses of upper L5BL neurons to contralateral stimulation are larger, often eliciting action potential firing on these neurons, when compared to those responses evoked in lower L5BL pyramidal neurons. This is in agreement with the specific pattern of innervation of callosal axons in upper L5B. Similarly, in the motor cortex, superficial pyramidal neurons preferentially target those L5B corticospinal pyramidal neurons located closer to the boundary with L5A (Anderson et al. 2010). In sensory areas, L5B bursting pyramidal neurons with large somas are known to directly integrate thalamocortical input (Constantinople and Bruno 2013). In the barrel cortex, these neurons have been reported to lay close to the boundary with layer 6. A suggestive hypothesis is that while lower layer 5B pyramidal neurons are mainly driven by direct input from the thalamus, forming a microcircuit homologous to the primitive reptilian dorsal cortex, upper L5B neurons could have segregated from this pathway to be integrated in a more elaborated loop of intracortical processing, including thalamus to L4, L4 to L2/3 and L2/3 to L5 steps. It will be worth to test this hypothesis in the close future.

Inhibitory networks recruited by callosal input

Anatomical and physiological evidence for callosal to interneuron connectivity is extensive (Carr and Sesack 1998; Cissé et al. 2003, 2007; Karayannis et al. 2006, Petreanu et al. 2007). Accordingly, we show that PV-FS and non PV-FS gabaergic interneurons from layers 2/3 and 5 receive direct callosal input. In addition, we have demonstrated that, in response to single-pulse stimulation of the contralateral cortex, suprathreshold PSPs

were only found in PV-FS cells, indicating that in these conditions, inhibition evoked by contralateral input on pyramidal neurons is PV-FS dependent. In fact, it is known that PV-FS responsiveness to local excitatory input is larger than in other inhibitory neurons (Mateo et al. 2011, Avermann et al. 2012), stressing the similarities in the impact of callosal and local ipsilateral input.

In response to single-pulse stimulation of the contralateral cortex, large IPSCs were evoked in L2/3 and L5BL pyramidal neurons, while only small amplitude IPSCs were observed in L5A and L5Bm pyramidal neurons. This suggests that PV-FS inhibitory networks are not as unspecific as previously suspected (Packer and Yuste 2011), and that functional specialization must exist, at least in the case of layer 5, where projection-specific pyramidal neurons subtypes are intermingled. Again, the comparison of our results on inhibitory input to layer 5 pyramidal neurons with reports by others gives insight on the organization of layer 5 circuits. Our results are in agreement with a report demonstrating that thicked-tufted but not thin-tufted pyramidal neurons of the medial prefrontal cortex receive input from L5 PV-FS cells (Lee et al. 2014). However, they contrast with a study in the auditory cortex (Rock and Apicella 2015), in which a larger PV-FS dependent inhibitory drive affects layer 5 corticocortical vs corticocollicular pyramidal neurons in response to contralateral input. Overall, these data indicate that a different organization of inhibitory circuits recruited by contralateral input exist across cortical areas, reinforcing the idea of specialization of the local cortical circuits in different cortical regions.

Laminar-dependent effect of callosal input on contralateral circuits

We have also demonstrated that in our preparation, callosal axons from superficial CPNs exert an opposed effect on their two main pyramidal targets. In response to single-pulse

stimulation, the low E/I balance of the callosal response in L2/3 pyramidal neurons transiently clamped these cells at a membrane potential below the action potential threshold, and therefore, spikes were elicited in these neurons with a low probability, even when held at a depolarized membrane potential. A similar scenario applies to the reciprocal connection among layer 2/3 pyramidal neurons in their home column (Mateo et al. 2011, Avermann et al. 2012).

In contrast, callosal input potently recruited large pyramidal neurons from layer 5B. The intrinsic electrophysiological properties of these neurons, including their low input resistance, depolarized resting potential, large voltage sag in response to square current pulse injection and their tendency to fire bursts of action potentials indicate that these neurons correspond to the thick-tufted extratelencephalic projection neurons (Molnár and Cheung 2006). The strong responsiveness of these neurons to callosal input was explained by a larger E/I balance of the callosal response compared to L2/3 ones.

Mechanisms explaining the differential recruitment of L2/3 and L5BL pyramidal neurons (I): callosal convergence

A larger amplitude of the evoked EPSCs on L5BL pyramidal neurons was a major determinant of the larger E/I balance of the callosal response in these neurons, and of the differential recruitment of L5BL and L2/3 pyramidal subtypes. In the case of ipsilateral cortical circuits, studies employing multiple simultaneous whole-cell recordings have shown that a larger convergence exists in the L2/3 to L5BL projection than in the reciprocal L2/3 pathway (compare Thomson and Bannister 1998, Avermann et al 2012, Jouhanneau et al 2015). Accordingly, our estimates of callosal convergence were 2-fold larger on L5BL pyramidal neurons than on L2/3 ones, , stressing the similarities between the callosal input and the projections of superficial pyramidal neurons in their home

column, but no difference was detected in the peak amplitude and area of putative unitary callosal EPSCs evoked with a minimal stimulation protocol.

Mechanisms explaining the differential recruitment of L2/3 and L5BL pyramidal neurons (II): PV-FS dependent feedforward and feedback inhibition

Several lines of evidence indicated that a differential laminar recruitment of PV-FS interneurons in response to callosal input also contributed to the larger responsiveness of L5BL neurons. Superficial PV-FS cells showed large amplitude PSPs even with weak stimulus intensities (about 200µA), reaching the threshold for action potential firing much earlier than surrounding pyramidal neurons. In contrast, layer 5 PV-FS cells showed smaller responses, and only with strong stimuli (>400µA), the AP threshold was reached. In these conditions, the response in many L5BL pyramidal neurons was already suprathreshold. Even more, the response of the L5 PV-FS cells were delayed with respect to the responses in superficial PV-FS neurons, and interestingly, their temporal properties fitted with the firing activity of surrounding L5BL pyramidal neurons. Altogether, these data suggests that in superficial layers, PV-FS dependent inhibition acts as a feedforward mechanism reducing the pool of postsynaptic pyramidal neurons that will response with and AP, therefore increasing the specificity in the response, while in layer 5, PV-FS inhibition acts as a feedback control with a reduced influence in the size of the recruited pool of L5BL neurons.

A similar scenario to the one described here for the integration of callosal input in superficial layers seems to apply for the case of the thalamocortical projection to layer 4 in sensory areas. In a thalamocortical slice preparation, input from the ventrobasal nucleus to layer 4 of the barrel cortex triggers the strong recruitment of PV-FS neurons but not of the pyramidal cells (Gabernet et al. 2005, Cruikshank et al. 2007). In this interneurons,

EPSCs are larger and appear with a lower latency than in the excitatory neurons (Cruikshank et al. 2007), similarly to what we have observed in our preparation. This is in part due to the GluR2 lacking AMPA receptors of PV-FS neurons, which show larger unitary conductance and faster kinetics than AMPA receptors in pyramidal cells (Hull et al. 2009). In addition, thalamic axonal convergence is also larger on PV-FS cells than in pyramidal neurons (Gabernet et al. 2005), further increasing the responsiveness difference among both cell types and favoring the role of PV-FS neurons as the origin of a potent feedforward inhibitory drive.

Nonetheless, less is known regarding the organization of cortical input to superficial and deep PV-FS neurons. Recently, it has been reported that the excitability of PV-FS cells is under control of the transcription factor Er81 (Dehorter et al. 2015). Those PV-FS neurons with higher expression levels of Er81 protein showed a higher frequency of mEPSCs and a lower frequency of mIPSCs, suggesting their larger excitability in response to neuronal activity. Er81 is more abundant among superficial PV-FS cells, and therefore it is expected that the responsiveness of these cells should be larger than those of deeper layers 5, which fits with our observations.

The fact that a potent PV-FS dependent feedforward inhibition controls the initial steps of cortical processing (thalamus to L4 projection and L2/3 reciprocal connectivity) but not the last steps of it (L2/3 to L5 projection) ascribes the allocation of the specificity in the cortical response to a given stimuli in supragranular layers. It would be of interest to check whether if this feedforward inhibitory system is also present in the reptilian cortex, or if it is a mammalian innovation linked to supragranular layers.

Mechanisms explaining the differential recruitment of L2/3 and L5BL pyramidal neurons (III): short-term dynamics of inhibitory currents

The net inhibitory effect of callosal input in L2/3 neurons was maintained in response to long, 40Hz trains of contralateral stimuli, while in L5BL pyramidal cells, the firing activity was sustained under these conditions. The same results were obtained *in vivo* in recordings from L2/3 and L5 pyramidal neurons in response to photoinduced local gamma oscillations in superficial layers (Adesnik and Scanziani 2010). In line with this, we observed that under 40Hz train stimulation, IPSC depression was lower on L2/3 than in L5BL pyramidal neurons, while EPCS short-term dynamics was similar among both cell types. Overall, L2/3 neurons maintained the E/I balance of the callosal response along the train, while L5BL pyramidal cells increased it, explaining why the former were inhibited and the latter sustained their firing in response to ongoing contralateral stimuli.

Interestingly, we found that a subpopulation of superficial non PV-FS cells responded with potentiating callosal EPSCs to 40Hz, but not to 4Hz, stimulation. Inhibitory gabaergic neurons expressing somatostatin form a dense inhibitory matrix in superficial layers of the cortex with a preference for the dendritic domain of pyramidal neurons (Kawaguchi and Kubota 1997, Fino and Yuste 2011). These neurons respond with potentiating EPSCs (Beierlein et al. 2003, Fanselow et al. 2008, Liu et al. 2014), and are known to be recruited with high frequency local pyramidal input. It is likely then, that the long 40Hz trains of contralateral input recruited the population of superficial somatostatin-positive neurons, which in turn, would explain the inhibition of L2/3 pyramidal neurons and the scarce depression of their IPSCs in response to high-frequency stimulation, a scenario in which PV-FS firing was markedly reduced. However, the strong depression of IPSCs in L5BL neurons in response to the same high-frequency stimulation indicates a clear difference between the dynamics of the inhibitory networks in superficial

and deep layers. It is feasible then that, despite somatostatin-positive interneurons also exist in the deeper layers of the neocortex (Lee et al. 2010, Xu et al. 2010), those in layer 5 may be less responsive to callosal input than their superficial counterparts, similarly to what happens with PV-FS cells. This possibility is further suggested by the striking laminar differences existing in the genetic, electrophysiological and morphological properties of these population of gabaergic interneurons (Ma et al. 2006).

Limitations of this study

We have employed an extracellular electrical stimulation approach to study callosal synaptic responses. A potential problem with extracellular stimulation is the antidromic activation of neurons projecting to the recording site, which is exacerbated in our case given the reciprocal nature of callosal connections. However, in our experimental conditions, the contribution of responses caused by the antidromic stimulation of CPN was minimal, at least when using low of medium stimulus intensities. The proportion of recorded neurons quantified in a large sample of neurons was very low: in superficial neurons, which include most CPNs (Fame et al., 2011), less than 4% responded antidromically to stimuli of 100 and 200 μA while in layers 5 and 6, antidromic spikes were never detected.

A second major consideration was the laminar origin of the callosal input being studied. As already mentioned, it is known that most CPNs are located in superficial layers (Fame et al. 2011), and our stimulus electrode was directly placed on these neurons, suggesting a strong bias for this source with respect to the minor populations of CPNs in layers 5 and 6. In addition, we studied the arborization of callosal axons originated in superficial CPNs of the agranular RSC. Their terminal branches occupied two strips, in the boundary of layers 1 and 2 and in the upper part of layer 5B (but not in the lower 5B).

This distribution nicely fitted with the specificity of the responses recorded across pyramidal neurons, with those in layers 2/3 and upper layer 5B showing the larger responses. Altogether, this strongly pointed to the fact that the observations reported here reflect the properties of the callosal input originated in superficial layers.

Finally, the fact that in our conditions, a significant proportion of the subpopulation of upper L5B large pyramids reached the firing threshold implies an additional difficulty. Nonetheless, the impact of local L5BL input in other pyramidal neurons during our experiments must be reduced, since it is known that the connectivity between these neurons and other pyramidal cells is scarce, and mainly limited to synapses formed with other L5BL pyramidal neurons (Markram 1997, Bannister 2005, Le Bé et al. 2007). A further point that reinforces the minimal influence of L5BL firing activity on the responses of pyramidal neurons is that with weak stimulation (100μA), which causes little firing among the upper L5BL neurons, some L5A neurons responded, and the PSP amplitude distribution across the pyramidal neurons was already bimodal indicating that this pattern is already imposed by callosal axons connectivity and that the influence of L5BL firing in our results must be marginal.

A final comment

Overall, the response properties of L2/3 and L5BL pyramidal neurons to callosal input are in line with studies on cortical circuits indicating the sparness in the firing activity of superficial pyramidal neurons and the dense firing regime followed by the large bursting pyramidal neurons in layer 5B (de Kock et al. 2007, Sakata and Harris 2009, Petersen and Crochet 2013). The tight similarities between our observations regarding the callosal input from superficial CPNs and the results from others studying the input from superficial pyramidal neurons in their home column reinforces the hypothesis of a

integrative role of the callosal projection in retrosplenial circuits. Even more, the specificity of the callosal response across the different pyramidal subtypes indicates that superficial CPNs sustain a transhemispheric subnetwork formed by L2/3 and upper L5BL pyramidal neurons, which, as indicated by the specific innervation from PV-FS interneurons, is at least partially segregated from cortical microcircuits including other types of pyramidal neurons.

CONCLUSIONS

1. Els axons callosos de les neurones piramidals superficials del còrtex retrosplenial es ramifiquen en la regió homotòpica contralateral seguint una distribució bimodal, innervant densament el límit entre les capes 1 i 2 i la part superior de la capa 5B.

2. Les neurones piramidals superficials amb projecció callosa del còrtex retrosplenial agranular sinapsen preferentment sobre neurones piramidals contralaterals situades en les capes 2/3 i a la part superior de la capa 5B, en aquest darrer cas específicament sobre aquelles gran piramidals de descàrrega en ràfega.

3. Les neurones piramidals superficials amb projecció callosa del còrtex retrosplenial agranular també sinapsen sobre interneurons inhibidores contralaterals. El tamany de les respostes inhibidores depenent d'interneurones de descàrrega ràpida sobre piramidals contralaterals seguix la mateixa especificitat que les respostes excitadores. Açò indica que la connectivitat entre neurones piramidals i interneurones de descàrrega ràpida es més específica del que previament es pensava.

4. Sota les nostres condicions, l'efecte de l'entrada callosal és netament inhibidor sobre piramidals superficials i excitador sobre les grans piramidals de capa 5B.

5. La diferència en el comportament d'ambdós tipus de neurones piramidals s'explica pel diferent balanç E/I de la resposta callosa, que al seu torn depén del següents factors:

a. Les corrents postsinàptiques calloses excitadores son majors a les grans piramidals de capa 5B. Açò depén d'una major convergència d'axons callosos sobre les segones, pero no de diferències en el tamany de la corrent callosa unitària.
b. Les corrents postsinàptiques inhibidores depenents d'interneurones de descàrrega ràpida evocades en resposta a l'entrada callosa en neurones piramidals superficials aparèixen amb intensitats d'estímul moderades i coincideixen temporalment amb l'excitació callosa. A les grans piramidals de capa 5B, aquestes mateixes corrents inhibidores apareixen amb intensitats d'estímul més elevades i amb major latència. Açò depén del reclutament d'interneurones de descàrrega rápida. A les capes superficials, aquestes interneurones es recluten directa i ràpidament per l'entrada callosa, inhibint les piramidals superficials de forma potent. En canvi, a capa 5, aquestes interneurones responen dèbilment a l'excitació contralateral, i requerixen la descàrrega prèvia de les grans piramidals de capa 5B per disparar.
c. Les diferències en el balanç E/I de la resposta callosa s'accentuen en resposta a trens de 40Hz. Sota aquestes condicions, el balanç es manté constant en neurones piramidals de capa 2/3, ja que la dinàmica a curt termini de les corrents excitadora i inhibidora es similar. En canvi, a les grans piramidals de capa 5B, el component inhibidor deprimeix més que l'excitador, i per tant, el balanç E/I augmenta durant el tren. Aquesta diferència podria estar explicada pel reclutament d'interneurones positives per a somatostatina a les capes superficials.

CONCLUSIONS

1. Superficial CPNs in the agranular RSC project to the contralateral homotopic region where their axons branch following a bimodal pattern, with terminal arbors densely innervating the boundary between layers 1 and 2 and the upper part of layer 5B.

2. Superficial CPNs in the agranular RSC preferentially target contralateral superficial pyramidal neurons and large bursting pyramidal neurons in upper layer 5B, with respect to other subtypes of pyramidal cells.

3. Superficial CPNs also target inhibitory interneurons in the contralateral cortex. PV-FS dependent IPSCs on pyramidal neurons recruited by callosal input follow the same specificity shown by direct callosal excitation, indicating that PV-FS to pyramidal connectivity is not as unspecific as previously thought.

4. In our conditions, the net effect of the callosal input on superficial pyramidal neurons is inhibitory while those large bursting pyramidal cells in layer 5B are potently recruited.

5. The differential effect of callosal input on both targets depends on the different E/I balance of the callosal response on both cell types. This difference is explained by the following reasons:

a. Callosal EPSCs are larger on the large pyramidal neurons from L5B. This depends on a larger degree of callosal convergence on these neurons but not by a larger amplitude of the callosal uEPSC.

b. PV-FS dependent IPSCs on superficial pyramidal neurons appear with relatively moderate stimulus intensities and closely overlapping with callosal excitation, while on large pyramidal neurons from layer 5B, IPSCs require a higher stimulus intensity and show longer latencies. This depends on the larger responsiveness of superficial PV-FS interneurons to callosal input. While these interneurons are directly recruited by callosal axons and provide a potent feedforward inhibitory wave to surrounding pyramidal cells, those PV-FS interneurons in layer 5 only weakly respond to contralateral input but require the previous firing of the L5B pyramidal neurons to reach the threshold.

c. The E/I balance of the callosal response evoked with 40Hz trains is maintained constant in L2/3 pyramidal neurons as similar short-term dynamics apply for both, the callosal EPSCs and feed-forward IPSCs. In contrast, the IPSCs evoked in large pyramidal neurons from layer 5B depress more than callosal EPSCs, increasing the E/I balance of the callosal response during the train in these pyramidal neurons. This difference may be explained by the differential recruitment of somatostatin interneurons in superficial and deep layers of the cortex by callosal input.

REFERENCES

Aboitiz F, Montiel J. 2003. One hundred million years of interhemispheric communication: the history of the corpus callosum. Braz J Med Biol Res. 36:409-20

Adesnik H, Scanziani M. 2010. Lateral competition for cortical space by layer-specific horizontal circuits. Nature. 464:1155-60

Allmann J. 1990. Evolution of the neocortex. In Cerebral cortex vol8A:269-83. Plenum Press.

Anderson CT, Sheets PL, Kiritani T, Shepherd GM. 2010. Sublayer-specific microcircuits of corticospinal and corticostriatal neurons in motor cortex. Nat Neurosci. 13:739-44

Angulo MC, Rossier J, Audinat E. 1999. Postsynaptic glutamate receptors and integrative properties of fast-spiking interneurons in the rat neocortex. J Neurophysiol. 82:1295-302

Apicella AJ, Wickersham IR, Seung HS, Shepherd GM. 2012. Laminarly orthogonal excitation of fast-spiking and low-threshold-spiking interneurons in mouse motor cortex. J Neurosci. 32:7021-33

Atallah BV, Bruns W, Carandini M, Scanziani M. 2012. Parvalbumin-expressing interneurons linearly transform cortical responses to visual stimuli. Neuron. 73:159-70

Avermann M, Tomm C, Mateo C, Gerstner W, Petersen CC. 2012. Microcircuits of excitatory and inhibitory neurons in layer 2/3 of mouse barrel cortex. J Neurophysiol. 107:3116-34

Azevedo FA, Carvalho LR, Grinberg LT, Farfel JM, Ferretti RE, Leite RE, Jacob Filho W, Lent R, Herculano-Houzel S. 2009. Equal numbers of neuronal and nonneuronal cells make the human brain an isometrically scaled-up primate brain. J Comp Neurol. 513:532-41

Bannister AP. 2005. Inter- and intra-laminar connections of pyramidal cells in the neocortex. Neurosci Res. 53:95-103

Bartos M, Vida I, Jonas P. Synaptic mechanisms of synchronized gamma oscillations in inhibitory interneuron networks. Nat Rev Neurosci. 8:45-56

Beaulé V, Tremblay S, Théoret H. 2012. Interhemispheric control of unilateral movement. Neural Plast. 2012:627816

Beierlein M, Gibson JR, Connors BW. 2003. Two dynamically distinct inhibitory networks in layer 4 of the neocortex. J Neurophysiol. 90:2987-3000

Berezovskii VK, Nassi JJ, Born RT. 2011. Segregation of feedforward and feedback projections in mouse visual cortex. J Comp Neurol. 519:3672-83

Binzegger T, Douglas RJ, Martin KA. 2004. A quantitative map of the circuit of cat primary visual cortex. J Neurosci. 24:8441-53

Blakemore C, Diao YC, Pu ML, Wang YK, Xiao YM. 1983. Possible functions of the interhemispheric connexions between visual cortical areas in the cat. J Physiol. 337:331-49

Blasdel GG. 1992. Orientation selectivity, preference, and continuity in monkey striate cortex. J Neurosci. 12:3139-61.

Bloom JS, Hynd GW. 2005. The role of the corpus callosum in interhemispheric transfer of information: excitation or inhibition? Neuropsychol Rev. 15:59-71

Bock DD, Lee WC, Kerlin AM, Andermann ML, Hood G, Wetzel AW, Yurgenson S, Soucy ER, Kim HS, Reid RC. 2011. Network anatomy and in vivo physiology of visual cortical neurons. Nature. 471:177-82

Borrell V, Reillo I. 2012. Emerging roles of neural stem cells in cerebral cortex development and evolution. Dev Neurobiol. 72:955-71

Bortone DS, Olsen SR, Scanziani M. 2014. Translaminar inhibitory cells recruited by layer 6 corticothalamic neurons suppress visual cortex. Neuron. 82:474-85

Boucsein C, Nawrot MP, Schnepel P, Aertsen A. 2011. Beyond the cortical column: abundance and physiology of horizontal connections imply a strong role for inputs from the surround. Front Neurosci. 2011 5:32

Brodmann K. 2006. Localisation in the cerebral cortex. Springer.

Carlo CN, Stevens CF. 2013. Structural uniformity of neocortex, revisited. PNAS. 110:1488-93

Carr DB, Sesack SR. 1998. Callosal terminals in the rat prefrontal cortex: synaptic targets and association with GABA-immunoreactive structures. Synapse. 29:193-205

Cissé Y, Grenier F, Timofeev I, Steriade M. 2003. Electrophysiological properties and input-output organization of callosal neurons in cat association cortex. J Neurophysiol. 89:1402-13.

Cissé Y, Nita DA, Steriade M, Timofeev I. 2007. Callosal responses of fast-rhythmic-bursting neurons during slow oscillation in cats. Neuroscience 147:272-6

Czajkowski R, Jayaprakash B, Wiltgen B, Rogerson T, Guzman-Karlsson MC, Barth AL, Trachtenberg JT, Silva AJ. 2014. Encoding and storage of spatial information in the retrosplenial cortex. Proc Natl Acad Sci U S A. 111:8661-6

Chowdhury SA, Matsunami KI. 2002. GABA-B-related activity in processing of transcallosal response in cat motor cortex. J Neurosci Res. 68:489-95.

Cheung AF, Pollen AA, Tavare A, DeProto J, Molnár Z. 2007. Comparative aspects of cortical neurogenesis in vertebrates. J Anat 211:164-76

Collins CE, Airey DC, Young NA, Leitch DB, Kaas JH. 2010. Neuron densities vary across and within cortical areas in primates. PNAS. 107:15927-32

Connors BW, Gutnick MJ, Prince DA. 1982. Electrophysiological properties of neocortical neurons in vitro. J Neurophysiol. 48:1302-20.

Connors BW, Kriegstein AR. 1986. Cellular physiology of the turtle visual cortex: distinctive properties of pyramidal and stellate neurons. J Neurosci. 6:164-77

Connors BW, Gutnick MJ. 1990. Intrinsic firing patterns of diverse neocortical neurons. Trends Neurosci. 13:99-104

Constantinople CM, Bruno RM. 2011. Effects and mechanisms of wakefulness on local cortical networks. Neuron. 69:1061-8

Constantinople CM, Bruno RM. 2013. Deep cortical layers are activated directly by thalamus. Science. 340:1591-4

Covic EN, Sherman SM. 2011. Synaptic properties of connections between the primary and secondary auditory cortices in mice. Cereb Cortex. 21:2425-41

Cruikshank SJ, Lewis TJ, Connors BW. 2007. Synaptic basis for intense thalamocortical activation of feedforward inhibitory cells in neocortex. Nat Neurosci. 10:462-8

Decosta-Fortune TM, Li CX, de Jongh Curry AL, Waters RS. 2015. Differential pattern of interhemispheric connections between homotopic layer V regions in the forelimb representation in rat barrel field cortex. Anat Rec (Hoboken). 298:1885-902

DeFelipe J. 2011. The evolution of the brain, the human nature of cortical circuits, and intellectual creativity. Front Neuroanat. 5:29

Dehorter N, Ciceri G, Bartolini G, Lim L, del Pino I, Marín O. 2015. Tuning of fast-spiking interneuron properties by an activity-dependent transcriptional switch. Science. 349:1216-20

de Kock CP, Bruno RM, Spors H, Sakmann B. 2007. Layer- and cell-type-specific suprathreshold stimulus representation in rat primary somatosensory cortex. J Physiol. 581:139-54

De Pasquale R, Sherman SM. 2011. Synaptic properties of corticocortical connections between the primary and secondary visual cortical areas in the mouse. J Neurosci. 31:16494-506

Deuchars J, West DC, Thomson AM. 1994. Relationships between morphology and physiology of pyramid-pyramid single axon connections in rat neocortex in vitro. J Physiol. 478:423-35

Donkelaar HJT. Reptiles. In: The central nervous system of vertebrates Volume 2. Springer-Verlag. 1998:1315

Donkelaar HJT b. Anurans. In: The central nervous system of vertebrates Volume 2. Springer-Verlag. 1998:1151

Douglas RJ, Martin KAC. Canonical cortical circuits. In Handbook of brain microcircuits. Oxford University Press. 2010:15-21.

Engel AK, König P, Kreiter AK, Singer W. 1991. Interhemispheric synchronization of oscillatory neuronal responses in cat visual cortex. 252:1177-9

Fanselow EE, Richardson KA, Connors BW. 2008. Selective, state-dependent activation of somatostatin-expressing inhibitory interneurons in mouse neocortex. J Neurophysiol. 100:2640-52

Feldmeyer D, Egger V, Lubke J, Sakmann B. 1999. Reliable synaptic connections between pairs of excitatory layer 4 neurones within a single 'barrel' of developing rat somatosensory cortex. J Physiol. 521:169-90

Feldmeyer D, Lübke J, Silver RA, Sakmann B. 2002. Synaptic connections between layer 4 spiny neurone-layer 2/3 pyramidal cell pairs in juvenile rat barrel cortex: physiology and anatomy of interlaminar signalling within a cortical column. J Physiol. 538:803-22

Feldmeyer D, Lübke J, Sakmann B. 2006. Efficacy and connectivity of intracolumnar pairs of layer 2/3 pyramidal cells in the barrel cortex of juvenile rats. J Physiol. 575:583-602

Fishell G, Rudy B. 2011. Mechanisms of inhibition within the telencephalon: "where the wild things are". Annu Rev Neurosci. 34:535-67

Frick A, Feldmeyer D, Helmstaedter M, Sakmann B. 2008. Monosynaptic connections between pairs of L5A pyramidal neurons in columns of juvenile rat somatosensory cortex. Cereb Cortex. 18:397-406

Florio M, Huttner WB. 2014. Neural progenitors, neurogenesis and the evolution of the neocortex. Development. 141:2182-94

Fino E, Yuste R. 2011. Dense inhibitory connectivity in neocortex. Neuron. 69:1188-203

Fuster JM, Bressler SL. 2015. Past makes future: role of pFC in prediction. J Cogn Neurosci. 27:639-54

Gabernet L, Jadhav SP, Feldman DE, Carandini M, Scanziani M. 2005. Somatosensory integration controlled by dynamic thalamocortical feed-forward inhibition. Neuron. 48:315-27

Georgopoulos AP, Merchant H, Naselaris T, Amirikian B. 2007. Mapping of the preferred direction in the motor cortex. PNAS 104:11068-72

Glasser MF, Coalson TS, Robinson EC, Hacker CD, Harwell J, Yacoub E, Ugurbil K, Andersson J, Beckmann CF, Jenkinson M, Smith SM, Van Essen DC. 2016. A multi-modal parcellation of human cerebral cortex. Nature. doi: 10.1038

Goldman PS, Nauta WJ. 1977. Columnar distribution of cortico-cortical fibers in the frontal association, limbic, and motor cortex of the developing rhesus monkey. Brain Res. 122:393-413

Gray CM, König P, Engel AK, Singer W. 1989. Oscillatory responses in cat visual cortex exhibit inter-columnar synchronization which reflects global stimulus properties. Nature. 338:334-7

Harris KD, Mrsic-Flogel TD. 2013. Cortical connectivity and sensory coding. Nature. 503:51-8

Harwell CC, Parker PR, Gee SM, Okada A, McConnell SK, Kreitzer AC, Kriegstein AR. 2012. Sonic hedgehog expression in corticofugal projection neurons directs cortical microcircuit formation. Neuron 73:1116-26

Helmstaedter M, Staiger JF, Sakmann B, Feldmeyer D. 2008. Efficient recruitment of layer 2/3 interneurons by layer 4 input in single columns of rat somatosensory cortex. J Neurosci. 28:8273-84

Herculano-Houzel S, Collins CE, Wong P, Kaas JH, Lent R. 2008. The basic nonuniformity of the cerebral cortex. PNAS. 105:12593-8

Hippenmeyer S, Vrieseling E, Sigrist M, Portmann T, Laengle C, Ladle DR, Arber S. 2005. A developmental switch in the response of DRG neurons to ETS transcription factor signaling. PLoS Biol. 3:e159.

Hirsch JA, Martinez LM. 2006. Laminar processing in the visual cortical column. Curr Opin Neurobiol. 16:377-84

Hlushchuk Y, Hari R. 2006. Transient suppression of ipsilateral primary somatosensory cortex during tactile finger stimulation. J Neurosci. 26:5819-24

Holtzman JD, Gazzaniga MS. 1982. Dual task interactions due exclusively to limits in processing resources. Science. 218:1325-7

Horton JC, Adams DL. 2005. The cortical column: a structure without a function. Philos Trans R Soc Lond B Biol Sci. 360:837-62

Hubel DH, Wiesel TN. 1967. Cortical and callosal connections concerned with the vertical meridian of visual fields in the cat. J Neurophysiol. 30:1561-73

Hubel DH, Wiesel TN. 1968. Receptive fields and functional architecture of monkey striate cortex. J Physiol. 195:215-43

Hull C, Isaacson JS, Scanziani M. 2009. Postsynaptic mechanisms govern the differential excitation of cortical neurons by thalamic inputs. J Neurosci. 29:9127-36

Hutsler JJ, Lee DG, Porter KK. 2005. Comparative analysis of cortical layering and supragranular layer enlargement in rodent carnivore and primate species. Brain Res. 1052:71-81

Irlbacher K, Brocke J, Mechow JV, Brandt SA. 2006. Effects of GABA(A) and GABA(B) agonists on interhemispheric inhibition in man. Clin Neurophysiol. 118:308-16

Isaacson JS, Scanziani M. 2011. How inhibition shapes cortical activity. Neuron. 72:231-43

Iwamura Y. 2000. Bilateral receptive field neurons and callosal connections in the somatosensory cortex. Philos Trans R Soc Lond B Biol Sci. 355:267-73.

Jouhanneau JS, Kremkow J, Dorrn AL, Poulet JF. 2015. In vivo monosynaptic excitatory transmission between layer 2 cortical pyramidal neurons. Cell Rep. 13:2098-106

Kaneko T. 2013. Local connections of excitatory neurons in motor-associated cortical areas of the rat. Front Neural Circuits. 7:75

Karayannis T, Huerta-Ocampo I, Capogna M. 2007. GABAergic and pyramidal neurons of deep cortical layers directly receive and differently integrate callosal input. Cereb Cortex. 17:1213-26

Kätzel D, Zemelman BV, Buetfering C, Wölfel M, Miesenböck G. 2011. The columnar and laminar organization of inhibitory connections to neocortical excitatory cells. Nat Neurosci. 14:100-7

Kawaguchi Y. 1992. Receptor subtypes involved in callosally-induced postsynaptic potentials in rat frontal agranular cortex in vitro. Exp Brain Res. 88:33-40

Kawaguchi Y, Kubota Y. 1997. GABAergic cell subtypes and their synaptic connections in rat frontal cortex. Cereb Cortex. 7:476-86

Kerlin AM, Andermann ML, Berezovskii VK, Reid RC. 2010. Broadly tuned response properties of diverse inhibitory neuron subtypes in mouse visual cortex. Neuron. 67:858-71

Kim EJ, Juavinett AL, Kyubwa EM, Jacobs MW, Callaway EM. 2015. Three types of cortical layer 5 neurons that differ in brain-wide connectivity and function. Neuron. 88:1253-67

Kim J, Matney CJ, Blankenship A, Hestrin S, Brown SP. 2014. Layer 6 corticothalamic neurons activate a cortical output layer, layer 5a. J Neurosci. 34:9656-64

Ko H, Hofer SB, Pichler B, Buchanan KA, Sjöström PJ, Mrsic-Flogel TD. 2011. Functional specificity of local synaptic connections in neocortical networks. Nature. 473:87-91

Kumar SS, Huguenard JR. 2001. Properties of excitatory synaptic connections mediated by the corpus callosum in the developing rat neocortex. J Neurophysiol. 86:2973-85

Kumar SS, Huguenard JR. 2003. Pathway-specific differences in subunit composition of synaptic NMDA receptors on pyramidal neurons in neocortex. J Neurosci. 23:10074-83

Lamme VA, Zipser K, Spekreijse H. 1998. Figure-ground activity in primary visual cortex is suppressed by anesthesia. PNAS. 95:3263-8

Le Bé JV, Silberberg G, Wang Y, Markram H. 2007. Morphological, electrophysiological, and synaptic properties of corticocallosal pyramidal cells in the neonatal rat neocortex. Cereb Cortex. 17:2204-13

Lee AT, Gee SM, Vogt D, Patel T, Rubenstein JL, Sohal VS. 2014. Pyramidal neurons in prefrontal cortex receive subtype-specific forms of excitation and inhibition. Neuron. 81:61-8

Lee S, Hjerling-Leffler J, Zagha E, Fishell G, Rudy B. 2010. The largest group of superficial neocortical GABAergic interneurons expresses ionotropic serotonin receptors. J Neurosci. 30:16796-808

Lee S, Kruglikov I, Huang ZJ, Fishell G, Rudy B. 2013. A disinhibitory circuit mediates motor integration in the somatosensory cortex. Nat Neurosci. 16:1662-70

Lee WC, Bonin V, Reed M, Graham BJ, Hood G, Glattfelder K, Reid RC. 2016. Anatomy and function of an excitatory network in the visual cortex. Nature. 532:370-4

Lefort S, Tomm C, Floyd Sarria JC, Petersen CC. 2009. The excitatory neuronal network of the C2 barrel column in mouse primary somatosensory cortex. Neuron. 61:301-16

Lewis WB. 1880. Researches on the comparative structure of the cortex cerebri. Phil. Trans. R. Soc. Lond. 171:35-64

Liu YC, Cheng JK, Lien CC. 2014. Rapid dynamic changes of dendritic inhibition in the dentate gyrus by presynaptic activity patterns. J Neurosci. 34:1344-57

Lorente de Nó R. Arquitectonics and structure of the cerebral cortex. In Physiology of the nervous system. Oxford University Press. 1938: 291-330.

Luck SJ, Hillyard SA, Mangun GR, Gazzaniga MS. 1989. Independent hemispheric attentional systems mediate visual search in split-brain patients. Nature. 342:543-5.

Ma Y, Hu H, Berrebi AS, Mathers PH, Agmon A. 2006. Distinct subtypes of somatostatin-containing neocortical interneurons revealed in transgenic mice. J Neurosci. 26:5069-82

Ma Y, Hu H, Agmon A. 2012. Short-term plasticity of unitary inhibitory-to-inhibitory synapses on the presynaptic interneuron subtype. J Neurosci. 32:983-8

Markram H. 1997. A network of tufted layer 5 pyramidal neurons. Cereb Cortex. 7:523-33.

Markram H, Lübke J, Frotscher M, Roth A, Sakmann B. 1997. Physiology and anatomy of synaptic connections between thick tufted pyramidal neurones in the developing rat neocortex. J Physiol. 500:409-40

Markram H, Toledo-Rodriguez M, Wang Y, Gupta A, Silberberg G, Wu C. 2004. Interneurons of the neocortical inhibitory system. Nat Rev Neurosci. 5:793-807

Markram H, Muller E, Ramaswamy S, Reimann MW, Abdellah M, Sanchez CA, Ailamaki A, Alonso-Nanclares L, Antille N, Arsever S, Kahou GA, Berger TK, Bilgili A, Buncic N, Chalimourda A, Chindemi G, Courcol JD, Delalondre F,

Delattre V, Druckmann S, Dumusc R, Dynes J, Eilemann S, Gal E, Gevaert ME, Ghobril JP, Gidon A, Graham JW, Gupta A, Haenel V, Hay E, Heinis T, Hernando JB, Hines M, Kanari L, Keller D, Kenyon J, Khazen G, Kim Y, King JG, Kisvarday Z, Kumbhar P, Lasserre S, Le Bé JV, Magalhães BR, Merchán-Pérez A, Meystre J, Morrice BR, Muller J, Muñoz-Céspedes A, Muralidhar S, Muthurasa K, Nachbaur D, Newton TH, Nolte M, Ovcharenko A, Palacios J, Pastor L, Perin R, Ranjan R, Riachi I, Rodríguez JR, Riquelme JL, Rössert C, Sfyrakis K, Shi Y, Shillcock JC, Silberberg G, Silva R, Tauheed F, Telefont M, Toledo-Rodriguez M, Tränkler T, Van Geit W, Díaz JV, Walker R, Wang Y, Zaninetta SM, DeFelipe J, Hill SL, Segev I, Schürmann F. 2015. Reconstruction and simulation of neocortical microcircuitry. Cell. 163:456-92

Mateo C, Avermann M, Gentet LJ, Zhang F, Deisseroth K, Petersen CC. 2011. In vivo optogenetic stimulation of neocortical excitatory neurons drives brain-state-dependent inhibition. Curr Biol. 21:1593-602

Mioche L, Singer W. 1989. Chronic recordings from single sites of kitten striate cortex during experience-dependent modifications of receptive-field properties. J Neurophysiol. 62:185-97

Mitchell BD, Macklis JD. 2005. Large-scale maintenance of dual projections by callosal and frontal cortical projection neurons in adult mice. J Comp Neurol. 482:17-32

Mizuno H, Hirano T, Tagawa Y. 2007. Evidence for activity-dependent cortical wiring: formation of interhemispheric connections in neonatal mouse visual cortex requires projection neuron activity. J Neurosci. 27:6760-70

Molnár Z, Cheung AF. 2006. Towards the classification of subpopulations of layer V pyramidal projection neurons. Neurosci Res. 55:105-15

Molyneaux BJ, Arlotta P, Fame RM, MacDonald JL, MacQuarrie KL, Macklis JD. 2009. Novel subtype-specific genes identify distinct subpopulations of callosal projection neurons. J Neurosci. 29:12343-54.

Morgenstern NA, Bourg J, Petreanu L. 2016. Multilaminar networks of cortical neurons integrate common inputs from sensory thalamus. Nat Neurosci. 19:1034-40

Mountcastle VB. 1957. Modality and topographic properties of single neurons of cat's somatic sensory cortex. J Neurophysiol 20:408-34

Mountcastle VB. An organizing principle for cerebral function: the unite module and the distributed system. In The Mindful Brain. 1978:7-50.

Mountcastle VB. 2003. Introduction. Computation in cortical columns. Cereb Cortex. 13:2-4

Mumford D. 1992. On the computational architecture of the neocortex. II. The role of cortico-cortical loops. Biol Cybern. 66:241-51

Narayanan RT, Egger R, Johnson AS, Mansvelder HD, Sakmann B, de Kock CP, Oberlaender M. 2015. Beyond columnar organization: cell type- and target layer-specific principles of horizontal axon projection patterns in rat vibrissal cortex. Cereb Cortex. 25:4450-68

Naumann RK, Ondracek JM, Reiter S, Shein-Idelson M1 Tosches MA, Yamawaki TM, Laurent G. 2015. The reptilian brain. Curr Biol. 25:R317-21.

Neher E, Sakmann B. 1976. Single-channel currents recorded from membrane of denervated frog muscle fibres. Nature. 260:799-802

Nelson S. 2002. Cortical microcircuits: diverse or canonical? Neuron. 36:19-27

Nieuwenhuys JVR, van Dongen PAM, Donkelaar HJT. Mammals. In The central nervous system of vertebrates Volume 3. Springer-Verlag. 1998:1637

Nishikimi M, Oishi K, Tabata H, Torii K, Nakajima K. 2011. Segregation and pathfinding of callosal axons through EphA3 signaling. J Neurosci. 31:16251-60

Nomura T, Ohtaka-Maruyama C, Yamashita W, Wakamatsu Y, Murakami Y, Calegari F, Suzuki K, Gotoh H, Ono K. 2016. The evolution of basal progenitors in the developing non-mammalian brain. Development. 143:66-74

Olivares R, Montiel J, Aboitiz F. 2001. Species differences and similarities in the fine structure of the mammalian corpus callosum. Brain Behav Evol. 57:98-105

Olkowicz S, Kocourek M, Lučan RK, Porteš M, Fitch WT, Herculano-Houzel S, Němec P. 2016. Birds have primate-like numbers of neurons in the forebrain. PNAS. 113:7255-60

Otsuka T, Kawaguchi Y. 2008. Firing-pattern-dependent specificity of cortical excitatory feed-forward subnetworks. J Neurosci. 28:11186-95

Packer AM, Yuste R. 2011. Dense, unspecific connectivity of neocortical parvalbumin-positive interneurons: a canonical microcircuit for inhibition? J Neurosci. 31:13260-71

Palmer LM, Schulz JM, Murphy SC, Ledergerber D, Murayama M, Larkum ME. 2012. The cellular basis of GABA(B)-mediated interhemispheric inhibition. Science 335:989-93

Petersen CC, Crochet S. 2013. Synaptic computation and sensory processing in neocortical layer 2/3. Neuron. 78:28-48

Petilla Interneuron Nomenclature Group. 2008. Petilla terminology: nomenclature of features of GABAergic interneurons of the cerebral cortex. Nat Rev Neurosci. 9:557-68

Petreanu L, Huber D, Sobczyk A, Svoboda K. 2007. Channelrhodopsin-2-assisted circuit mapping of long-range callosal projections. Nat Neurosci. 10:663-8

Pfeffer CK, Xue M, He M, Huang ZJ, Scanziani M. 2013. Inhibition of inhibition in visual cortex: the logic of connections between molecularly distinct interneurons. Nat Neurosci. 16:1068-76

Pi HJ, Hangya B, Kvitsiani D, Sanders JI, Huang ZJ, Kepecs A. 2013. Cortical interneurons that specialize in disinhibitory control. Nature. 503:521-4

Pouille F, Scanziani M. 2001. Enforcement of temporal fidelity in pyramidal cells by somatic feed-forward inhibition. Science. 293:1159-63

Puelles L. 2001. Brain segmentation and forebrain development in amniotes. Brain Res Bull 55:695–710

Puelles L, Harrison M, Paxinos G, Watson C. 2013. A developmental ontology for the mammalian brain based on the prosomeric model. Trends Neurosci. 36:570-8

Purves D, Riddle DR, LaMantia AS. 1992. Iterated patterns of brain circuitry (or how the cortex gets its spots). Trends Neurosci. 15:362-8

Rakic P. 1971. Guidance of neurons migrating to the fetal monkey neocortex. Brain Res. 33:471-6

Rakic P. 1972. Mode of cell migration to the superficial layers of fetal monkey neocortex. J Comp Neurol. 145:61-83

Rakic P. 1974. Neurons in rhesus monkey visual cortex: systematic relation between time of origin and eventual disposition. Science 183:425-7

Rakic P. 1988. Specification of cerebral cortical areas. Science 241:170-6

Rakic P. 2008. Confusing cortical columns. PNAS. 105:12099-100

Ramos RL, Tam DM, Brumberg JC. 2008. Physiology and morphology of callosal projection neurons in mouse. Neuroscience. 153:654-63

Rehkämper G, Frahm HD, Zilles K. 1991. Quantitative development of brain and brain structures in birds (galliformes and passeriformes) compared to that in mammals (insectivores and primates). Brain Behav Evol. 37:125-43.

Reiner A. 1993. Neurotransmitter organization and connections of turtle cortex: implications for the evolution of mammalian isocortex. Comp Biochem Physiol Comp Physiol. 104:735-48

Reis J, Swayne OB, Vandermeeren Y, Camus M, Dimyan MA, Harris-Love M, Perez MA, Ragert P, Rothwell JC, Cohen LG. 2008. Contribution of transcranial magnetic stimulation to the understanding of cortical mechanisms involved in motor control. J Physiol. 586:325-51

Reyes-Puerta V, Sun JJ, Kim S, Kilb W, Luhmann HJ. 2015. Laminar and columnar structure of sensory-evoked multineuronal spike sequences in adult rat barrel cortex in vivo. Cereb Cortex. 25:2001-21.

Ringach DL, Mineault PJ, Tring E, Olivas ND, Garcia-Junco-Clemente P, Trachtenberg JT. 2016. Spatial clustering of tuning in mouse primary visual cortex. Nat Commun. 7:12270

Ringo JL, Doty RW, Demeter S, Simard PY. 1994. Time is of the essence: a conjecture that hemispheric specialization arises from interhemispheric conduction delay. Cereb Cortex. 4:331-43

Rock C, Apicella AJ. 2015. Callosal projections drive neuronal-specific responses in the mouse auditory cortex. J Neurosci. 35:6703-13

Rockel AJ, Hiorns RW, Powell TP. 1974. Proceedings: numbers of neurons through full depth of neocortex. J Anat. 118:371

Rockel AJ, Hiorns RW, Powell TP. 1980. The basic uniformity in structure of the neocortex. Brain 103:221-44

Sakata S, Harris KD. 2009. Laminar structure of spontaneous and sensory-evoked population activity in auditory cortex. Neuron. 64:404-18

Shanahan M, Bingman VP, Shimizu T, Wild M, Güntürkün O. 2013. Large-scale network organization in the avian forebrain: a connectivity matrix and theoretical analysis. Front Comput Neurosci. 7:89.

Shao Z, Burkhalter A. 1996. Different balance of excitation and inhibition in forward and feedback circuits of rat visual cortex. J Neurosci. 16:7353-65

Sheets PL, Suter BA, Kiritani T, Chan CS, Surmeier DJ, Shepherd GM. 2011. Corticospinal-specific HCN expression in mouse motor cortex: I(h)-dependent synaptic integration as a candidate microcircuit mechanism involved in motor control. J Neurophysiol.106:2216-31

Sherman SM, Guillery RW. 1998. On the actions that one nerve cell can have on another: distinguishing "drivers" from "modulators". PNAS. 95:7121-6

Smith DM, Barredo J, Mizumori SJ. 2012. Complimentary roles of the hippocampus and retrosplenial cortex in behavioral context discrimination. Hippocampus. 22:1121-33

Sohal VS, Zhang F, Yizhar O, Deisseroth K. 2009. Parvalbumin neurons and gamma rhythms enhance cortical circuit performance. Nature. 459:698-702

Song S, Sjöström PJ, Reigl M, Nelson S, Chklovskii DB. 2005. Highly nonrandom features of synaptic connectivity in local cortical circuits. PLoS Biol. 3:e68

Sousa VH, Miyoshi G, Hjerling-Leffler J, Karayannis T, Fishell G. 2009. Characterization of Nkx6-2-derived neocortical interneuron lineages. Cereb Cortex. 19 Suppl 1:i1-10

Stark E, Eichler R, Roux L, Fujisawa S, Rotstein HG, Buzsáki G. 2013. Inhibition-induced theta resonance in cortical circuits. Neuron. 80:1263-76

Tamamaki N, Yanagawa Y, Tomioka R, Miyazaki J-I, Obata K, Kaneko T. 2003. Green fluorescent protein expression and colocalization with calretinin, parvalbumin, and somatostatin in the GAD67-GFP knock-in mouse. J Comp Neurol. 467:60–79

Thomson AM, Girdlestone D, West DC. 1989. A local circuit neocortical synapse that operates via both NMDA and non-NMDA receptors. Br J Pharmacol. 96:406-8

Thomson AM, Bannister AP. 1998. Postsynaptic pyramidal target selection by descending layer III pyramidal axons: dual intracellular recordings and biocytin filling in slices of rat neocortex. Neuroscience. 84:669-83

Thomson AM, Lamy C. 2007. Functional maps of neocortical local circuitry. Front Neurosci. 1:19-42

Thomson AM. 2010. Neocortical layer 6, a review. Front Neuroanat. 4:13

Ulinski PS. Visual cortex of turtles. In: Evolution of Nervous Systems. Volume 2. Oxford Academic Press. 2007: 195–203

Valverde F. 2002. Estructura de la corteza cerebral. Organización intrínseca y análisis comparativo del neocórtex. Rev Neurol. 34:758-80

Vann SD, Aggleton JP, Maguire EA. 2009. What does the retrosplenial cortex do? Nat Rev Neurosci. 10:792-802

van der Knaap LJ, van der Ham IJ. 2011. How does the corpus callosum mediate interhemispheric transfer? A review. Behav Brain Res. 223:211-21

Vogt BA, Gorman AL. 1982. Responses of cortical neurons to stimulation of corpus callosum in vitro. J Neurophysiol. 48:1257-73

Vogt BA, Paxinos G. 2014. Cytoarchitecture of mouse and rat cingulate cortex with human homologies. Brain Struct Funct. 219:185-92

Wang CL, Zhang L, Zhou Y, Zhou J, Yang XJ, Duan SM, Xiong ZQ, Ding YQ. 2007. Activity-dependent development of callosal projections in the somatosensory cortex. J Neurosci. 27:11334-42

Watkins PV, Kao JP, Kanold PO. 2014. Spatial pattern of intra-laminar connectivity in supragranular mouse auditory cortex. Front Neural Circuits. 8:15

Weiler N, Wood L, Yu J, Solla SA, Shepherd GM. 2008. Top-down laminar organization of the excitatory network in motor cortex. Nat Neurosci. 11:360-6

Wolbers T, Büchel C. 2005. Dissociable retrosplenial and hippocampal contributions to successful formation of survey representations. J Neurosci. 25:3333-40

Woolsey TA, Van der Loos H. 1970. The structural organization of layer IV in the somatosensory region (SI) of mouse cerebral cortex. The description of a cortical field composed of discrete cytoarchitectonic units. Brain Res. 17:205-42

Yamawaki N, Borges K, Suter BA, Harris KD, Shepherd GM. 2014. A genuine layer 4 in motor cortex with prototypical synaptic circuit connectivity. Elife. 3:e05422

Yamashita T, Pala A, Pedrido L, Kremer Y, Welker E, Petersen CC. 2013. Membrane potential dynamics of neocortical projection neurons driving target-specific signals. Neuron. 80:1477-90

Yorke CH Jr, Caviness VS Jr. 1975. Interhemispheric neocortical connections of the corpus callosum in the normal mouse: a study based on anterograde and retrograde methods. J Comp Neurol. 164:233-45

Yoshimura Y, Dantzker JL, Callaway EM. 2005. Excitatory cortical neurons form fine-scale functional networks. Nature. 433:868-73

Zaitsev AV, Lewis DA. 2013. Functional properties and short-term dynamics of unidirectional and reciprocal synaptic connections between layer 2/3 pyramidal cells and fast-spiking interneurons in juvenile rat prefrontal cortex. Eur J Neurosci. 38:2988-98